# BEAT-TO-BEAT ESTIMATION OF STROKE VOLUME USING IMPEDANCE CARDIOGRAPHY

*THESIS*

*submitted in partial fulfillment of the requirements*

*for the degree of*

**Doctor of Philosophy**

*by*

**S. Mohan Mahalakshmi Naidu**

(Roll No. 09407801)

*under the supervision of*

**Prof. P. C. Pandey**


**Department of Electrical Engineering**

**Indian Institute of Technology Bombay**

**December 2017**

## Indian Institute of Technology Bombay

### Department of Electrical Engineering

# *Ph.D. Thesis Approval*

The Ph.D. thesis entitled "**Beat-to-beat estimation of stroke volume using impedance cardiography**" by **S. Mohan Mahalakshmi Naidu (Roll No. 09407801)** is approved, after the successful completion of viva voce examination, for the award of the degree of **Doctor of Philosophy**.

Supervisor: _____ (Prof. P. C. Pandey)

Internal Examiner: _____ (Prof. V. Rajbabu)

External Examiner: _____ (Prof. K. K. Deepak)

Chairman: _____ (Prof. P. P. Date)

Date: 20th December, 2017

Place: Mumbai

# DECLARATION

I declare that this written submission represents my ideas in my own words and where others' ideas or words have been included, I have adequately cited and referenced the original sources. I also declare that I have adhered to all principles of academic honesty and integrity and have not misrepresented or fabricated or falsified any idea/data/fact/source in my submission. I understand that any violation of the above will be cause for disciplinary action by the Institute and can also evoke penal action from the sources which have thus not been properly cited or from whom proper permission has not been taken when needed.

S. Mohan Mahalakshmi Naidu

Roll no.: 09407801

Date: 20th December, 2017

Place: Mumbai

S. Mohan Mahalakshmi Naidu / Supervisor: Prof. P. C. Pandey, "Beat-to-beat estimation of stroke volume using impedance cardiography," *PhD Thesis*, Department of Electrical Engineering, IIT Bombay, 2017.

## Abstract

Impedance cardiography is a low-cost noninvasive technique, based on monitoring of the thoracic impedance, for estimation of stroke volume (SV) and some other cardiovascular indices. Impedance cardiogram (ICG) is the negative of the first derivative of the impedance signal. Detection of its characteristic points B, C, and X is used for SV estimation. Our research objective is to develop a method for automatic beat-to-beat SV estimation to improve the acceptability of this technique for use in clinical practice. For this purpose, two investigations are carried out: (i) development of a technique for characteristic point detection and (ii) use of artificial neural network (ANN) for SV estimation using echocardiography as the reference technique. An ICG-echocardiography database is developed with recordings from subjects with normal health under rest and in the post-exercise condition and from subjects with cardiovascular disorders under rest.

A technique for automatic detection of B, C, and X points is proposed. It uses wavelet-based artifact suppression and multiple time-domain features in ICG along with R and T peaks of ECG as reference points to reduce errors due to morphological variations. Evaluation with reference to the visually marked points in ICG and with reference to the intervals measured from echocardiography showed its performance to be better than the established techniques. For estimation of the B-X interval, the mean and standard deviation of differences, as referred to the mean R-R interval, were 3.2% and 7.1%, respectively.

An ANN-based technique for SV estimation is proposed, with the input ICG parameters obtained by automatic detection of the characteristic points and the target values obtained by beat-to-beat SV measurements from time-aligned Doppler echocardiogram. A three-layer feed-forward ANN with error back-propagation algorithm is optimized by examining the effects of the number of neurons in the hidden layer, activation function, training algorithm, and set of input parameters. Performance of the optimized ANN was much better than that of equation-based estimations. Results showed that the ANN trained using the pooling of the under-rest and post-exercise recordings from subjects with normal health can be used for SV estimation for the recordings from subjects with cardiovascular disorders, it resulted in mean error of −0.1 mL, standard deviation of errors of 7.2 mL, and correlation coefficient of 0.93. Thus the proposed method may be helpful in improving the acceptability of impedance cardiography in clinical practice and as a research tool for study of SV variability.

[Blank Page]

# Contents

**Appendices**

# List of Symbols

| | |
|---|---|
| $A$ | cross-sectional area |
| $(-dz/dt)_{\max}$ | maximum of the negative of the derivative of the impedance |
| $H$ | subject's height |
| $L$ | distance between voltage sensing electrodes |
| $r$ | correlation coefficient |
| $T_{\text{lvet}}$ | left ventricular ejection time |
| $V_{\text{ITBV}}$ | intra-thoracic blood volume |
| $W$ | body weight |
| $z(t)$ | change in the thoracic impedance |
| $Z(t)$ | total sensed thoracic impedance |
| $Z_0$ | basal impedance across thorax |
| $\bar{\varepsilon}$ | mean error |
| $\rho$ | blood resistivity |
| $\sigma_{\varepsilon}$ | standard deviation of errors |

# List of Abbreviations

| | |
|---|---|
| ANN | artificial neural network |
| AVC | aortic valve closure |
| AVO | aortic valve opening |
| BFGS | Broyden-Fletcher-Goldfarb-Shanno |
| CGPB | conjugate gradient with Powell-Beale restarts |
| CO | cardiac output |
| ECG | electrocardiogram |
| EQKB | SV estimation using Kubicek equation |
| EQSR | SV estimation using Sramek equation |
| EQBR | SV estimation using Berstein equation |
| FPCG | Fletcher-Powell conjugate gradient |
| ICG | impedance cardiogram |
| LM | Levenberg-Marquardt |
| LVOT | left ventricular outflow tract |
| OSS | one-step secant |
| PAV | peak aortic velocity |
| PCG | phonocardiogram |
| PE | post-exercise |
| PRCG | Polak-Ribiere conjugate gradient |
| RBP | resilient back-propagation |
| SCD | subjects with cardiovascular disorders |
| SCD-UR | subjects with cardiovascular disorder under-rest |
| SCG | scaled conjugate gradient |
| S.D. | standard deviation |
| SNH | subjects with normal health |
| SNH-PE | subjects with normal-health post-exercise |
| SNH-UR | subjects with normal-health under-rest |
| SNR | signal-to-noise ratio |
| SV | stroke volume |
| UR | under-rest |
| VLRB | variable learning rate back-propagation |
| VTI | velocity-time integral |

# List of Tables

# List of Figures

# Chapter 1
# INTRODUCTION

## 1.1 Problem Overview

The time interval between two successive contractions of the heart is known as the cardiac cycle. Stroke volume (SV) is the amount of blood pumped out in one cardiac cycle and cardiac output (CO) is the amount of blood pumped by the heart in one minute and is obtained as the product of SV and the heart rate (Guyton and Hall 2006). SV and CO are important parameters for assessing the functioning of the cardiovascular system (Kerr *et al* 1998, Korhonen *et al* 1999, Siebert *et al* 1999, Nelson and Janerot-Sjoberg 2001, Liu *et al* 2004, Siebert *et al* 2004).

The established techniques for CO estimation are Fick's method, dye dilution, and thermodilution. These techniques are invasive and expensive. Risks associated with them restrict their use for subjects with cardiovascular disorders. Further, they are not usable for continuous monitoring (Kubicek *et al* 1974, Pianosi and Garros 1996, De Maria and Raisinghani 2000, Scherhag *et al* 2005, Tang and Tong 2009). The commonly used noninvasive technique is transthoracic echocardiography (Lewis *et al* 1984, Peterson *et al* 2003, Baumgartner *et al* 2009). It requires expensive equipment and skilled manpower. Several studies have investigated SV variability and its relationship with respiration (Marik *et al* 2009, Hoff *et al* 2014, Elstad and Walloe 2015, Holme *et al* 2016). Automatic beat-to-beat SV monitoring over an extended period using impedance cardiography can facilitate use of SV variability, like that of heart rate variability, for diagnosis of cardiovascular disorders.

Impedance cardiography is a low-cost noninvasive technique, based on monitoring of the thoracic impedance, for SV estimation (Kubicek *et al* 1974, Qu *et al* 1986, Kim 1989, Patterson 1989, Van De Water *et al* 2003). It involves applying a low-level current (< 5 mA) of high frequency (20 – 100 kHz) through a pair of electrodes placed on the thorax and measuring the resulting amplitude-modulated voltage developed across another pair of electrodes placed inside the region bounded by the current injecting electrodes. It can be used as a tool for early diagnosis of cardiovascular disorders (Kubicek *et al* 1974, Woltjer *et al* 1997, Ventura *et al* 2000, Van De Water *et al* 2003, Heinroth *et al* 2007, Bour and Kellett 2008). However, it is still not considered as a replacement for the existing techniques for use in clinical diagnosis or as part of patient bedside monitor, due to lack of repeatability of the measurements and agreement with the reference techniques. Areas of further investigation for

improving acceptance of this technique include establishing the sources of the impedance signal and mathematical modelling of the thorax, establishing the most suitable electrode configuration, SV estimation technique, establishing the effect of physical parameters (weight, height, age, etc.) in SV estimation, suppression of respiratory and motion artifacts to enable beat-to-beat estimation, and clinical applications (Jensen *et al* 1995, Raaijmakers *et al* 1997, Kamath *et al* 2009, Pandey and Pandey 2009, Tang and Tong 2009, Patterson 2010).

The negative of the derivative of the thoracic impedance signal is known as the impedance cardiogram (ICG). Landmarks in ICG associated with significant events in the cardiac cycle are known as the characteristic points, named as the A, B, C, X, and O points (Lababidi *et al* 1970, Takada *et al* 1977, Patterson 1989, Hurwitz *et al* 1990, Summers *et al* 2003). The B, C, and X points are detected for obtaining the parameters for SV estimation. As ICG is often contaminated with motion and respiratory artifacts, ensemble averaging of the waveform is generally employed to suppress the artifacts (Kubicek *et al* 1974, Qu *et al* 1989, Hurwitz *et al* 1990, Sherwood *et al* 1998, Riese *et al* 2003). It leads to averaging of event latencies and distortion in the ICG features and therefore the estimated parameters from ensemble-averaged ICG may not be well related to SV.

Several equations for SV estimation, based on models of the thoracic impedance and the aortic blood flow profile, have been proposed (Kubicek *et al* 1966, Kubicek *et al* 1970, Kubicek *et al* 1974, Kubicek 1989, Patterson 1989, Sramek *et al* 1983, Sramek 1984, Sherwood *et al* 1990, Van De Water *et al* 2003, Bernstein and Lemmens 2005). These equations use parameters obtained from the ICG waveform and patient-dependent physical parameters. Several studies have compared the measurements using impedance cardiography with those using reference techniques like thermodilution and echocardiography (Lababidi *et al* 1971, Aust *et al* 1982, Lewis *et al* 1984, Wang *et al* 1989, Northridge *et al* 1990, Castor *et al* 1994, Kizakevich *et al* 1994, Jensen *et al* 1995, Woltjer *et al* 1996, van der Meer *et al* 1999, De Maria and Raisinghani 2000, Summers *et al* 2003, Van De Water *et al* 2003, Summers *et al* 2004, Bernstein and Lemmens 2005, Fortin *et al* 2006, Arora *et al* 2007, Baumgartner *et al* 2009, Fellahi *et al* 2009, Kieback *et al* 2009, Tang and Tong 2009). Most of these studies involved subjects with normal health and some involved subjects with cardiovascular disorders. The results generally do not show a good agreement in case of subjects with cardiovascular disorders. Assuming the estimation from the reference technique to be error-free, the disagreements could be due to three sources: (i) errors in estimation of ICG parameters due to artifacts, smearing during ensemble averaging, and errors in detection of the characteristic points; (ii) inadequacies of the ICG parameter set and the SV equation; and (iii) use of body-related measurements that are unrelated to the type of disorder.

Therefore, further investigations are needed to develop a technique for SV estimation under clinical conditions.

## 1.2 Research Objectives

The research objective is to develop a technique for automatic beat-to-beat SV estimation using ICG parameters, without using models of the thoracic impedance and the aortic blood flow profile. For this purpose, two investigations are carried out: (i) development of a technique for improved detection of the ICG characteristic points as needed for SV estimation and (ii) use of artificial neural network (ANN) for SV estimation using Doppler echocardiography as the reference technique.

A time-domain technique for automatic detection of ICG characteristic points is proposed. It does not require estimation of the baseline and manual selection of the processing parameters. The technique is validated on recordings from subjects with normal health under rest and in the post-exercise condition with an increase in the heart rate introduced by exercise and the recordings from subjects with cardiovascular disorders under rest. A technique for beat-to-beat SV estimation using artificial neural network is developed using Doppler echocardiography as the reference technique. The proposed technique is investigated on the recordings from subjects with normal health for finalizing the set of input parameters and optimizing the network. Subsequently, the technique is evaluated on the recordings from both sets of subjects by comparing the results with those from the equation-based estimations.

## 1.3 Thesis Outline

The second chapter provides an overview of impedance cardiography and presents the scope of research. The third chapter presents the proposed technique for automatic detection of ICG characteristic points and its validation. The investigations for beat-to-beat SV estimation using artificial neural networks and the evaluation results are presented in the fourth chapter. Summary of the investigations carried out, conclusions, and some suggestions for further investigations are presented in the last chapter. Supplementary information is provided in the four appendices.

# Chapter 2
# IMPEDANCE CARDIOGRAPHY

## 2.1 Introduction

Impedance cardiography is a noninvasive technique, based on monitoring of the thoracic impedance during the cardiac cycle, for estimation of several cardiovascular indices. It was primarily developed by Kubicek *et al* (1966) as a low-cost technique for SV estimation. It can be used for early diagnosis of cardiovascular disorders (Kubicek *et al* 1974, Woltjer *et al* 1997, Ventura 2000, Van De Water *et al* 2003, Ono *et al* 2004, Heinroth *et al* 2007, Bour and Kellett 2008). This chapter provides an overview of the instrumentation for impedance cardiography, the physiological correlates of the impedance signal, equations for SV estimation, applications of impedance cardiography, and clinical studies on SV estimation. The last section presents the scope of research reported in the thesis.

## 2.2 Instrumentation for Impedance Cardiography

The technique involves applying a low-level current (< 5 mA) of high frequency (20 – 100 kHz) into the thorax through a pair of electrodes placed on the thorax and measuring the resulting voltage developed across another pair of electrodes placed inside the region bounded by the current injecting electrodes (Kubicek *et al* 1966, Kubicek 1970, Kubicek *et al* 1974, Qu *et al* 1986, Kim 1989, Patterson 1989, Van De Water *et al* 2003). The impedance cardiography instrument generally consists of a current source, an impedance detector and differentiator, an ECG extraction circuit, and two pairs of electrodes, as shown in Figure 2.1. The picked-up voltage has two components. The first component is the voltage drop caused by the excitation current passing through the thoracic impedance. This component is an amplitude modulated waveform with the frequency of the excitation current as the carrier frequency and a very small modulation index due to variation in the thoracic impedance. The second component is contributed by ECG. The impedance detector comprises a difference amplifier and bandpass filter to supress common-mode interference, ECG component, and high-frequency noise, followed by an amplitude demodulator to extract a voltage proportional to the thoracic impedance. The impedance of a body segment measured using low-level high-frequency current is nearly resistive (Rosell and Webster 1995) and the term impedance in the context of impedance cardiography refers to the resistance of the thoracic segment. The impedance signal refers to the voltage waveform proportional to the time-varying thoracic

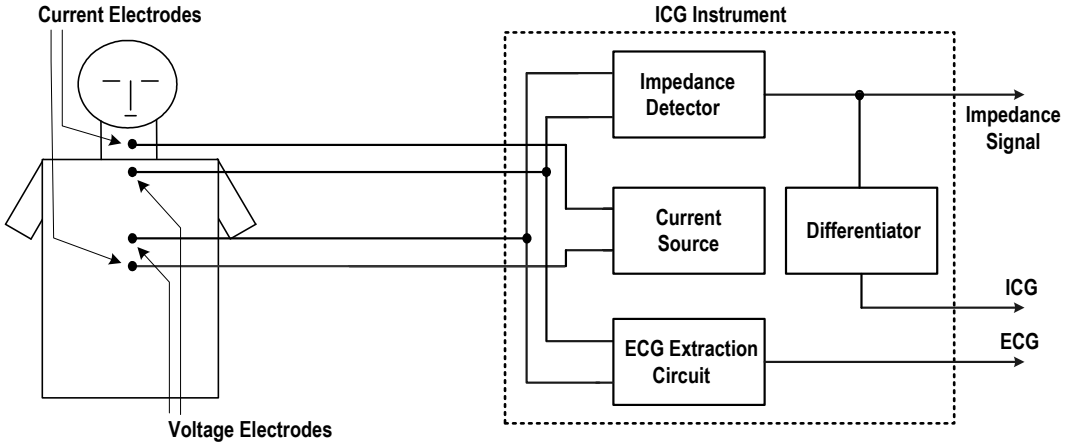


**Figure 2.1** Block diagram of instrumentation for impedance cardiography.

resistance. Negative of the first derivative of the impedance signal is known as the impedance cardiogram (ICG) and it is obtained as the output of the differentiator. The ECG extraction circuit extracts the ECG signal which is used as reference for processing the ICG signal.

In impedance cardiography, generally four-electrode configuration is used, with surface electrodes in the form of either band or spot electrodes. Several studies have been conducted regarding the placement of electrodes for recording the ICG signals (Bonjer *et al* 1952, Kubicek *et al* 1966, Kubicek *et al* 1970, Sramek 1984, Penney *et al* 1985, Bernstein *et al* 1986, as cited in Woltjer *et al* 1997, Boomsma *et al* 1989, Patterson *et al* 1991, Ragheb *et al* 1992, Yamakoshi *et al* 2003, Ikarashi *et al* 2006).

Bonjer *et al* (1952) used four band electrodes, with the outer pair of electrodes to inject the current and the inner pair to measure the voltage. Use of separate electrode pairs for current injection and voltage measurement helps in reducing the contribution of electrode-tissue interface impedances in the sensed voltage and therefore in reducing motion artifacts in the detected impedance signal. Use of the four-band electrode configuration, as shown in Figure 2.2(a), has been reported in many studies (Kubicek *et al* 1966, Kubicek *et al* 1970, Woltjer *et al* 1997, Patterson 2010). Use of band electrodes for current injection is meant to provide a uniform current distribution in the thoracic region. However, band electrodes may not be suitable for clinical use and their use in long-term monitoring can cause a chocking sensation. To overcome these limitations, Sramek (1984) proposed a twelve-spot electrode configuration, replacing each band electrode by a set of shorted together spot electrodes. In this configuration, two spot electrodes placed laterally on the neck at the intersection of the circumference of the neck with the frontal plane and shorted together serve as the upper

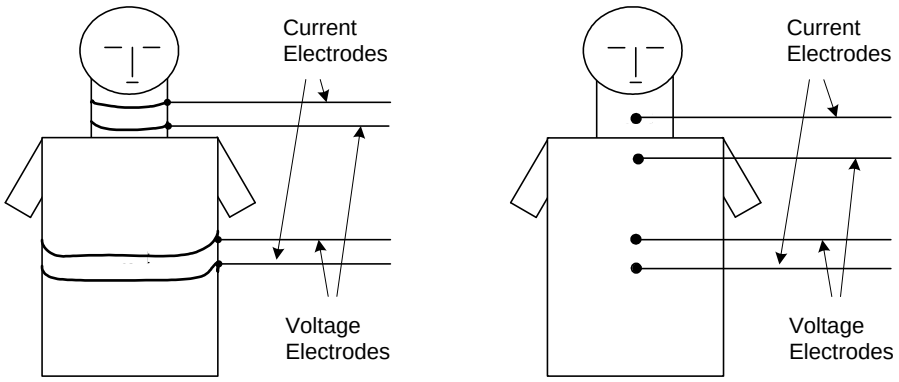


(a) (b)

**Figure 2.2** Electrode configurations: (a) Four-band electrode configuration, (b) Four-spot electrode configuration.

voltage electrode. Two spot electrodes placed on the neck approximately 3 – 5 cm above the upper voltage electrodes and shorted together serve as the upper current electrode. Two spot electrodes are placed at the anterior intercostal space at each mid-clavicular line at the level of xiphoidal process and two spot electrodes are placed at the same level on the back. These four spot electrodes shorted together serve as the lower voltage electrode. Four spot electrodes are placed approximately 4 – 6 cm below the lower set of voltage electrodes. These spot electrodes are shorted together and serve as lower current electrode.

Penney *et al* (1985) used four-spot electrode configuration, as shown in Figure 2.2(b), to avoid the practical difficulty associated with band electrodes for critically ill patients. In this configuration, two electrodes are placed with approximately 6 cm separation at the base of the neck. Two electrodes are placed on the lower left anterolateral of the thorax, with one near the mid-clavicular line and the other one at 8 cm from the first and in the tenth inter-costal space near mid-auxiliary line. They used two-channel impedance cardiography for recordings from spot and band electrodes and reported a good similarity between the two signals, in terms of peak and shape of the waveform. Qu *et al* (1986) evaluated different placements of the four-spot electrode configurations. They concluded that better SNR was achieved with the current electrode pair placed at the back of the sternum, with one electrode on the neck and the other electrode above the xiphoidal process, and the voltage electrode pair in the front, with the two electrodes placed inside the region of the current electrodes.

Bernstein *et al* (1986, as cited in Woltjer *et al* 1997) proposed an eight-spot electrode configuration. In this configuration, two spot electrodes placed laterally on the neck at the intersection of the circumference of the neck with the frontal plane and shorted together serve as the upper voltage electrode. Two spot electrodes placed on the neck approximately 5 cm

above the upper voltage electrodes and shorted together serve as the upper current electrode. Two spot electrodes placed laterally at the level of xiphoidal process and shorted together serve as the lower voltage electrode. Two spot electrodes placed approximately 5 cm below the lower set of voltage electrodes and shorted together serve as the lower current electrode. Woltjer *et al* (1997) reported that the results from the lateral spot electrode array were different from those obtained using band electrodes, possibly due to the inhomogeneous electrical field caused by these spot electrodes. They modified the electrode array to nine-spot electrode array, called as modified semi-circular configuration. In this configuration, an electrode placed on the forehead serves as the upper current electrode. Two spot electrodes placed laterally on the neck at the intersection of the circumference of the neck with the frontal plane and shorted together serve as the upper voltage electrode. The lower voltage electrode is formed by two shorted-together spot electrodes placed on the two lateral sides at the level of xiphoidal process. The lower current electrode is formed by four shorted-together spot electrodes placed horizontally on the frontal line and below the lower voltage electrodes. It was reported that this configuration generated a relatively homogeneous electrical field in the thoracic region and was interchangeable with the band electrode configuration.

Several instrument designs and electrode configurations have been reported and some instruments are commercially available. A test setup is needed for comparing the performance of these instruments in terms of linearity, sensitivity, accuracy, frequency response, and noise rejection. For this purpose, thoracic bioimpedance simulators have been reported with settable step changes in the impedance (Pandey *et al* 2008, Ulbrich *et al* 2015). As the step change in the simulated impedance is not suitable for extraction of ICG, there is a need to develop a thoracic bioimpedance simulator to simulate the time-varying bioimpedance with selectable waveform along with settable basal impedance, and simulation of noise and artifacts.

## 2.3 Impedance Signal and Its Physiological Correlates

The source of the impedance signal has been subject of several studies involving experiments on animals and humans, using electrical model of the thorax, and those using 3D finite difference thorax models developed using magnetic resonance imaging (Bonjer *et al* 1952, Kubicek *et al* 1970, Visser *et al* 1977, Kim *et al* 1988, Wang and Patterson 1995, Patterson 2010). Initially it was assumed that the lung was the major contributor to the impedance signal (Kubicek *et al* 1970). Later, it was reported that aorta was the source of the impedance signal (Kubicek *et al* 1974, Kim *et al* 1988). Visser *et al* (1977) found from an experiment conducted on dogs that impedance change was caused by, apart from the cardiac related volume changes, change in blood resistivity due to change of orientation of the erythrocytes.

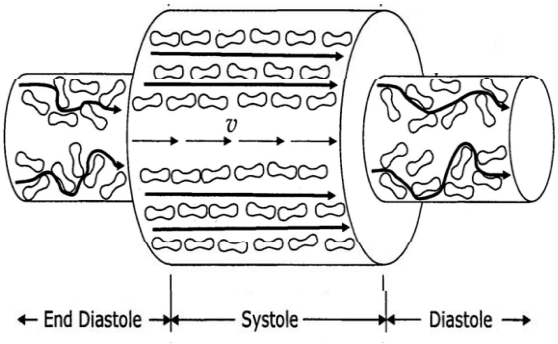


**Figure 2.3** Orientation of erythrocytes during different phases of the cardiac cycle. Adapted from Bernstein (2010).

This has been supported by several studies conducted on humans (Sakamoto and Kanai 1979, Wang and Patterson 1995, Bernstein 2010). Figure 2.3 shows the change in erythrocyte orientations during the cardiac cycle, from random during the diastole to align along the flow direction during the systole.

The landmarks in ICG associated with the significant events in the cardiac cycle are known as the ICG characteristic points and these are labeled as A, B, C, X, and O (Lababidi *et al* 1970, Takada *et al* 1977, Kim 1989, Patterson 1989, Hurwitz *et al* 1990, Woltjer *et al* 1997, Summers *et al* 2003). The simultaneously recorded thoracic impedance signal, ICG along with its characteristic points marked on it, phonocardiogram (PCG) showing the heart sounds, and ECG are shown in Figure 2.4.

*A point*: It follows the P wave of the ECG signal and it is the negative deflection before the B point in the ICG waveform. It generally coincides with the atrial contraction, but the contribution of the contraction of the left and right atria has not been established (Karnegis and Kubicek 1970, Lababidi *et al* 1970, Takada *et al* 1977, Woltjer *et al* 1997).

*B point*: It occurs after the QRS complex, in the region of the first heart sound, as a notch in the ICG waveform just before the rapid upstroke ascending towards the C point. It is associated with the aortic valve opening, as confirmed by echocardiography and aortic pressure technique (Lababidi *et al* 1970, Kizakevich *et al* 1993, Visser *et al* 1993).

*C point*: It is the highest peak in the ICG waveform during the systole and it is associated with the peak in the aortic blood flow (Karnegis and Kubicek 1970, Kubicek *et al* 1974, Welham *et al* 1978, Kizakevich *et al* 1993, Woltjer *et al* 1997). Kizakevich *et al* (1993) used Doppler echocardiography to measure peak aortic blood velocity and found the C point to be associated with the ventricular contraction.

*X point*: It is below the baseline and is the lowest point in the ICG waveform followed by the O point in a cardiac cycle. It is associated with the aortic valve closure (Lababidi *et al*

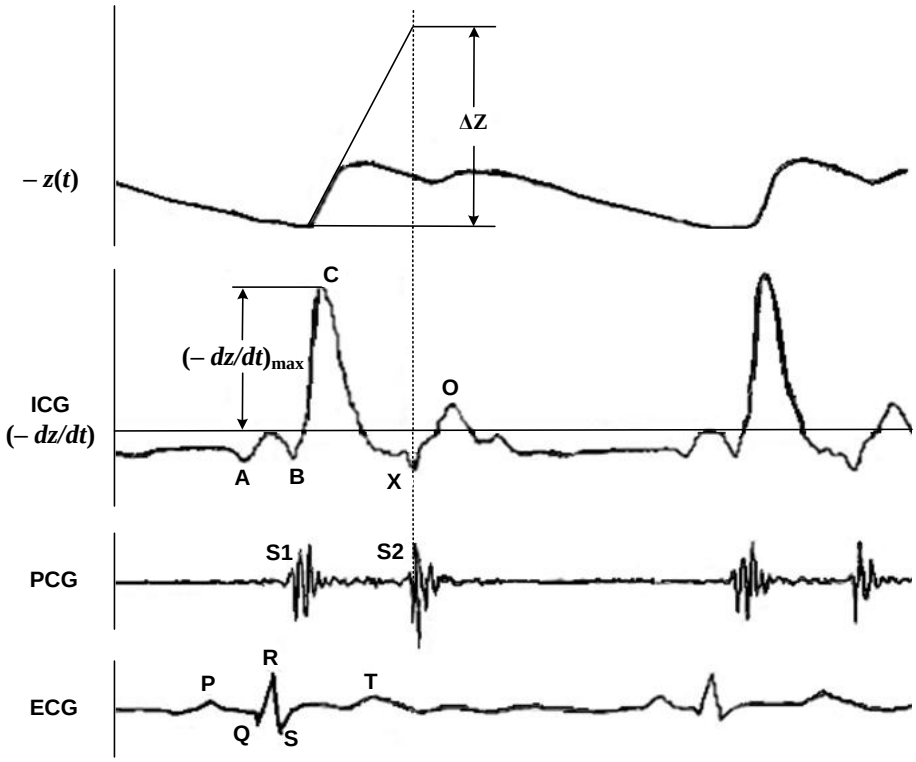


**Figure 2.4** ICG with its characteristic points and other related signals. Adapted from Patterson (1989).

1970, Kubicek *et al* 1974) and occurs in the region of the second heart sound. Its association with the aortic valve closure has been confirmed by studies using echocardiography and aortic pressure technique (Kizakevich *et al* 1993, Visser *et al* 1993).

*O point*: It is the peak after the X point. It coincides with the wide opening of the mitral valve. It lies in the interval from the mitral transition, above the lowest point i.e. aortic valve closure to the A point during the early diastole (Lababidi *et al* 1970, Bour and Kellett 2008). It is strongly influenced by the pulmonary venous return and abnormalities in its location are associated with aortic valve insufficiency or acute myocardial injury in heart failure patients (Woltjer *et al* 1997).

## 2.4 Equations for SV Estimation

Several equations for estimating the stroke volume from the parameters of ICG waveform have been developed. Some of these equations are based on physiological models and some are empirically derived (Kubicek *et al* 1966, Nyboer *et al* 1970, Sramek *et al* 1984, Raaijmakers *et al* 1997, Van De Water *et al* 2003, Bernstein and Lemmens 2005). In all these equations, the thoracic impedance is assumed to be resistive.

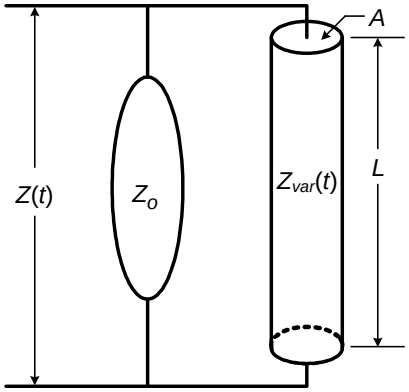


**Figure 2.5** Parallel column model. Adapted from Patterson (1989)

Nyboer *et al* (1970) proposed the relationship between change in impedance and change in blood volume in a body segment during the cardiac cycle, modelling the segment as two parallel columns, as shown in Figure 2.5. The first column has constant impedance $Z_0$ representing the basal impedance. The second column is modelled as a cylindrical conductor of resistivity $\rho$, fixed length $L$, and time-varying cross-sectional area $A$, and it represents the time-varying impedance $Z_{\text{var}}(t)$. The equivalent impedance $Z(t)$ of the parallel-column model is

$$Z(t) = Z_0 \,||\, Z_{\text{var}}(t) \tag{2.1}$$

The small change in the time-varying impedance, with reference to the basal impedance $Z_0$ is given as $z(t) = Z(t) - Z_0$, or as

$$z(t) = = \frac{-Z_0^2}{Z_0 + Z_{\text{var}}(t)} \tag{2.2}$$

Assuming that $Z_{\text{var}}(t) >> Z_0$, the time-varying component is given as

$$z(t) \approx -Z_0^2 / Z_{\text{var}}(t) \tag{2.3}$$

The impedance of the variable impedance column is $\rho L / A(t)$. With volume $V(t) = LA(t)$, the variable impedance is given as

$$Z_{\text{var}}(t) = \rho L^2 / V(t) \tag{2.4}$$

The time-varying component of the impedance, from (2.3) and (2.4), is given as

$$z(t) = -\frac{Z_0^2}{\rho L^2} V(t) \tag{2.5}$$

Therefore, $V(t)$ can be obtained as

$$V(t) = \frac{\rho L^2}{Z_0^2}(-z(t)) \tag{2.6}$$

Nyboer (1970) assumed that the blood inflow into the thorax was the cause of impedance change and there was insignificant outflow during the ejection phase. Impedance decreases with increase in the blood volume, and hence the maximum decrease in the impedance, $\Delta Z = \max(-z(t))$, corresponds to maximum change in the blood volume in the thorax. It can be given as

$$\Delta V = \rho \frac{L^2}{Z_0^2} \Delta Z \tag{2.7}$$

As the change in the blood volume is the net result of inflow and outflow of the blood, the backward slope extrapolation was proposed to estimate the change in the blood volume due to inflow during the cardiac cycle (Nyboer 1970). It is based on the assumption that the inflow lasts for a short interval at the beginning of the cardiac cycle and outflow rate remains nearly constant. Hence the maximum change in the impedance is calculated by drawing a linear extrapolation line to the down slope edge of the "volume difference graph", a plot of the impedance as a function of time, and extending the line upward and downward until it intersects the vertical coordinates determined by the end of systole and the beginning of the diastole as shown in Figure 2.6. The upward intersecting point is the probable height of the curve due to outflow, which is equal to the change due to inflow had there been no outflow. Thus the measured maximum change in the impedance as estimated using the backward extrapolation is proportional to the maximum volume change due to ventricular ejection (SV). Possibly due to difficulty in applying the backward extrapolation, this technique has not been reported in subsequent studies.

To take care of the blood that leaves the thoracic region during the ejection phase, a forward-slope extrapolation technique was reported by Kubicek *et al* (1966, 1970, 1974). It is based on the assumptions that the blood ejection from the ventricle is in the form of a square pulse, i.e., the flow rate is constant over the blood ejection phase, that the blood starts significantly leaving the thoracic region sometime after the aortic valve opens, and that the maximum rate of change in the impedance is proportional to the rate of blood ejection. As shown in Figure 2.4, a straight line is drawn from the steepest part of $-z(t)$ until the end of the ejection phase. Thus $\Delta Z$ is obtained as the product of the slope of the straight line and the left ventricular ejection time $T_{\text{lvet}}$. The slope is measured by finding the peak height (C point) of the ICG, i.e., maximum of $-dz/dt$. The interval $T_{\text{lvet}}$ is the interval from the opening of

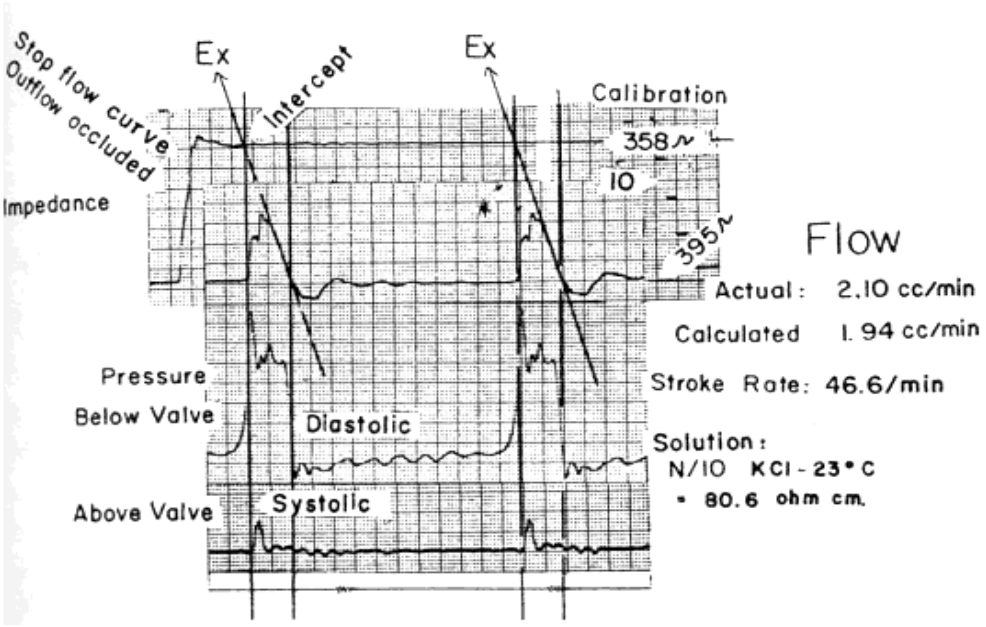


**Figure 2.6** Volume difference curve (impedance) with backward extrapolation used by Nyboer (1970).

aortic valve as marked by the B point to the aortic valve closure as marked by the X point. The stroke volume is estimated using Kubicek equation as

$$\mathrm{SV}_{\mathrm{Kubicek}} = \rho \frac{L^2}{Z_0^2} \left( -\frac{dz}{dt} \right)_{\max} T_{\mathrm{lvet}} \tag{2.8}$$

The main shortcomings of the Kubicek equation are associated with the validity of fixed-length conductor model of the thorax, difficulty in determining $\rho$, and inconsistencies in measurement of $L$. Sramek *et al* (1983, as cited in Van De Water *et al* 2003, Sramek 1984) substituted the cylindrical conductor model with a truncated cone model. They approximated $L$ as 0.17*H*, where $H$ is the subject height, and related $\rho$ with $Z_0$ and $L$, resulting in the following equation, known as the Sramek SV equation:

$$\mathrm{SV}_{\mathrm{Sramek}} = \frac{(0.17H)^3}{4.25} \frac{(-dz/dt)_{\max}}{Z_0} T_{\mathrm{lvet}} \tag{2.9}$$

where $H$ is in cm, $Z_0$ is in $\Omega$, $(-dz/dt)_{\max}$ is in $\Omega \cdot \mathrm{s}^{-1}$, $T_{\mathrm{lvet}}$ is in s, and SV is in mL.

Bernstein *et al* (1986, as cited in Van De Water *et al* 2003, Bernstein and Lemmens 2005) modified the Sramek's equation by introducing the weight deviation term $\delta = \sqrt{\mathrm{BMI}_{\mathrm{actual}} / \mathrm{BMI}_{\mathrm{ideal}}}$, where $\mathrm{BMI}_{\mathrm{actual}}$ is the body mass index (calculated as weight /

height$^2$, with weight in kg and height in m) and $\mathrm{BMI_{ideal}} = 24\ \mathrm{kg \cdot m^{-2}}$. The modified equation, known as the Sramek-Bernstein equation is given as

$$\mathrm{SV_{Sramek\text{-}Bernstein}} = \delta \frac{(0.17H)^3}{4.25} \frac{(-dz/dt)_{\max}}{Z_0} T_{\mathrm{lvet}} \tag{2.10}$$

To improve the estimation accuracy, Bernstein and Lemmens (2005) proposed an SV equation derived from a multi-component parallel column model of the thorax. It uses square root of $(-dz/dt)_{\max}$ normalized with $Z_0$, in order to relate $(-dz/dt)$ to the variation in the blood resistivity caused by variation in the blood velocity. With $Z_0$ in $\Omega$, $(-dz/dt)_{\max}$ in $\Omega \cdot \mathrm{s^{-1}}$, and $T_{\mathrm{lvet}}$ in s, SV in mL is given as

$$\mathrm{SV_{Bernstein}} = \frac{16W^{1.02}}{\zeta^2} \sqrt{(-dz/dt)_{\max} / Z_0}\ T_{\mathrm{lvet}} \tag{2.11}$$

where $W$ = body weight (kg),

$\zeta$ = index of transthoracic conduction

$$= \begin{cases} \dfrac{Z_C^2 - Z_C Z_0}{2Z_C^2 + Z_0^2 - 3Z_C Z_0}, & Z_0 < Z_C \\ 1, & Z_0 \geq Z_C \end{cases}$$

$Z_C$ = critical impedance (taken empirically as 20 Ω).

Some of the SV equations are based on the physiological models and some are empirically derived. Validity of the models used in SV equations in explaining the origin of the impedance signal and its physiological correlates has been questioned due to inconsistency of the results obtained using them (Jensen *et al* 1995, Raaijmakers *et al* 1997, Woltjer *et al* 1997, Ventura *et al* 2000, Scherhag *et al* 2005, Patterson 2010). Several simulation models (Kim *et al* 1988, Wang and Patterson 1995, Patterson 2010) have been used to investigate the origin of the impedance signal. Some of the parameters in the SV equations are body related and may lead to a bias in case of subjects with cardiovascular disorders, because they are unrelated to the type of cardiovascular disorder. Therefore, further investigations are needed to develop a technique using an appropriate set of contributing inputs, which can give error-free SV estimation under clinical conditions.

## 2.5 Impedance Cardiography Applications

Impedance cardiography has been developed primarily as a noninvasive technique for SV measurement. The ICG waveform can also be used for estimating several indices with

potential applications in diagnosis of cardiovascular disorders (Kim 1989, Visser *et al* 1993, Summers *et al* 1999, Summers *et al* 2003, Braun *et al* 2005, Sodolski and Kutarski 2007).

The thoracic fluid content (TFC) is related to the total fluid in the thorax, including the intravascular and extravascular fluids (Kubicek *et al* 1974, Saunders 1988) and it is given as

$$\text{TFC} = 1/Z_0 \tag{2.12}$$

The velocity index (VI) index is related to the peak velocity of the blood in the aorta (Packer *et al* 2006) and it is given as

$$\text{VI} = \left(-dz/dt\right)_{\max} / Z_0 \tag{2.13}$$

Acceleration index (ACI) is related to the peak acceleration of the blood flow in the aorta (Packer *et al* 2006) and it is defined as

$$\text{ACI} = \left(d^2z/dt^2\right)_{\max} / Z_0 \tag{2.14}$$

Pre-ejection period (PEP) is the time interval from the Q peak of ECG to the opening of the aortic valve. Systolic time ratio (STR) is the ratio of the pre-ejection period to the left ventricular ejection time (Packer *et al* 2006) and is given as

$$\text{STR} = \text{PEP} / T_{\text{lvet}} \tag{2.15}$$

Heather index (HI) is the ratio of the maximum rate of change in the impedance to the time interval from the Q wave of ECG to the C point of ICG, $T_{QC}$ (Kubicek *et al* 1974) and is given as

$$\text{HI} = \left(-dz/dt\right)_{\max} / T_{QC} \tag{2.16}$$

Systolic vascular resistance (SVR) is the index of the arteriolar constriction of the body (Packer *et al* 2006). It is the ratio of difference of mean arterial pressure (MAP) and central venous pressure (CVP) to the cardiac output (CO) and is given as

$$\text{SVR} = (\text{MAP} - \text{CVP})/\text{CO} \tag{2.17}$$

These indices are related to the electromechanical events of the heart and have been reported to be useful in diagnosing atrial and ventricular dysfunctions, valve related disorders, and arterial disorders.

The A point abnormality in ICG may be indicative of diastolic dysfunction related to the atrial and ventricular premature contractions (Lababidi *et al* 1970, Kubicek *et al* 1974). Double peaking at the C point is generally related with the ventricular abnormality, particularly ventricular asynchrony or severe mitral insufficiency (Kubicek *et al* 1974, Bour and Kellett 2008). The O point generally coincides with the opening of the mitral valve and corresponds to the E wave in the Doppler echocardiogram. Abnormality in the O point is seen in cases of the aortic stenosis or increased venous return. Ratio of the O peak to the C peak is

related to the pulmonary capillary wedge pressure and it may be useful in classification of heart failure patients (Karnegis and Kubicek 1970, Lababidi *et al* 1970, Visser *et al* 1977, Scherhag *et al* 2005, Bour and Kellett 2008). Left ventricular ejection fraction is the ratio of the amount of blood pumped out of the ventricle to the total blood in it at the end of diastole. On the basis of several earlier studies, Bour and Kellett (2008) concluded that 40 – 60% of heart failure patients have normal values of left ventricular ejection fraction and have heart failure due to diastolic dysfunction, i.e., relative shift in the left ventricular filling towards the late diastole. In such patients, the ICG shows an enlargement of the O and A points. In atrial fibrillation, both A and O points may disappear (Bour and Kellett 2008).

Effects of exercise related stress and drugs on ICG have also been reported (Lababidi *et al* 1970, Kubicek *et al* 1974). High-level exercise introduced enlargement of the O point during the rapid filling phase of the ventricles and that of the A point during the left atrial contraction. After low-level exercise, effects of the cardiac problems related to the mechanical activity of the heart were much more visible in ICG than in ECG. In healthy subjects, SV increased with exercise and $T_{\text{lvet}}$ decreased. Pulmonary oedema, pleural effusion or haemorrhage into the chest resulted in lower value of $Z_0$. In healthy subjects, the R-C interval (interval from the R peak of ECG to the C point of ICG) shortened in post-exercise stress condition and in response to drugs.

Several researchers have reported the usefulness of ICG for estimation of SV (Kubicek *et al* 1974, Woltjer *et al* 1997, Ventura *et al* 2000, Ono *et al* 2004, Heinroth *et al* 2007, Bour and Kellett 2008). Kim *et al* (1992) reported the use of ICG for diagnosing the cardiac diseases related to pulmonary artery, dilated cardiomyopathy, aortic stenosis and other valvular diseases by monitoring the SV during exercise. Zhang and Li (2008) reported that ICG can be used to monitor cardiac function under transient conditions. Sherwood *et al* (1998) reported that the ICG may be useful for assessing the effect of physical exercise, sleep, and use of drugs on the cardiac system.

Strickberger *et al* (2005) reported the use of ICG in cardiac resynchronization therapy (CRT). Objective of CRT is to correct ventricular dysfunction in severe heart failure patients by simultaneously pacing both the left and right ventricles. It has been reported to work well in patients with QRS complex wider than 120 ms. Tissue Doppler imaging echocardiography (TDI) is currently used for detection of ventricular dys-synchrony for CRT (Tassan-Mangina *et al* 2006). Bour and Kellett (2008) and Heinroth *et al* (2007) have also reported use of ICG for this purpose.

ICG may be useful in emergency departments because it is a noninvasive technique providing primary information about the cause and severity of attack in heart patients (Ventura *et al* 2000, Summers *et al* 2003, Lo *et al* 2007). It can be used for examining the effects of various stimuli (exercise, sleep, during drug testing, etc.) on the cardiovascular system (Sherwood *et al* 1998, Ono *et al* 2004). It has been reported to be useful in determining the coronary artery diseases and ischemia, a localized vasoconstriction during exercise (Kizakevich *et al* 1989, Summers *et al* 2003). It has been used as a prognostic tool in predicting short-term risk in stable chronic heart failure patients (Packer *et al* 2006). Hill and Lowe (1973) used it for monitoring blood flow during anaesthesia. Lopez-Saucedo *et al* (1989) used it to monitor resuscitation of a patient during the treatment in intensive care unit. Yu *et al* (2001) used hemodynamic parameters measured from ICG to explore the psychological mood states. Variations in R-C time intervals and CO have been used to examine the effect of different diseases on the autonomic nervous system (Jindal *et al* 2003, Meijer *et al* 2007). You-ten *et al* (2008) used ICG for continuous monitoring of the cardiac hemodynamic parameters during the caesarean delivery under spinal anaesthesia and used SV, systolic blood pressure, and cardiac indices to maintain the normal baseline blood pressure by drug administration to avoid hypotension. A study by Wong *et al* (2009), involving subjects with normal blood pleasure, reported that ECG and ICG together can be used for monitoring the systolic blood pressure.

## 2.6 Clinical Studies on SV Estimation

Several studies have been reported for comparison of SV and CO estimated using impedance cardiography with those measured using some of the established techniques (Jensen *et al* 1995, Woltjer *et al* 1996, Woltjer *et al* 1997, De Maria and Raisinghani 2000, Summers *et al* 2003, Bernstein and Lemmens 2005, Kamath *et al* 2009, Tang and Tong 2009).

Woltjer *et al* (1996) estimated SV using ICG on subjects with cardiovascular disorders, with lateral spot and modified semi-circular spot electrode configurations. They compared both sets of values with those obtained using thermodilution as the reference technique. Kubicek and Sramek-Bernstein equations were used for SV calculation in both the electrode configurations. Comparison with reference technique was carried out by calculating the mean difference, standard deviation of differences, linear regressing (intercept and slope), and correlation coefficient. The results, summarized in Table 2.1, showed that the best performance was observed for Kubicek equation with modified semi-circular spot electrode array (correlation coefficient of 0.90, mean difference of 0.5 mL, and standard deviation of differences = 8.6 mL). Lateral spot electrode array gave relatively poor results for both the

**Table 2.1** Comparison of SV estimation from ICG using Kubicek (K) and Sramek-Bernstein (SB) equations with those from thermodilution, as reported by Woltjer *et al* (1996). Number of subjects: 37 (28 males, 9 females).

| Electrode array | Equa-tion | Mean diff. (mL) | Std. dev. of diff. (mL) | Linear regress. intercept | Linear regress. slope | Corr. coeff. |
|---|---|---|---|---|---|---|
| Lateral spot | K | −27.9 | 11.6 | 0.2 | 0.5 | 0.69 |
| | SB | −2.7 | 14.6 | 12.4 | 0.8 | 0.64 |
| Modified semi-circular spot | K | 0.5 | 8.6 | −5.0 | 1.1 | 0.90 |
| | SB | 19.3 | 16.6 | 11.8 | 1.1 | 0.73 |

equations. The authors emphasized the need for further studies to examine the validity of impedance cardiography for monitoring SV variation under different conditions in the same patient. Bernstein and Lemmens (2005) compared CO estimation from ICG using their proposed SV equation with the Kubicek, Sramek, and Sramek-Bernstein equations, using thermodilution as the reference technique. They used lateral spot electrode configuration (eight-spot electrode configuration) in their study. The ICG parameters were obtained after ensemble averaging of the signal over 30 cardiac cycles. The bias and precision errors for the Kubicek equation were 51% and 32%, respectively. The corresponding values were 41% and 34% for the Sramek equation, and 36% and 33% for the Sramek-Bernstein equation. Their proposed equation resulted in much better performance, with bias of −1% and with precision error of 16%.

Summers *et al* (2003) have summarized results from around 201 studies on estimation of SV using ICG and those with some of the other established techniques, using weighted average and meta-analytic values of correlation coefficients. The values as given in Table 2.2 show a large variation across the reference techniques. Tang and Tong (2009), in a review of impedance cardiography and its suitability for clinical use, have summarised results from several studies involving CO measurement on patients with cardiovascular disorders with thermodilution as the reference technique. They reported correlation coefficients ranging from 0.34 to 0.93, with large interpatient variation.

There is no universally accepted reference technique for SV measurement (Tang and Tong 2009, Kieback *et al* 2010). The thermodilution technique is considered as the gold standard, but it is invasive and expensive. It cannot be used for continuous monitoring and has the limitation of being usable only for patients with severe cardiovascular disorders (Pianosi and Garros 1996, De Maria and Raisinghani 2000, Scherhag 2005). In several recent studies on use of impedance cardiography for estimation of SV and some other cardiovascular indices,

**Table 2.2** Correlation coefficients (*r*) between SV values using ICG and those using some of the established methods: weighted average and meta-analytic values from 201 studies, as reported by Summers *et al* (2003).

| Reference method | No. of measurements | Average *r* | Meta-analytic *r* |
|---|---|---|---|
| Thermodilution | 10,959 | 0.81 | 0.95 |
| Direct Fick | 587 | 0.79 | 0.95 |
| Indirect Fick | 541 | 0.80 | 0.90 |
| Doppler | 284 | 0.61 | 0.86 |
| Dye-dilution | 902 | 0.81 | 0.93 |
| Ventriculography | 295 | 0.72 | 0.81 |
| Echocardiography | 281 | 0.69 | 0.92 |
| Isotope dilution | 41 | 0.88 | 0.88 |
| Integrated flow | 49 | 0.83 | 0.83 |
| Pulsatile flow | 17 | 0.76 | 0.76 |
| LVAD | 30 | 0.89 | 0.89 |
| MRI | 20 | 0.92 | 0.98 |
| EM flow probe | 2,807 | 0.84 | 0.88 |
| Overall | 16,803 | 0.81 | 0.94 |

Doppler echocardiography, which is noninvasive, has been used as the reference technique (Aust *et al* 1982, Lewis *et al* 1984, Northridge *et al* 1990, Kizakevich *et al* 1993, Castor *et al* 1994, van der Meer *et al* 1999, Arora *et al* 2007, Baumgartner *et al* 2009, Fellahi *et al* 2009, Kieback *et al* 2010). A summary of results reported in some of the earlier studies on evaluation of impedance cardiography with reference to Doppler echocardiography is given in Table 2.3.

Aust *et al* (1982) estimated SV using ICG and Doppler echocardiograms recorded from six healthy subjects under transient conditions. SV values were estimated using the Kubicek equation and subject-specific blood resistivity measurement. Despite large errors, the correlation coefficient was 0.83 and it was concluded that impedance cardiography was better suited for monitoring SV variation than for absolute measurement. In the study by Northridge *et al* (1990) on 25 cardiac patients with acute myocardial infraction, the range with 95% confidence limits for CO estimated with thermodilution as the reference technique was –1.43 to 1.11 L/min for Doppler echocardiography and –1.23 to 1.32 L/min for ICG.

Kizakevich *et al* (1993) measured systolic events and indices by impedance cardiography and Doppler echocardiography from 31 subjects admitted for coronary

**Table 2.3.** A summary of results reported in some earlier studies on evaluation of impedance cardiography with reference to Doppler echocardiography.

| Study | Subjects | Results |
|---|---|---|
| Aust *et al* (1982) | 6 healthy subjects | Correlation coefficient of SV estimation with reference to Doppler echocardiography = 0.83. |
| Northridge *et al* (1990) | 24 cardiac patients | 95% limits of agreement of CO estimation with thermodilution: –1.23 to 1.32 L/min for Doppler echocardiography, –1.43 to 1.11 L/min for ICG. |
| Kizakevich *et al* (1993) | 5 healthy subjects & 26 patients with coronary artery disease | Correlation coefficients of systolic ejection measures with reference to Doppler echocardiography: 0.78 for aortic valve opening time, 0.86 for peak ejection velocity time, 0.73 for aortic valve closure time, 0.74 for peak acceleration, 0.79 for normalized acceleration. |
| Castor *et al* (1994) | 10 cardiac patients | Mean difference of CO estimation with reference to thermodilution: –2.2% to 1.4% for ICG, –16% to –32% for Doppler echocardiography. |
| van der Meer *et al* (1999) | 26 cardiac patients | Correlation coefficient of CO estimation with reference to Doppler echocardiography = 0.85. |
| Fellahi *et al* (2009) | 25 healthy subjects | Correlation coefficient of cardiac index (CO / body surface area) with reference to Doppler echocardiography = 0.36. |

angiography and who could exercise to a moderate symptom-limited Bruce protocol. ICG was recorded using four-band electrode configuration. They observed that the aortic valve opening in Doppler echocardiogram was closely associated with the onset of the rapid systolic rise of $-z(t)$. The characteristic points were detected and parameters were obtained after ensemble averaging over 32 cardiac cycles. Using ICG and Doppler echocardiography, locations of systolic events were measured, as time intervals with reference to the Q wave of ECG. The mean differences of aortic valve opening time, peak ejection velocity time, and aortic valve closure time were 20 ms, 25 ms, −21 ms, respectively. Regression coefficients for aortic valve opening time, peak ejection velocity time, aortic valve closure time, and peak aortic acceleration were 0.78, 0.86, 0.73, and 0.74 respectively.

Castor *et al* (1994) measured CO using impedance cardiography, Doppler echocardiography, and thermodilution, from 10 subjects with severe cardiovascular disorders, under the conditions of controlled ventilation, apnoea, and spontaneous breathing. Mean difference and standard deviation of differences of CO measurement using impedance cardiography and Doppler echocardiography with reference to thermodilution were calculated in three

conditions. The mean differences were –2.2% to 1.4% for impedance cardiography and –16% to –32% for Doppler echocardiography. The corresponding values of standard deviations of differences were 11% to 16% and 12% to 21%. They concluded that the measurement errors with impedance cardiography were less than those with Doppler echocardiography. van der Meer *et al* (1999) used impedance cardiography, with 8-spot electrode configuration, ensemble averaging over six cardiac cycles, and Sramek-Bernstein equation, for CO measurement on 26 patients (17 patients with no valvular disorders, 9 with mitral regurgitation), along with Doppler echocardiography as the reference technique. For all patients grouped together, the mean of differences was 0.20 L/min, the standard deviation of differences was 0.74 L/min, and the correlation coefficient was 0.85. The performance for the patients with valvular disorders was somewhat lower than that for those without valvular disorders.

Fellahi *et al* (2009) used impedance cardiography, with SV calculated using Sramek-Bernstein equation every cardiac cycle and averaged over 15 cycles, for the measurement of cardiac index (CO/body surface area) on 25 healthy subjects, along with Doppler echocardiography as the reference technique. The measurements were made under the conditions of (i) normal rest, (ii) positive end-expiratory pressure of 10 cm $H_2O$ by means of a continuous positive airway pressure ventilator, and (iii) 30 cm $H_2O$ positive pressure on the lower body applied by means of inflated medical anti-shock trousers. Doppler echocardiography showed a significant decrease in the values for the second condition with reference to the first condition and a significant increase in the values for the third condition. Impedance cardiography did not show such changes. The correlation coefficients were 0.36 (significant) for the three conditions taken together, 0.21 (not significant) for the second condition, and 0.22 (not significant) for the third condition, indicating that the impedance cardiography was not suited for monitoring of CO changes during hemodynamic load challenges.

## 2.7 Scope of Research

Impedance cardiography is a noninvasive and low-cost technique for monitoring of SV and several other cardiovascular indices. Studies on evaluation of the technique have often reported lack of repeatability in estimation and poor agreement between the estimated values and the measurements using the reference techniques. Therefore, impedance cardiography is still not considered as a replacement for the existing techniques for clinical diagnosis, continuous monitoring in intensive care unit, and for decision making in emergency

departments. Based on the review of earlier investigations, it emerges that further work in the following areas may be helpful for clinical application of this technique:

(i) Development of instrumentation for acquisition of ICG signal with low distortion, low ripple, and high SNR;

(ii) Establishing most suitable electrode configuration;

(iii) Developing signal processing techniques for suppression of respiratory and motion artifacts in order to avoid distortions associated with ensemble averaging and detection of characteristic points to enable study of beat-to-beat variability of parameters;

(iv) Developing a technique for estimating SV from ICG parameters with low bias and high precision, for signals acquired from a large number of subjects (subjects with normal health and patients with different cardiovascular disorders and with different weight, height, and age) under different physiological conditions.

Our research objective is to develop a technique for automatic beat-to-beat SV estimation using impedance cardiography. Most of the existing techniques use the ICG parameters along with a few patient-dependent parameters (blood resistivity, inter-electrode distance, patient height, weight, etc.). Disagreement between the estimation using impedance cardiography and the measurements using the reference techniques could be due to (i) errors in ICG parameters due to artifacts, smearing introduced by ensemble averaging, and errors in automatic detection of the characteristic points; (ii) inadequacies of the parameter set and the SV equations; and (iii) use of body-related measurements that are not related to the type of disorder. As validation using ensemble-averaged ICG and measurement across subjects cannot help in isolating these sources, we use beat-to-beat estimation over a large number of cardiac cycles. To address the inadequacies of the model-based techniques, use of artificial neural networks (ANN) for SV estimation is investigated, as this technique does not involve models of the thoracic impedance and the aortic blood flow profile. Doppler echocardiography is used as the reference technique as it is noninvasive and can be used for beat-to-beat SV measurements on healthy subjects and patients and it can be used simultaneously along with impedance cardiography.

For the purpose of developing a technique for automatic beat-to-beat SV estimation, two investigations are carried out: (i) development of a technique for improved detection of the ICG characteristic points as needed for SV estimation and (ii) use of artificial neural networks for SV estimation using Doppler echocardiography as the reference technique. For these investigations, a database of simultaneously acquired ICG related signals and Doppler echocardiograms is developed by recording the signals from subjects with normal health and subjects with cardiovascular disorders.

On the basis of examination of morphological variations of ICG signals, a time-domain technique for automatic beat-to-beat detection of ICG characteristic points is developed. It does not require estimation of the baseline and manual selection of the processing parameters. It retains information related to beat-to-beat variability in event latencies. The technique is validated on recordings from subjects with normal health under rest and in the post-exercise condition with an increase in the heart rate introduced by exercise and subjects with cardiovascular disorders under rest. The proposed technique is subsequently used for obtaining the ICG parameters for SV estimation.

Use of artificial neural network is investigated for automatic beat-to-beat SV estimation using the ICG parameters, without involving models of the thoracic impedance and the aortic blood flow profile. The network is trained using beat-to-beat datasets from the recordings from subjects with normal health under rest and in post-exercise condition and investigations are carried out for optimizing the network and the set of input parameters. The optimized network is subsequently evaluated on the recordings from both sets of subjects and the results are compared with those from the model-based techniques.

# Chapter 3
# DETECTION OF ICG CHARACTERISTIC POINTS

## 3.1 Introduction

Estimation of SV and several other cardiovascular indices from ICG requires error-free detection of the B, C, and X points. The ICG signal is often contaminated with components related to respiration and body movements, collectively known as artifacts (Miyamoto *et al* 1981, Qu *et al* 1986, Zhang *et al* 1986, Hurwitz *et al* 1990, Wang *et al* 1991, Raza *et al* 1992, Barrows *et al* 1995, Webster 1998, Yamamoto *et al* 1998, Ernst *et al* 1999, Riese *et al* 2003, Krivoshei *et al* 2008). These artifacts cause errors in detection of the characteristic points, particularly in the detection of the less prominent B and X points (Ono *et al* 2004, Shyu *et al* 2004, Rizzi *et al* 2009). Difficulties in detection of these points also occur due to significant morphological variations in the waveform, particularly in recordings from subjects with cardiovascular disorders.

A technique is proposed and investigated for automatic detection of B, C, and X points. It is a time-domain technique using multiple features and reference points obtained from ECG and it has been developed after an empirical examination of a large number of artifact-free and artifact-contaminated recordings. It does not require estimation of the baseline and selection of the processing parameters. It does not involve high-order derivatives and therefore is not significantly affected by noise in the input signal. Unlike the wavelet-based techniques, it can be used on short record lengths.

The second section provides a review of the signal processing techniques for detection of the B, C, and X points, followed by a description of the proposed technique. The material and method used for validation of the technique are described in the third section followed by the results and discussion in the subsequent sections.

## 3.2 Signal Processing

### *A. Detection of the B, C, and X Points*

A denoising technique is generally employed to suppress the artifacts before attempting detection of the characteristic points. As the spectra of the artifacts related to respiration (0.4 – 2 Hz) and body movements (0.1 – 10 Hz) overlap with that of ICG (0.8 – 20 Hz), it is difficult to suppress

the artifacts by filtering. Several signal processing techniques have been developed for artifact suppression. Ensemble averaging, coherent ensemble filtering, adaptive filtering, and wavelet-based techniques have been reported for suppressing the artifacts (Zhang *et al* 1986, Shyu *et al* 1988, Nagel *et al* 1989, Wang *et al* 1989, Hurwitz *et al* 1990, Kim *et al* 1992, Raza *et al* 1992, Ono *et al* 2004, Pandey and Pandey 2005, Pandey and Pandey 2007, Pandey and Pandey 2009, Rizzi *et al* 2009, Pandey *et al* 2011). Kim *et al* (1992) reported that an averaging technique can effectively suppress the respiratory artifacts in ICG. However, ensemble average suppresses the beat-to-beat information related to event latencies and variable shape of ICG signal during respiration (Raza *et al* 1992). To retain the beat-to-beat information, a wavelet-based denoising technique with scale-dependent thresholding for processing of the ICG signals has been developed by Pandey and Pandey (2007). It has been reported to provide SNR improvement of 23 dB in case of ICG signals contaminated with respiratory artifact.

Several techniques have been reported for detection of ICG characteristic points (Kubicek *et al* 1966, Kubicek *et al* 1970, Ono *et al* 2004, Shyu *et al* 2004, Rizzi *et al* 2009, Carvalho *et al* 2011). The highest peak in the ICG waveform in a cardiac cycle is taken as the C point. It is generally prominent and its detection is not significantly affected by the artifacts. The B and X points are much less distinct and their detection gets severely affected. The notch representing the B point in ICG waveform is often difficult to detect and it may be indistinct or disappear during exercise (Sherwood *et al* 1990, Ono *et al* 2004, Ermishkin *et al* 2014). The techniques used for artifact suppression often introduce some distortions in the waveform and therefore may degrade the detection of the less distinct characteristic points.

Some of the morphological variations in ICG are shown in Figure 3.1 from the recordings from subjects with normal-health under-rest and post-exercise conditions and subjects with cardiovascular disorders under-rest. The waveform of Figure 3.1(a), from a recording under-rest from a subject with normal-health, has a clear notch just before the upstroke preceding the C point. In the waveform in Figure 3.1(b), from a post-exercise recording from a subject with normal-health, the B point may be considered to be the nearly flat segment before the upstroke. The waveform of Figure 3.1(c), from another post-exercise recording, has no notch or flat segment and the B point may be considered to be the point of significant change in the slope of the upstroke preceding the C point.

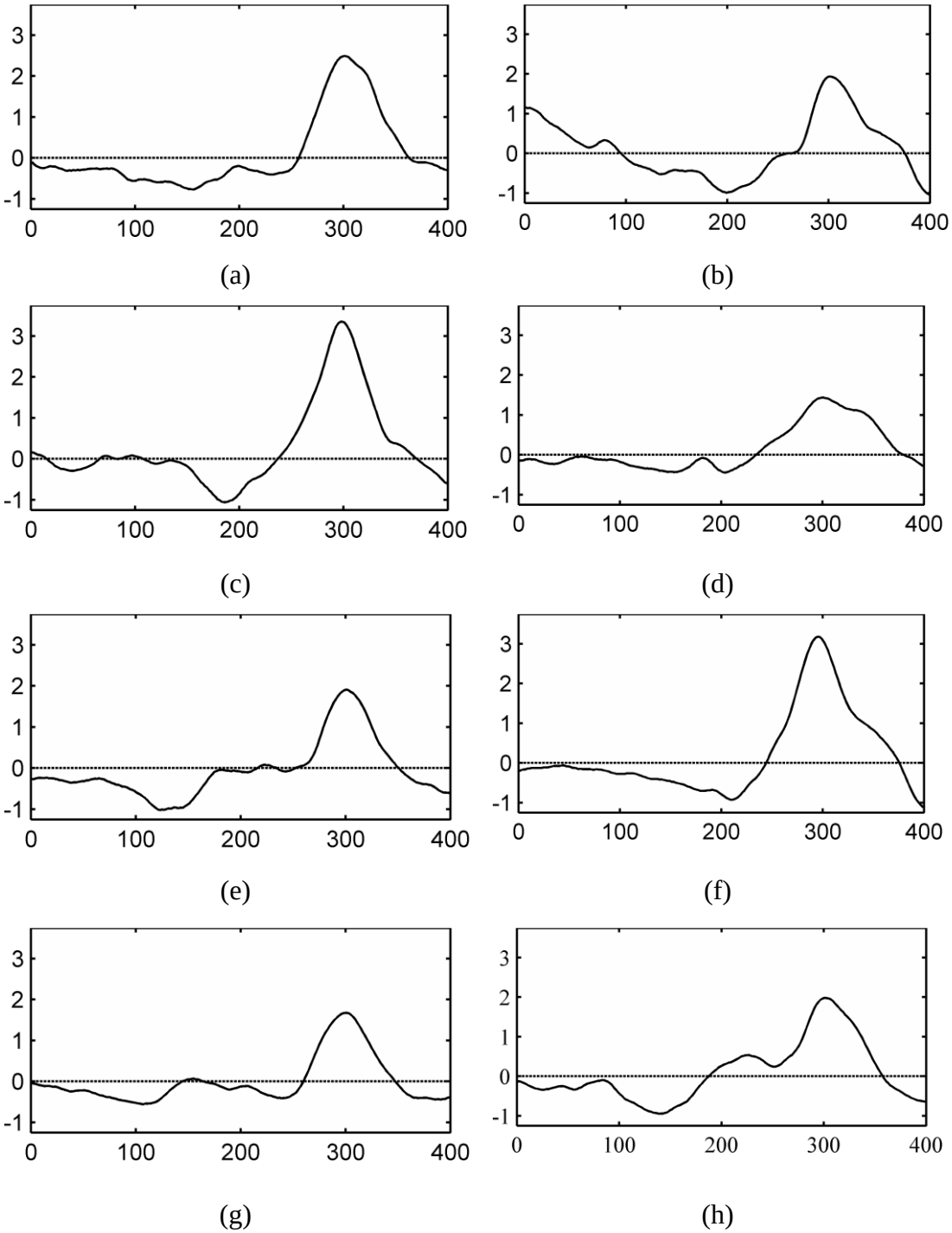


**Figure 3.1.** ICG waveform examples. X-axis: time in ms, Y-axis: ICG in Ω/s.

The waveforms of Figures 3.1(d)–(h) are from under-rest recording from different subjects with cardiovascular disorders. The waveforms of Figures 3.1(d) and 3.1(e) have two valleys preceding the C point and the second valley may be considered as the B point. The waveforms in Figures 3.1(f) and 3.1(g) have single rapid upstroke before the C point and the B point has to be located within it. The waveform of Figure 3.1(h) is very different from that of Figure 3.1(a), but it has the notch corresponding to the B point.

The morphological variations in ICG pose difficulties in detection of the B and X points. As a solution for these difficulties, several techniques have been proposed. In the 'zero crossing' technique of Kubicek *et al* (1966), the zero crossing before the C point is marked as the B point and the valley after the C point is marked as the X point. To avoid ambiguities in marking the zero crossing in the presence of noise and artifacts, Kubicek *et al* (1970) proposed the '15% from baseline' technique in which the point at 15% of the peak value from the baseline is marked as the B point. In the 'baseline-upstroke intersection' technique proposed by Ono *et al* (2004), the upstroke is approximated by a line joining the points on ICG segment at 40% and 80% of the peak value from the baseline. The point on ICG corresponding to the intersection of upstroke with baseline is marked as the B point. They reported that the technique improved the consistency in calculation of pre-ejection period (PEP) and $T_{\text{lvet}}$. This technique is reported to be prone to significant errors in presence of baseline wander (Pandey and Pandey 2005).

Shyu *et al* (2004) reported a wavelet-based technique for detection of the B and X points and its validation by simultaneous recording of ICG and pressure-volume (PV) loop. The technique uses 7-level decomposition of the ICG with quadratic spline wavelet. The minimum before the C point in the sixth level of decomposition is taken as the B point. The first zero crossing after the C point in the fourth level is taken as the X point. The technique proposed by Zhao *et al* (2005) uses 5-level decomposition of the ICG with bior3.3 wavelet. The minimum points preceding and following the C point in the fourth level of decomposition are marked as the B and X points respectively.

Carvalho *et al* (2011) reported a technique using first four derivatives of the ICG to detect the B and X points as being related to the opening and closing movements of aortic cusps in systolic and diastolic phases, respectively. In this technique, the peak before the notch preceding the C point is taken as the B point and the onset of the notch following the C point is taken as the X point. The 'baseline-upstroke intersection' technique of Ono *et al* (2004) is used to get an initial estimate of the B point. The presence of notch before the C point is checked by locating

sign change in the second derivative. If the notch is present, the first minimum in the third derivative occurring before the initial estimate is taken as the revised estimate, otherwise the first zero crossing in the first derivative occurring before the initial estimate is taken as the revised estimate. The lowest ICG point occurring in the 0.75 of R-T interval after the T-peak is taken as the initial estimation of the X point. Use of the revised B and X points resulted in lower mean absolute errors. But it also resulted in lower correlation coefficients, possibly due to random errors in detection caused by noise associated with calculation of the high-order derivatives. In the B-point detection technique reported by DeMarzo and Lang (1996), first difference of the ICG is scanned backwards starting from the C point and the point of inflection is taken as the B point. The onset of the upward slope reaching towards the peak of the Doppler echocardiogram is marked as the aortic valve opening (AVO).

Rizzi *et al* (2009) investigated the variable threshold dependent multi-scale wavelet-based technique for C point detection. Hu *et al* (2014) proposed a wavelet-based technique for detection of B, C, and X points in ICG, using quadratic spline wavelet for decomposition of ICG signal. The ICG cycles in different levels of decomposition are examined for maximum-minimum pairs preceding the zero crossing. The points corresponding to zero crossing, maximum, and minimum are taken as B, C, and X points respectively. In the B-point detection technique by Arbol *et al* (2017), the highest point of the third derivative occurring in the 300-ms segment preceding the C is taken as the B point. In the time-domain technique by Naidu *et al* (2011) for automatic detection of the B, C, and X points, the R peak of simultaneously recorded ECG is used as the reference for cycle identification. The C point is detected as the highest point within the ICG segment starting at the point corresponding to the R peak and of duration equal to one-fifth of the R-R interval. The first minimum preceding the C point is taken as the B point. The lowest point in the ICG segment starting at the C point and of duration equal to one-third of the C-C interval is taken as the X point. It was reported that the technique resulted in lower errors in estimation of the B-X time intervals.

The earlier techniques for detections of ICG characteristic points have been generally evaluated on different recordings and using different performance indicators.

### *B. Proposed Technique for Automatic Detection of ICG Points*

Based on an empirical examination of the application of the earlier techniques on ICG signals with significant morphological variations, the technique by Naidu *et al* (2011) was modified to develop

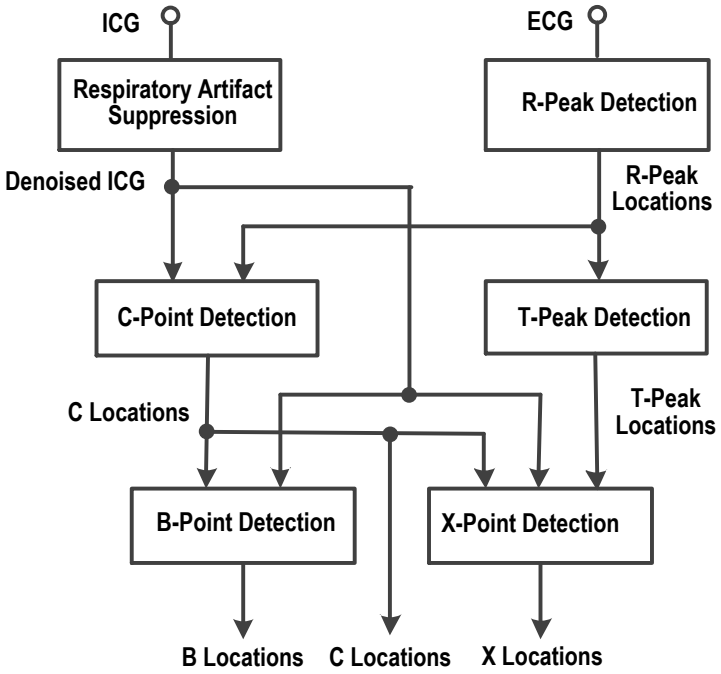


**Figure 3.2** Signal processing for detection of B, C, and X points in ICG.

a time-domain technique for automatic detection of B, C, and X points for use in beat-to-beat SV estimation. The technique uses simultaneously acquired ICG and ECG as inputs and its block diagram is shown in Figure 3.2. The ICG is denoised using a wavelet-based technique with scale-dependent thresholding (Pandey and Pandey 2007). The R-peaks in the ECG signal are located using Pan-Tompkins algorithm (Pan and Tompkins 1985) and these serve as reference points for cardiac cycle identification. In each cardiac cycle, the peak of the T wave is located as the peak of the ECG segment lying within 20% to 45% of the R-R interval.

The ICG segment starting at the point corresponding to the R peak and duration equal to 35% of the R-R interval is scanned and the highest point is marked as the C point. The ICG segment preceding the C point and of duration equal to one-fifth of the C-C interval is scanned and the point with the lowest value is marked as the valley point. The difference between the values at the C point and the valley point is calculated as the peak-to-valley height $H_{pv}$. The first difference of the ICG is scanned backwards starting from the point corresponding to $0.3H_{pv}$ below the C point to the point corresponding to the valley point, and the point with a change of sign is marked as the B point. If there is no sign change, the point $0.3H_{pv}$ above the valley point is marked as the

B point. The ICG segment starting at the point corresponding to the T peak in ECG and duration equal to one-third of the C-C interval is scanned and the lowest point is marked as the X point.

A qualitative visual examination of the automatically detected points in the recordings from six healthy subjects and four cardiac patients, consisting of a total of 447 cardiac cycles, showed that the proposed technique significantly reduced the errors in detection of the B and X points, as compared to the earlier technique (Naidu *et al* 2011). The technique was further evaluated, as described in the next section, on clinical recordings by comparing the automatically detected points with the visually marked ones and the corresponding points obtained using Doppler echocardiography as a reference technique.

## 3.3 Material and Method

### *A. Signal Recording*

The ICG, ECG, and Doppler echocardiogram signals were simultaneously recorded in a clinical setting from subjects with normal health and subjects with cardiovascular disorders. The same recordings were used for evaluation of characteristic point detection and SV estimation. Details of signal recording are given later in Section 4.2 of the next chapter.

For a subject with normal health, two recordings were carried out. The first recording was carried out with the subject having relaxed and rested. The second recording was carried out after the subject had undergone an exercise to significantly increase the heart rate. The first and second sets of recordings are referred to as ‘under-rest’ and ‘post-exercise’ recordings, respectively. For a subject with cardiovascular disorder, only the under-rest recording was carried out. The under-rest (UR) and post-exercise (PE) recordings from the 16 subjects with normal health (SNH) have 416 and 469 cardiac cycles, respectively and these are referred to as SNH-UR and SNH-PE. The under-rest recordings from the 14 subjects with cardiovascular disorders (SCD) have 632 cardiac cycles and these are referred to as SCD-UR.

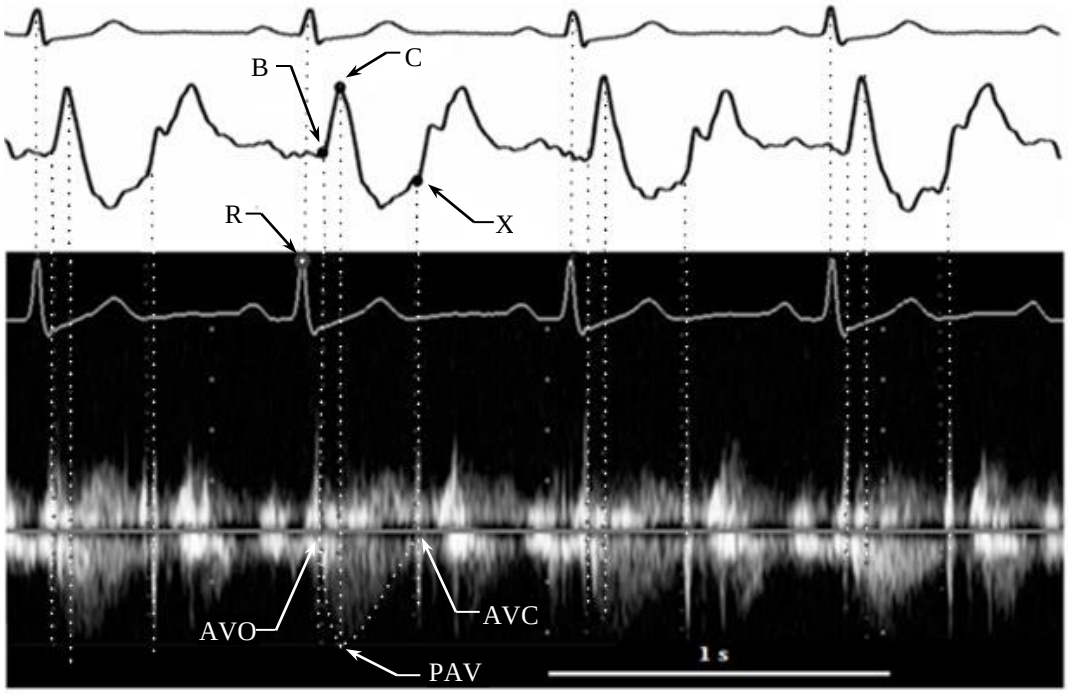


**Figure 3.3** Example of simultaneously recorded ICG and ECG with time-aligned Doppler echocardiogram showing the B, C, and X points of ICG along with the AVO, PAV, and AVC points of the Doppler echocardiogram from subject with normal health (SD) post-exercise. First trace (top): ECG from the ICG machine, second trace: ICG, third trace: ECG from the Doppler echocardiography machine, and fourth trace (bottom): blood velocity profile from the Doppler echocardiography machine. X-axis: time.

### *B. Evaluation Method*

The proposed technique for automatic detection of B and X points was applied on the recordings from (i) SNH-UR, (ii) SNH-PE, and (iii) SCD-UR as described in the previous section. Evaluation of the detection technique was carried out by comparing the automatically detected points with visually marked and the corresponding points obtained using Doppler echocardiography as a reference technique. For this purpose, the ICG signals and Doppler echocardiograms were time-aligned using the ECG waveforms simultaneously recorded by the two machines. An example of the simultaneously recorded ICG and ECG along with the time-aligned Doppler echocardiogram is shown in Figure 3.3.

For evaluation of the automatically detected points with reference to the visually marked points, the B, C, and X points were marked graphically by moving a cursor on the waveform and beat-to-beat recording of the positions of the points, without access to the automatically detected

ones. For evaluation with reference to the points observed using Doppler echocardiography, the corresponding points were graphically marked on the peak velocity profile in the Doppler echocardiogram time-aligned with the ICG. The B point was compared with the point of aortic valve opening (AVO) marked as the onset of the sharp rise of the velocity profile. The C point was compared with the peak of aortic velocity (PAV) profile. The X point was compared with the point of aortic valve closure (AVC) marked as the end of the velocity profile.

For evaluation of the detected points across cardiac cycles and across recordings, statistical analysis was applied on the intervals between the ECG-R peak and the detected points. The first set of evaluations involved comparison of R-B, R-C, and R-X intervals as obtained by automatic detection of the points with corresponding intervals as obtained by visual marking. For the second set of evaluations, the R-B, R-C, and R-X intervals obtained by automatic detection were compared with R-AVO, R-PAV, and R-AVC intervals obtained from time-aligned Doppler echocardiograms.

Comparisons were made by calculating the mean error as a bias indicator and standard deviation of errors as an imprecision indicator. As another performance indicator for B point detection, detection error was calculated by treating position errors exceeding 30 ms as failed detection. Agreement between the corresponding intervals was examined by calculating correlation coefficients and by using Bland-Altman plots of difference of the measurements versus mean of the measurements.

For comparing the results obtained using the proposed technique with the earlier techniques on the same set of recordings and same performance indicators, we implemented some of the earlier techniques. Two earlier techniques were implemented for B-point detection: (i) the ‘15% from baseline’ technique by Kubicek *et al* (1970) and (ii) the ‘baseline-upstroke intersection’ technique by Ono *et al* (2004) These techniques are subsequently referred to as the 'Kubicek' and 'Ono' techniques, respectively. The ‘minnimum after C peak’ technique by Kubicek *et al* (1966) was implemented for X-point detection and is subsequently referred to as the 'Kubicek' technique. The ICG signals in the recordings have significant respiratory artifacts. Therefore, processing for characteristic point detection was preceeded by artifact suppression using the wavelet-based denoising as used in the proposed technique.

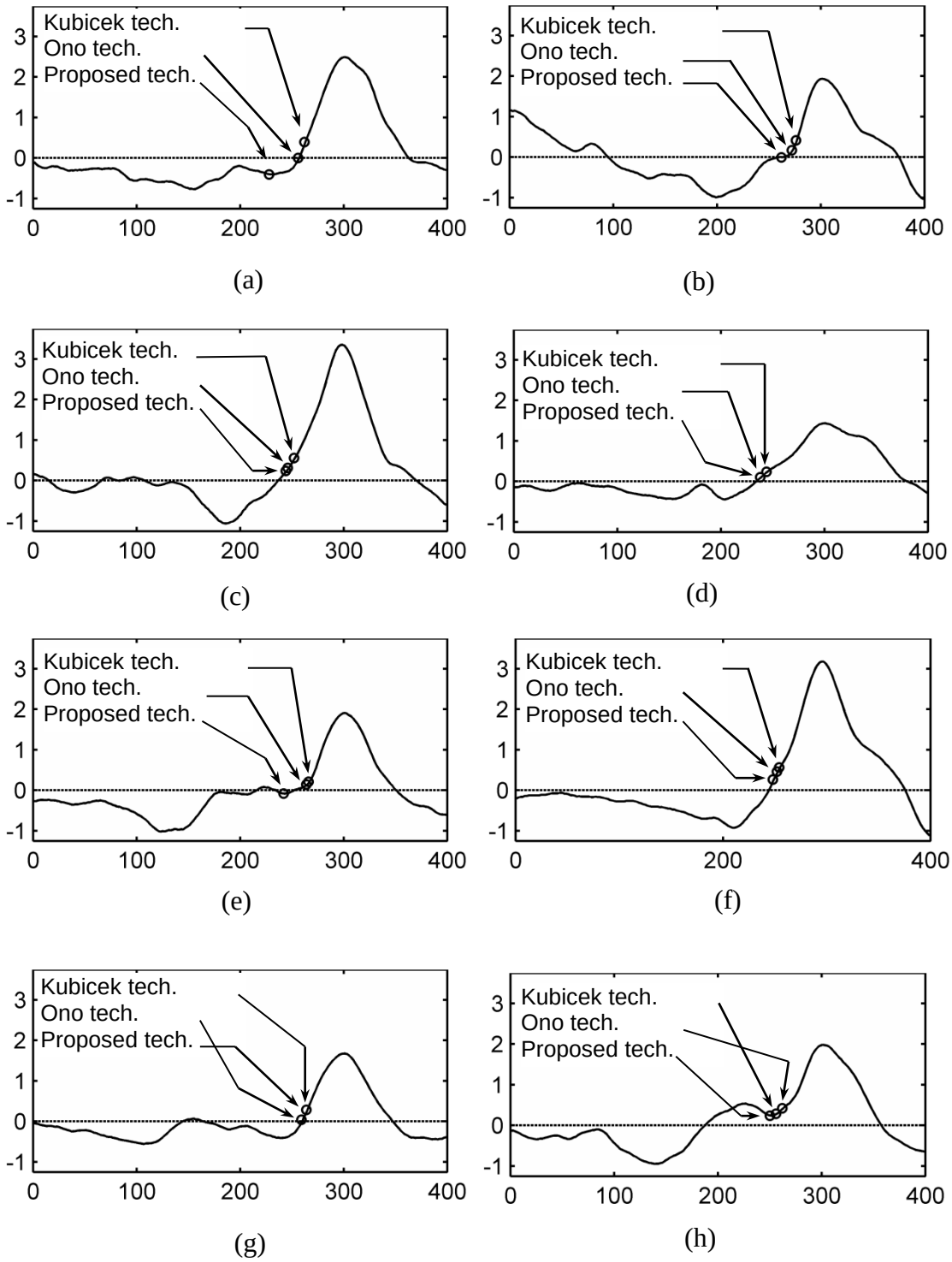


**Figure 3.4** Examples of the automatically detected B points in the ICG with different morphologies arround the B point.

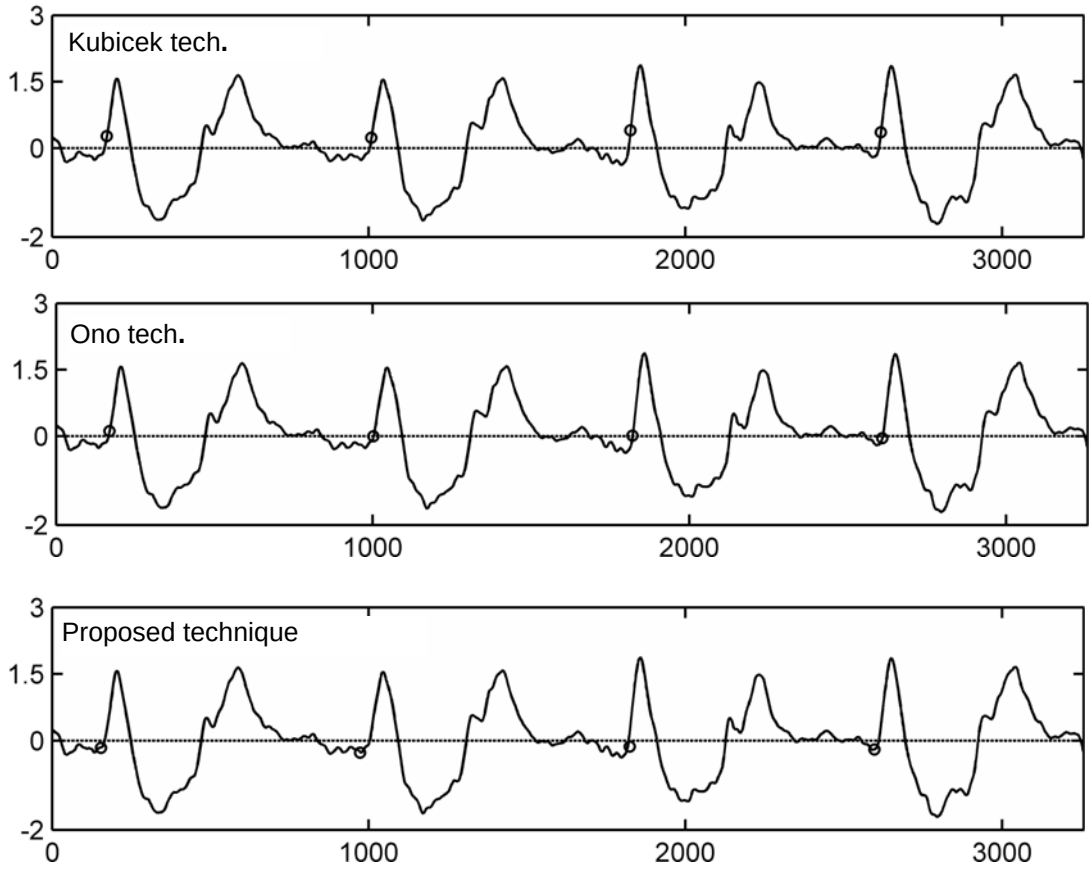


**Figure 3.5** Example of automatically detected B point in the ICG recording from a subject with normal health (SD) post-exercise. X-axis: time in ms, Y-axis: ICG in Ω/s.

The results of application of the proposed technique and the two earlier techniques for B-point detection on some of the waveforms with different morphologies around the B point (as shown earlier in Figure 3.1) are shown in Figure 3.4. An example of the application of the techniques on a waveform with multiple cycles is shown in Figure 3.5. An example of the application of the X point detection is shown in Figure 3.6.

## 3.4 Results

The recordings from both sets of subjects showed significant variation in heart rate as well as in the morphology of ICG waveforms. Evaluation of the automatic detection of the C, B, and X points was carried out by examining the agreement of automatically detected points with the visually marked ones. Further evaluation was carried out by comparing the beat-to-beat values of the R-C, R-B, and R-X intervals with the R-PAV, R-AVO, and R-AVC intervals, respectively.

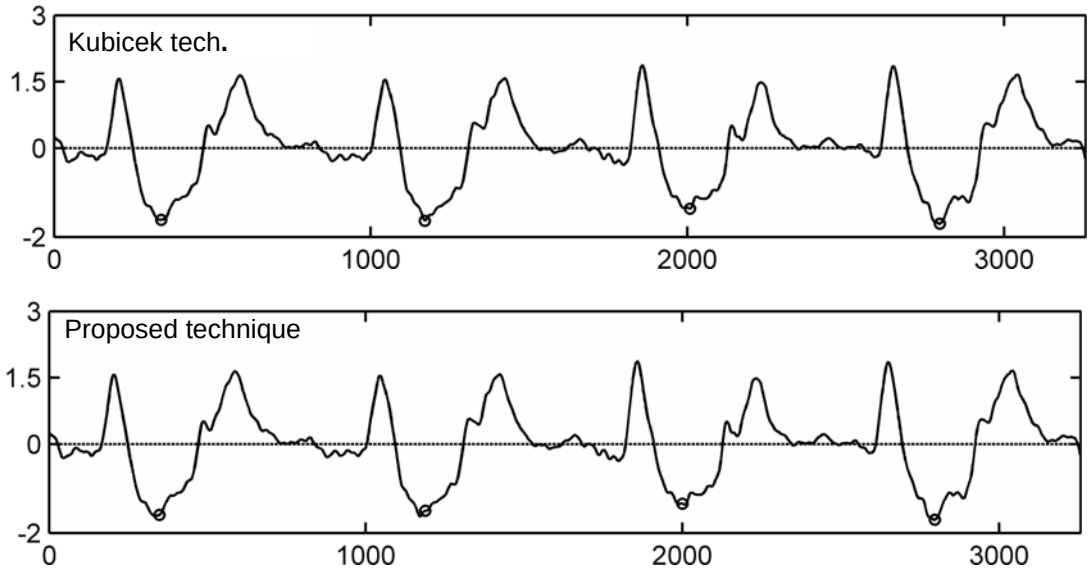


**Figure 3.6** Examples of automatically detected X points in the ICG recording from a subject with normal health (SD) post-exercise. X-axis: time in ms, Y-axis: ICG in Ω/s.

The automatically detected C points closely matched with the visually marked ones. Results of beat-to-beat comparison of the R-C intervals measured using automatic detection of C points with the R-PAV intervals measured using visual markings on the echocardiogram are summarized in Table 3.1. For the overall recordings, the mean and standard deviation (S.D.) of the R-PAV intervals were 94 and 22 ms, respectively. The values of correlation coefficients between the R-PAV and R-C intervals were 0.87, 0.85, 0.90, and 0.89 for the SNH-UR, SNH-PE, SCD-UR, and overall recordings, respectively. The mean differences between the R-PAV and R-C intervals were 4, 2, 6, and 8 ms for the SNH-UR, SNH-PE, SCD-UR, and overall recordings, respectively. The corresponding values of standard deviation of differences were 8, 10, 12, and 10 ms, which were less than 10% of the mean intervals.

**Table 3.1** Comparison of R-C intervals measured using ICG with R-PAV intervals measured using Doppler echocardiogram. $r$ = correlation coefficient, $\overline{\varepsilon}$ = mean of differences, and $\sigma_\varepsilon$ = standard deviation of differences.

| Measurement | | Signal recording (subject type, recording condition) | | | |
|---|---|---|---|---|---|
| | | SNH-UR | SNH-PE | SCD-UR | Overall |
| No. of cycles | | 416 | 469 | 632 | 1517 |
| R-R interval | Mean (ms) | 824 | 652 | 798 | 760 |
| | S.D. (ms) | 124 | 98 | 162 | 154 |
| R-PAV interval | Mean (ms) | 100 | 84 | 100 | 94 |
| | S.D. (ms) | 18 | 18 | 26 | 22 |
| R-C interval | Mean (ms) | 94 | 82 | 93 | 90 |
| | S.D. (ms) | 16 | 16 | 23 | 20 |
| | $r$ | 0.87 | 0.85 | 0.90 | 0.89 |
| | $\overline{\varepsilon}$ (ms) | 4 | 2 | 6 | 4 |
| | $\sigma_\varepsilon$ (ms) | 8 | 10 | 12 | 10 |

The positions of the automatically detected B points were compared with those of the visually marked points. Means of the differences in all cases were less than 1 ms, indicating no significant position bias. With the Kubicek technique, S.D. of differences for the SNH-UR, SNH-PE, SCD-UR, and overall recordings were 36, 28, 20, and 28 ms, respectively. The corresponding values were almost similar with the Ono technique. The corresponding values with the proposed technique were 22, 18, 18, and 20 ms, thus indicating a more precise detection. Considering a position difference beyond ± 30 ms as a failed detection, the percentage detection errors for overall recordings were 21% and 16%, with the Kubicek and Ono techniques, respectively. The corresponding error with the proposed technique was 8%.

The results of comparison of the beat-to-beat R-B intervals with the corresponding R-AVO intervals are summarized in Table 3.2. The mean and S.D. of the R-AVO intervals for the overall recordings were 38 and 12 ms, respectively. The correlation coefficients with the visual, Kubicek, Ono, and proposed techniques for overall recordings were 0.79, 0.25, 0.28, and 0.56, respectively. The mean differences with the visual, Kubicek, Ono, and proposed techniques for overall recordings were 2, –4, –2, and 2 ms, respectively. The corresponding S.D. of differences were 10, 26, 24, and 22 ms. Similar results were observed for the three sets of recordings. Therefore in

**Table 3.2** Comparison of R-B intervals measured using ICG with R-AVO intervals (AVO: aortic valve opening point) measured using Doppler echocardiogram. $r$ = correlation coefficient, $\overline{\varepsilon}$ = mean of differences, and $\sigma_\varepsilon$ = standard deviation of differences.

| Measurement | | | Signal recording (subject type, recording condition) | | | |
|---|---|---|---|---|---|---|
| | | | SNH-UR | SNH-PE | SCD-UR | Overall |
| No. of cycles | | | 416 | 469 | 632 | 1517 |
| R-AVO interval | Mean (ms) | | 40 | 34 | 38 | 38 |
| | S.D. (ms) | | 12 | 14 | 12 | 12 |
| R-B interval | Mean (ms) | Visual marking | 38 | 32 | 38 | 36 |
| | | Kubicek tech. | 36 | 36 | 50 | 42 |
| | | Ono tech. | 34 | 34 | 46 | 40 |
| | | Proposed tech. | 38 | 28 | 38 | 34 |
| | S.D. (ms) | Visual marking | 20 | 16 | 16 | 16 |
| | | Kubicek tech. | 30 | 24 | 22 | 26 |
| | | Ono tech. | 30 | 24 | 20 | 24 |
| | | Proposed tech. | 30 | 24 | 24 | 26 |
| | $r$ | Visual marking | 0.77 | 0.83 | 0.77 | 0.79 |
| | | Kubicek tech. | 0.00 | 0.22 | 0.55 | 0.25 |
| | | Ono tech. | 0.19 | 0.14 | 0.51 | 0.28 |
| | | Proposed tech. | 0.50 | 0.62 | 0.54 | 0.56 |
| | $\overline{\varepsilon}$ (ms) | Visual marking | 2 | 2 | 0 | 2 |
| | | Kubicek tech. | 6 | –2 | –12 | –4 |
| | | Ono tech. | 6 | 0 | –8 | –2 |
| | | Proposed tech. | 4 | 4 | 0 | 2 |
| | $\sigma_\varepsilon$ (ms) | Visual marking | 12 | 8 | 10 | 10 |
| | | Kubicek tech. | 32 | 24 | 18 | 26 |
| | | Ono tech. | 30 | 26 | 18 | 24 |
| | | Proposed tech. | 26 | 18 | 20 | 22 |

terms of agreement with the AVO points, the proposed technique performed better than the earlier ones. Similar results were obtained for the three sets of recordings separately.

The results of beat-to-beat comparison of R-X and R-AVC intervals are summarized in Table 3.3. The mean and standard deviation of the R-AVC intervals for the overall recordings were 322 and 42 ms, respectively. The correlation coefficients with the Kubicek and proposed techniques for overall recordings were 0.71 and 0.64, respectively. The mean differences with the Kubicek and proposed techniques for overall recordings were 58 and 26 ms, respectively. The

**Table 3.3** Comparison of R-X intervals measured using ICG with R-AVC intervals measured using Doppler echocardiogram. $r$ = correlation coefficient, $\overline{\varepsilon}$ = mean of differences, and $\sigma_\varepsilon$ = standard deviation of differences.

| Measurement | | | Signal recording (subject type, recording condition) | | | |
|---|---|---|---|---|---|---|
| | | | SNH-UR | SNH-PE | SCD-UR | Overall |
| No. of cycles | | | 416 | 469 | 632 | 1517 |
| R-AVC intervl | Mean (ms) | | 332 | 288 | 340 | 322 |
| | S.D. (ms) | | 30 | 36 | 38 | 42 |
| R-X interval | Mean (ms) | Kubicek tech. | 258 | 224 | 294 | 262 |
| | | Proposed tech. | 290 | 264 | 322 | 296 |
| | S.D. (ms) | Kubicek tech. | 60 | 56 | 75 | 72 |
| | | Proposed tech. | 56 | 44 | 68 | 64 |
| | $r$ | Kubicek tech. | 0.57 | 0.67 | 0.70 | 0.71 |
| | | Proposed tech. | 0.60 | 0.44 | 0.65 | 0.64 |
| | $\overline{\varepsilon}$ (ms) | Kubicek tech. | 74 | 64 | 44 | 58 |
| | | Proposed tech. | 42 | 24 | 16 | 26 |
| | $\sigma_\varepsilon$ (ms) | Kubicek tech. | 48 | 42 | 56 | 52 |
| | | Proposed tech. | 46 | 42 | 52 | 48 |

corresponding S.D. of differences were 52 and 48 ms. Thus in comparison to the Kubicek technique, the proposed technique significantly reduced the bias and also improved the precision.

For examining the suitability of the proposed technique for measurement of the left-ventricular ejection time, beat-to-beat comparison of the B-X and AVO-AVC intervals was carried out. The results are summarized in Table 3.4 for the proposed technique and the Kubicek technique. The mean and standard deviation of the AVO-AVC intervals for the overall recordings were 284 and 36 ms, respectively. The correlation coefficients with the Kubicek and proposed techniques for overall recordings were 0.56 and 0.50, respectively. The mean differences with the Kubicek and proposed techniques for overall recordings were 64 and 24 ms, respectively. The corresponding S.D. of differences were 58 and 54 ms. Thus in comparison to the Kubicek technique, the proposed technique significantly reduced the bias and slightly improved the precision of the beat-to-beat measurements.

**Table 3.4** Comparison of B-X intervals measured using ICG with AVO-AVC intervals measured using Doppler echocardiogram. $r$ = correlation coefficient, $\overline{\varepsilon}$ = mean of differences, and $\sigma_\varepsilon$ = standard deviation of differences.

| Measurement | | | Signal recording (subject type, recording condition) | | | |
|---|---|---|---|---|---|---|
| | | | SNH-UR | SNH-PE | SCD-UR | Overall |
| No. of cycles | | | 416 | 469 | 632 | 1517 |
| AVO-AVC interval | Mean (ms) | | 290 | 254 | 302 | 284 |
| | S.D. (ms) | | 26 | 33 | 32 | 36 |
| B-X interval | Mean (ms) | Kubicek tech. | 222 | 188 | 246 | 222 |
| | | Proposed tech. | 252 | 234 | 286 | 260 |
| | S.D. (ms) | Kubicek tech. | 64 | 50 | 70 | 70 |
| | | Proposed tech. | 56 | 50 | 62 | 62 |
| | $r$ | Kubicek tech. | 0.30 | 0.50 | 0.55 | 0.56 |
| | | Proposed tech. | 0.40 | 0.39 | 0.46 | 0.50 |
| | $\overline{\varepsilon}$ (ms) | Kubicek tech. | 68 | 68 | 56 | 64 |
| | | Proposed tech. | 38 | 20 | 16 | 24 |
| | $\sigma_\varepsilon$ (ms) | Kubicek tech. | 62 | 50 | 60 | 58 |
| | | Proposed tech. | 52 | 48 | 56 | 54 |

## 3.5 Discussion

The B, C, and X points in the ICG waveform are considered to be related to the aortic valve opening, peak of the aortic velocity, and aortic valve closure, respectively. These points need to be detected in an error-free manner for obtaining the ICG parameters for SV estimation. While the C point is generally prominent, the B and X points are much less distinct and their detection gets severely affected by artifacts and due to morphological variations in the waveform. The techniques for detection of these points are based on saliencies in the waveform, features based on higher-order derivatives, and features obtained by wavelet decomposition. These techniques often result in non-constant bias and random errors. The techniques using saliencies in the waveform show large errors or lack of detection in the cardiac cycles having significant deviations from the defined features or significant baseline wander. The techniques based on features derived from higher-order derivatives lead to significant random errors due to noise associated with these derivatives.

The techniques based on wavelet decomposition may result in inter-cycle smearing and cause errors during significant cardiac variability.

Based on an empirical examination of the morphological variations in the ICG waveforms, a time-domain technique for automatic detection of B, C, and X points for use in beat-to-beat SV estimation has been developed and evaluated. The proposed technique uses simultaneously acquired ECG and ICG data as inputs. It uses R and T peaks of ECG as reference points and multiple time-domain features to reduce errors due to morphological variations. Detection is carried out on a beat-to-beat basis after marking of the ICG cycles with reference to the R peaks and hence the technique avoids inter-cycle smearing. It does not require estimation of the baseline and selection of the processing parameters. As high-order derivatives are not used, the detection is not significantly affected by the presence of a moderate level of noise in the input signal. A wavelet-based denoising is employed for suppression of respiratory artifacts in ICG and the technique can be used without any restriction on breathing.

The proposed technique was evaluated on the ICG-echocardiography database comprising simultaneously acquired and time-aligned ICG, ECG, and Doppler echocardiogram recordings. The evaluation was carried out on data with 1517 cardiac cycles, consisting of 416 cardiac cycles recorded under the resting condition and 469 cycles in the post-exercise condition from 16 subjects with normal health and 632 cardiac cycles recorded from 14 subjects with cardiovascular disorders under resting condition. The data exhibited large heart rate and morphological variations. The mean R-R intervals for the three sets of recordings were 824, 652, and 798 ms and the corresponding standard deviations were 124, 98, and 162 ms. The corresponding values for the three sets of recordings pooled together were 760 ms and 154 ms. The performance of the technique was evaluated with reference to the visually marked points in the ICG waveform and with reference to the intervals measured using echocardiography.

Despite large heart rate and morphological variations in the data, there were no significant differences in the performance of the proposed technique across the three sets of recordings. Therefore, the performance can be discussed by examining the results for the cardiac cycles from the three sets of recordings pooled together. The C points detected by the proposed technique closely matched with the visually marked ones in all cycles. The beat-to-beat comparison of R-C intervals with the corresponding intervals measured using echocardiography showed mean difference and standard deviation of differences as 4 ms and 10 ms, respectively. For the B-point detection, the mean difference and standard deviation of differences with reference to the visually

marked points were 1 ms and 20 ms, respectively. Considering a position difference beyond ± 30 ms as a failed detection, the detection error was 8%. The mean difference and standard deviation of differences for beat-to-beat comparison of R-B intervals with the corresponding intervals measured using Doppler echocardiograms were 2 ms and 22 ms, respectively. The beat-to-beat comparison of R-X intervals with reference to the corresponding intervals measured from echocardiography showed the mean difference and the standard deviation of differences as 26 ms and 48 ms, respectively. In terms of bias and precision, the proposed technique performed better than the established techniques reported earlier. The bias-related errors (means of differences), as referred to the mean R-R interval, in the estimation of R-C, R-B, and R-X intervals with the corresponding measurements using echocardiography as the reference were 0.5%, 0.3%, and 3.4%, respectively. The corresponding precision related errors (standard deviations of differences) were 1.3%, 2.9%, and 6.3%. The bias and precision related errors for estimation of the B-X interval as a measure of the left ventricular ejection time were 3.2% and 7.1%, respectively.

The improved performance of the proposed technique in comparison to earlier techniques may be attributed to the use of artifact suppression, use of R and T peaks as reference points for marking ICG segments for locating the features, and use of multiple time-domain features for resolving ambiguities caused by morphological variations. The results of objective evaluation of the proposed technique, in terms of bias and precision in the estimation of R-C, R-B, R-X, and B-X intervals with the corresponding measurements using echocardiography as the reference, shows its usefulness for obtaining ICG parameters for automatic beat-to-beat SV estimation.

# Chapter 4
# SV ESTIMATION USING ARTIFICIAL NEURAL NETWORK

## 4.1 Introduction

The SV estimation methods using impedance cardiography are generally based on models of the thoracic impedance and the aortic blood flow profile. The results obtained do not show a good agreement with the established techniques like thermodilution and other invasive techniques or with the noninvasive technique of Doppler echocardiography. Considering the difficulties in developing models with adequate physiological justification, some researchers have proposed the use of artificial neural network (ANN) for SV estimation, assuming that the nonlinear relationship between SV and the ICG-related and other input parameters can be captured during the training of the network.

Mulavara *et al* (1998) reported an ANN-based method for SV estimation from ICG with Doppler echocardiography as the reference technique. They used a three-layer feed-forward neural network trained using error back-propagation algorithm. The study was conducted on recordings from 20 subjects with normal health, acquired in three supine body positions (horizontal, $10^{o}$ head down, and $30^{o}$ head up), during six 5-s breath-hold durations separated by 15-s normal breathing over a period of two minutes. The ICG recording from each breath-hold duration was ensemble averaged and used to get the values of ICG peak and left ventricular ejection time. These values along with average heart rate over the breath-hold duration, inter-electrode distance, basal impedance, volume of electrically participating thoracic tissues (calculated from height and weight) formed the set of inputs and the SV value measured from Doppler echocardiogram served as the target value. RMS error and maximum iteration count were used as the stopping criteria during training. The neurons in the hidden layer used hyperbolic tangent activation function and the optimal number of neurons was empirically determined. Half of the total 360 datasets (20 subjects, 3 positions, 6 recordings) were randomly selected for training and the other half of the datasets were used for testing. Eight networks with different combination of inputs as used in the Kubicek and the Sramek equations were evaluated and the network with the superset of the inputs as used in the two equations provided the best performance. Coefficients of determination for estimations using the Kubicek equation, the Sramek equation, and the ANN with the superset of inputs were 8.2%, 9.9%, and 77.4%, respectively, indicating the ANN-based approach to be better suited for SV estimation than the approaches based on biophysical modeling.

Baura (2001) in a patent has described an ANN-based technique for noninvasive cardiac output monitoring using ICG parameters with thermodilution as the reference technique. The method uses a three-layer feed-forward network, with three neurons in the hidden-layer and hyperbolic tangent activation function, trained using error back-propagation algorithm. The inputs to the network comprise the heart rate, basal impedance, ICG peak, left ventricular ejection time, inter-electrode distance, and the CO value as calculated by Kubicek equation. The training requires CO measurement on a large number of patients using thermodilution and the corresponding ICG parameters.

The earlier investigations on SV estimation used input parameters obtained from ensemble-averaged ICG and across-the-subjects training and testing. We propose to use an ANN for SV estimation, with ICG parameters from a large number of cycles without ensemble averaging as the inputs and the corresponding beat-to-beat SV values from Doppler echocardiography as the reference.

The second section presents the material and method for signal recording, parameter extraction, and ANN model implementation, optimization, and testing. The results are presented in the third section, followed by the discussion in the last section. An overview of SV estimation using Doppler echocardiography (Quinones *et al* 2002, Oh *et al* 2006) is provided in Appendix A.

## 4.2 Material and Method

The ANN-based technique for beat-to-beat estimation of stroke volume was applied and tested on signals recorded from a set of subjects with normal health and those with cardiovascular disorders. The following subsections describe the signal recording, parameter extraction, and ANN model implementation, optimization, and testing.

### *A. Signal Recording*

The ANN model is trained using the beat-to-beat values of SV estimated from Doppler echocardiography as the target values. Detection of ICG characteristic points for estimation of ICG parameters uses R and T peaks of simultaneously recorded ECG. For this purpose, the ICG, ECG, and Doppler echocardiogram signals were simultaneously recorded in a clinical setting from a number of subjects under rest and in post-exercise condition.

The signals were recorded in a clinical setting at Hardas Heart Care (Pune, Maharashtra, India), after approval of the protocol by the Ethics Committee of the hospital. The subjects for participating in the study were recruited from among the persons visiting the hospital for health check-up, diagnosis, or post-operative treatment, without efforts for gender

and age balancing. They were informed about the study and they read and signed the consent if willing to participate in it. There was no monetary cost or benefit for participation.

The subjects with normal health had no known history of cardiovascular disorders and were screened by a cardiologist on the basis of physical examination and ECG report. The subjects with cardiovascular disorders were the patients undergoing post-operative treatment or with past history of cardiovascular disorders. They were screened for suitability to participate in the study by the concerned cardiologist. The gender, age, height, and weight of the subjects were noted. The group of subjects with normal health comprised seventeen males and one female with age of 26 – 65 years (mean = 46.3 years, S.D. = 10.7 years), height of 1.54 – 1.80 m (mean = 1.69 m, S.D. = 0.06 m), and weight of 61 – 100 kg (mean = 76.2 kg, S.D. = 10.0 kg). The group of subjects with cardiovascular disorders had nineteen males and three females with age of 24 – 78 years (mean = 51.5 years, S.D. = 15.8 years), height of 1.43 – 1.76 m (mean = 1.66 m, S.D. = 0.08 m), and weight of 52 – 97 kg (mean = 71.6 kg, S.D. = 11.7 kg). The recordings were carried out during the period extending from June 2014 to June 2015.

The ICG related signals were recorded using 'HIC-2000 Impedance Cardiograph' from Bio-Impedance Technology (Chapel Hill, NC, USA). The impedance sensing was carried out using four-electrode configuration with Ag-AgCl disposable ECG spot electrodes. The outer two electrodes were used for injecting the excitation current and the resulting voltage was picked-up across the inner two electrodes. The upper current electrode was placed above the suprasternal notch on the front of the neck, with the lower one placed below the xiphoid process on the left lateral side of the thorax. The upper voltage electrode was placed at the base of the neck below the upper current electrode and the lower voltage electrode was placed at the level of xiphoid process on the left lateral side of the thorax above the lower current electrode. The placement of ICG electrodes is shown in Figure 4.1. The instrument used 1 mA excitation current of 100 kHz and provided analog output signals corresponding to basal impedance ($Z_0$), deviation from basal impedance $(-z(t))$, and ICG ($-dz/dt$) with the sensitivities of 40 mV/$\Omega$, 0.5 V/$\Omega$, and 400 mV/$(\Omega \cdot s^{-1})$, respectively. It also provided analog ECG signal as sensed using the voltage electrodes. The output signals from the ICG instrument were acquired using the 8-channel, 12-bit signal acquisition module 'KUSB-3102' from Keithley Instruments (Cleveland, Ohio, USA) and connected through USB to a battery-powered Notebook PC. The sampling frequency was set at 500 Hz. The distance between the voltage sensing electrodes was noted.

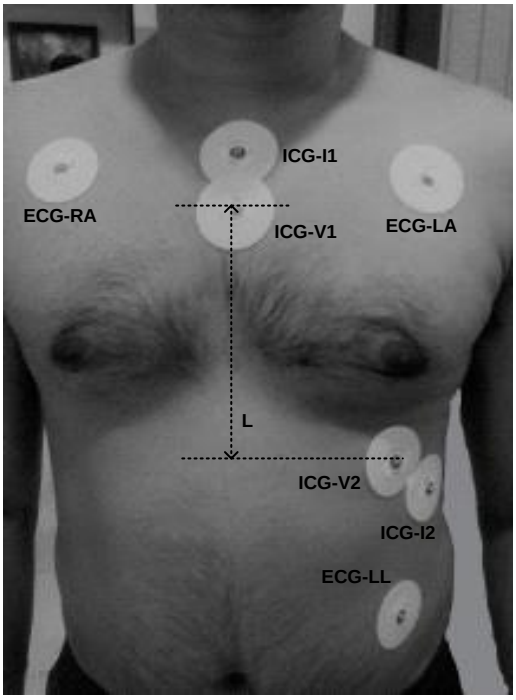


**Figure 4.1** Placement of electrodes on the chest: four electrodes of the ICG machine (current injection electrodes ICG-I1 and ICG-I2; voltage sensing electrodes ICG-V1 and ICG-V2) and three ECG electrodes of the echocardiogram machine.

The echocardiography recordings were carried out using 'iE33 echocardiography system' from Philips Ultrasound (Bothell, Wash., USA) with a 5 MHz phased-array probe placed on the chest after applying an ultrasound gel for good contact with the skin. The aortic blood flow velocity profile was recorded using apical five-chamber view of the ascending aorta. The aortic diameter was measured using parasternal long-axis view at the level of the aortic annulus during mid-systole. The velocity-time integral (VTI) was estimated as the area between the envelope of the Doppler spectrum and its baseline with the help of the built-in software of the echocardiography machine by tracing the spectral envelope with its track ball. As described later in Appendix A (Section A.3), the inter-operator variability of VTI measurement was observed to be less than 7% of the mean values. The machine has a facility for three-electrode ECG recording and this facility was used, with electrode placement as shown earlier in Figure 4.1, for time-aligned display of ICG and Doppler echocardiogram waveforms. As the recordings of ICG and Doppler echocardiogram waveforms employed independent time bases, the cardiac cycles of the two recordings were synchronized by alignment of the corresponding ECG-R peaks. An example of the simultaneously recorded ICG and ECG along with the time-aligned Doppler echocardiogram is shown in Figure 4.2.

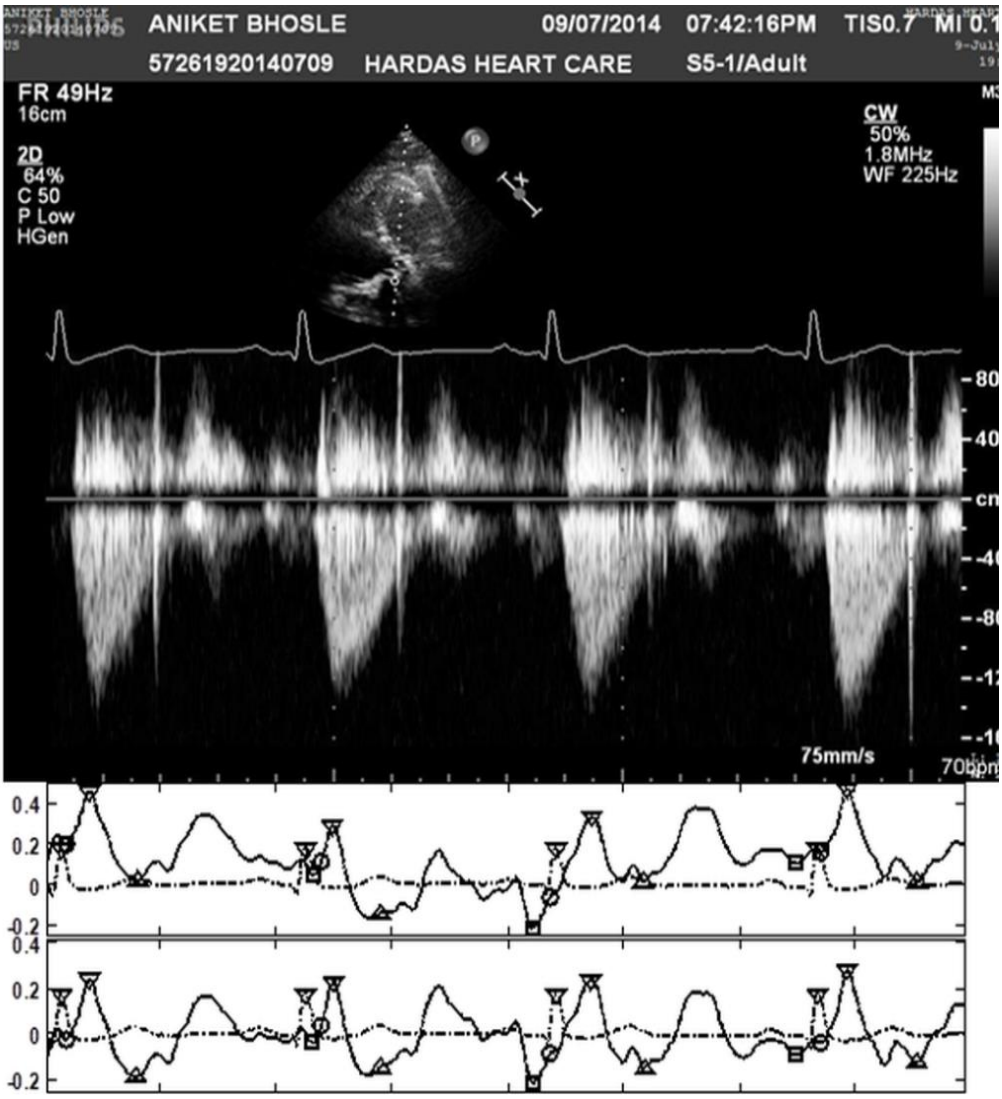


**Figure 4.2** Simultaneously recorded ICG and ECG with time-aligned Doppler echocardiogram frame. Upper trace is the blood velocity profile at aortic annulus with ECG recorded as recorded by the Doppler echocardiograph. The middle trace shows the unprocessed ICG and simultaneously acquired ECG by the impedance cardiograph. The lower trace shows the denoised ICG along with ECG. ICG: marked with the detected B, C, and X points. ECG: marked with R-peaks.

For a subject with normal health, two recordings were carried out. The first recording was carried out with the subject having relaxed and rested. The ICG electrodes and echocardiography probe were placed as described earlier and the ICG and Doppler echocardiogram signals were simultaneously recorded, with the subject lying in the left-lateral position with a slight folding of the right leg. For the second recording, the subject underwent an exercise to increase the heart rate. The exercise was carried out, following the first four stages of the Bruce exercise protocol (Bruce *et al* 1949), for about ten minutes on

the 'GE T-2100' treadmill from GE Healthcare (Wauwatosa, Wis., USA) attached with 'Smart Biphasic' defibrillator from Philips Healthcare (Andover, Mass., USA). The recording was carried out soon after cessation of the exercise and in the same way as the first recording. The subject was advised to avoid any movements during both the recordings in order to minimize the motion artifacts, but no restrictions were placed on breathing. The first and second sets of recordings are referred to as 'under-rest' and 'post-exercise' recordings. For a subject with cardiovascular disorder, only the under-rest recording was carried out. A summary of information on subjects with normal health and subjects with cardiovascular disorders along with the corresponding values of aortic annulus diameter, R-R interval of ECG, and stroke volume estimated using Doppler echocardiography are given in Table 4.1 and Table 4.2, respectively. The recordings have been organized as a database for ICG related research as described in Appendix C. The under-rest (UR) and post-exercise (PE) recordings from the 18 subjects with normal health (SNH) have 630 and 625 cardiac cycles, respectively and these are referred to as SNH-UR and SNH-PE. These cycles pooled together result in 1255 cardiac cycles and are referred to as SNH-UR+PE. The under-rest recordings from the 22 subjects with cardiovascular disorders (SCD) have 842 cardiac cycles and these are referred to as SCD-UR.

*B. Extraction of Parameters*

SV estimation uses three parameters obtained from impedance cardiography: the basal impedance $Z_0$, the ICG peak $(-dz/dt)_{\max}$, and the left ventricular ejection time $T_{\text{lvet}}$. Extraction of $(-dz/dt)_{\max}$ and $T_{\text{lvet}}$ requires detection of the B, C, and X points in the ICG waveform. The automatic beat-to-beat detection of these points was carried out using the technique presented in Chapter 3 (Naidu *et al* 2014), with the simultaneously recorded ICG and ECG waveforms as the inputs. The technique provides automatic marking of the R peak of ECG and the B, C, and X points of ICG in each cardiac cycle. From these markings, the time interval from the B point to the X point in a cardiac cycle was taken as $T_{\text{lvet}}$ and the height of the C point from the B point was taken as $(-dz/dt)_{\max}$. These values along with subject data are used as the inputs for SV estimation. The reference SV values are calculated as the product of VTI obtained from time-aligned Doppler echocardiogram and the cross-sectional area calculated from the measurement of aortic diameter at the annulus assuming circular cross-section, as described earlier as part of signal recording.

**Table 4.1** Information on subjects with normal health (SNH): age, aortic annulus diameter (Ao), recording condition (UR: under rest, PE: post-exercise), number of cardiac cycles, mean and S.D. of R-R intervals (RR), and mean and S.D. of stroke volume (SV) estimated using Doppler echocardiography.

| Subject | Age (year) | Ao (cm) | Condi-tion | No. of cycles | RR (ms) | | SV (mL) | |
|---|---|---|---|---|---|---|---|---|
| | | | | | Mean | S.D. | Mean | S.D. |
| SNH-AG | 44 | 2.15 | UR | 22 | 758 | 10.7 | 93.0 | 4.5 |
| | | | PE | 45 | 554 | 6.1 | 101.5 | 6.5 |
| SNH-BS | 50 | 2.10 | UR | 31 | 901 | 27.7 | 96.6 | 5.4 |
| | | | PE | 59 | 750 | 16.7 | 110.4 | 10.3 |
| SNH-GS | 26 | 2.36 | UR | 24 | 931 | 25.3 | 84.3 | 5.6 |
| | | | PE | 19 | 737 | 42.4 | 93.2 | 9.2 |
| SNH-KS | 47 | 2.06 | UR | 22 | 637 | 8.1 | 81.9 | 8.2 |
| | | | PE | 18 | 506 | 16.7 | 84.3 | 5.9 |
| SNH-MN | 32 | 1.62 | UR | 64 | 738 | 19.5 | 51.8 | 5.6 |
| | | | PE | 35 | 511 | 6.7 | 60.2 | 5.2 |
| SNH-MS | 58 | 1.86 | UR | 44 | 739 | 9.3 | 79.7 | 8.6 |
| | | | PE | 33 | 504 | 6.9 | 71.6 | 5.0 |
| SNH-NC | 58 | 2.12 | UR | 49 | 782 | 7.6 | 90.0 | 4.5 |
| | | | PE | 25 | 531 | 6.1 | 131.0 | 7.9 |
| SNH-NL | 60 | 2.13 | UR | 32 | 776 | 17.3 | 72.7 | 5.6 |
| | | | PE | 30 | 582 | 12.6 | 84.1 | 7.6 |
| SNH-RM | 37 | 2.10 | UR | 23 | 759 | 28.3 | 85.9 | 3.6 |
| | | | PE | 36 | 636 | 12.3 | 91.1 | 8.0 |
| SNH-SA | 50 | 1.98 | UR | 47 | 802 | 15.8 | 85.4 | 4.5 |
| | | | PE | 61 | 603 | 9.4 | 112.0 | 5.1 |
| SNH-SD | 42 | 1.90 | UR | 21 | 963 | 38.9 | 75.0 | 3.9 |
| | | | PE | 22 | 788 | 25.9 | 75.1 | 5.0 |
| SNH-SG | 39 | 2.30 | UR | 31 | 744 | 33.8 | 89.3 | 8.8 |
| | | | PE | 50 | 520 | 14.6 | 91.5 | 11.0 |
| SNH-SK | 60 | 2.29 | UR | 37 | 1011 | 52.7 | 96.4 | 7.7 |
| | | | PE | 31 | 743 | 21.9 | 104.0 | 6.7 |
| SNH-SM | 48 | 2.00 | UR | 15 | 769 | 26.9 | 68.8 | 3.8 |
| | | | PE | 40 | 586 | 12.9 | 81.0 | 3.7 |
| SNH-SP | 44 | 2.30 | UR | 25 | 650 | 9.1 | 94.7 | 5.6 |
| | | | PE | 26 | 553 | 6.8 | 97.3 | 5.7 |
| SNH-SZ | 65 | 2.34 | UR | 36 | 969 | 22.6 | 108.2 | 7.4 |
| | | | PE | 18 | 838 | 29.3 | 108.4 | 5.1 |
| SNH-VK | 35 | 2.02 | UR | 46 | 891 | 32.5 | 71.6 | 4.8 |
| | | | PE | 57 | 690 | 17.9 | 73.2 | 5.2 |
| SNH-ZP | 43 | 2.05 | UR | 57 | 830 | 39.7 | 72.8 | 3.5 |
| | | | PE | 24 | 628 | 20.1 | 82.7 | 4.3 |
| Across18 subjects | Mean = 46.3, S.D. = 10.7 | Mean = 2.09, S.D. = 0.19 | UR | 630 | 811 | 102.6 | 82.2 | 17.6 |
| | | | PE | 625 | 625 | 93.8 | 90.5 | 20.0 |
| | | | UR+PE | 1255 | 718 | 136.5 | 86.3 | 18.8 |

**Table 4.2** Information on subjects with cardiovascular disorders (SCD): age, aortic annulus diameter (Ao), recording condition (UR: under rest), number of cardiac cycles, mean and S.D. of R-R intervals (RR), and mean and S.D. of stroke volume (SV) estimated using Doppler echocardiography.

| Subject | Age (year) | Ao (cm) | Condi-tion | No. of cycles | RR (ms) | | SV (mL) | |
|---|---|---|---|---|---|---|---|---|
| | | | | | Mean | S.D. | Mean | S.D. |
| SCD-AB | 30 | 1.80 | UR | 41 | 866 | 35.8 | 76.1 | 2.7 |
| SCD-DS | 54 | 2.00 | UR | 64 | 703 | 6.4 | 77.5 | 5.2 |
| SCD-GH | 24 | 2.00 | UR | 40 | 514 | 35.8 | 42.1 | 4.7 |
| SCD-GU | 63 | 1.90 | UR | 39 | 884 | 34.8 | 71.9 | 3.1 |
| SCD-IP | 78 | 1.70 | UR | 21 | 1089 | 10.8 | 66.5 | 2.4 |
| SCD-JS | 28 | 1.90 | UR | 44 | 783 | 42.0 | 70.9 | 4.2 |
| SCD-KP | 60 | 1.98 | UR | 17 | 782 | 44.5 | 104.3 | 4.1 |
| SCD-MB | 58 | 1.67 | UR | 21 | 1001 | 13.8 | 70.7 | 2.1 |
| SCD-MJ | 53 | 1.96 | UR | 44 | 834 | 11.7 | 61.9 | 3.4 |
| SCD-PK | 39 | 1.98 | UR | 46 | 924 | 49.9 | 67.9 | 4.2 |
| SCD-RH | 55 | 2.02 | UR | 15 | 801 | 20.5 | 92.5 | 2.8 |
| SCD-RP | 60 | 1.82 | UR | 18 | 1135 | 92.7 | 75.8 | 2.3 |
| SCD-SC | 53 | 2.20 | UR | 55 | 808 | 46.7 | 111.6 | 6.7 |
| SCD-SD | 61 | 2.20 | UR | 22 | 1188 | 25.5 | 89.9 | 4.3 |
| SCD-SK | 76 | 2.09 | UR | 44 | 1054 | 23.2 | 93.5 | 8.2 |
| SCD-SP | 69 | 2.30 | UR | 35 | 1098 | 27.9 | 109.3 | 10.4 |
| SCD-SS | 50 | 2.10 | UR | 45 | 644 | 28.5 | 38.0 | 5.2 |
| SCD-ST | 28 | 1.77 | UR | 19 | 881 | 21.2 | 95.7 | 2.7 |
| SCD-SU | 48 | 1.87 | UR | 41 | 927 | 17.4 | 79.5 | 3.8 |
| SCD-SY | 31 | 1.80 | UR | 54 | 533 | 7.8 | 59.9 | 3.2 |
| SCD-TH | 67 | 1.70 | UR | 50 | 801 | 3.4 | 50.8 | 3.4 |
| SCD-TS | 63 | 2.10 | UR | 67 | 646 | 20.6 | 87.9 | 2.8 |
| Across 22 subjects | Mean = 52.2, S.D.= 15.9 | Mean = 1.95, S.D.= 0.17 | UR | 842 | 834 | 176.3 | 76.7 | 19.5 |

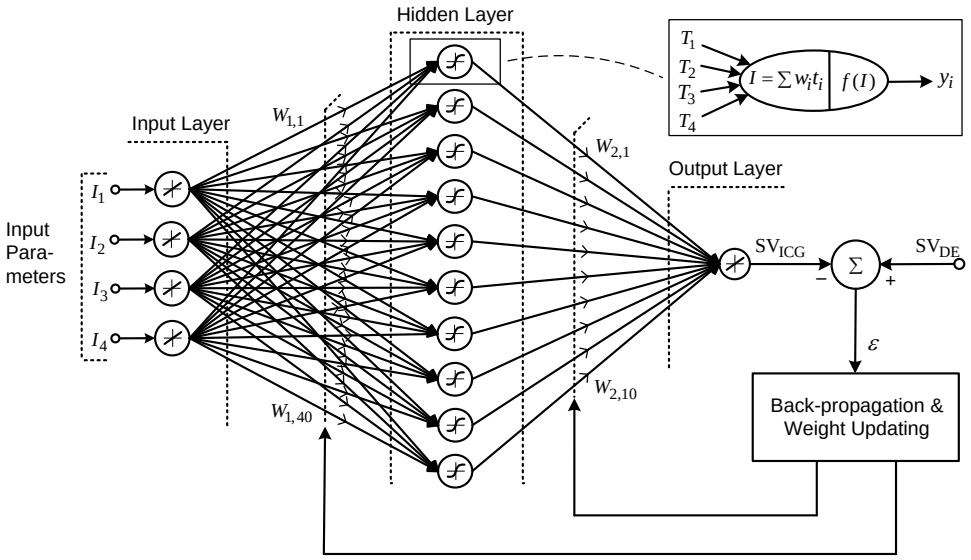


**Figure 4.3** A three-layer feed-forward ANN, with training using error back-propagation algorithm and nonlinear activation function in the hidden-layer, for SV estimation.

### *C. ANN Model Implementation, Optimization, and Testing*

Artificial neural networks (ANN) are data-driven and self-learning systems whose development was inspired by the biological neural systems (Hagan *et al* 1996, Samarasinghe 2006, Haykin 2009). An overview of ANN and some of its applications on estimation are provided in Appendix B. It has been reported that a three-layer feed-forward neural network with Levenberg-Marquardt or gradient decent class of learning algorithm can track a nonlinear input-output relationship (Nocedal and Wright 1999). Normally, the number of neurons in the input layer is equal to the number of inputs in the parameter set. The hidden layer typically consists of an empirically determined optimal number of neurons with a nonlinear transfer function (Haykin 2009). Designing ANN model for an estimation application involves a careful selection of ANN structure, training algorithm, the number of hidden layers and the number of neurons in each layer, the set of input parameters, pre-processing of the input data, and criterion to stop training. Overfitting is a common issue in ANN model development and it can be controlled by varying the number of neurons in the hidden layers. A smaller number of neurons than the required may lead to under-fitting or bias.

We have used a three-layer feed-forward ANN, with training using error back-propagation algorithm and nonlinear activation function in the hidden-layer, for SV estimation as shown in Figure 4.3. The implementation was carried out using MATLAB and

Neural Network Toolbox Release 2013a (MathWorks, Inc., Natick, Mass., USA). In this implementation, the input parameters (subject-related data and beat-to-beat ICG parameters) and the target values (beat-to-beat SV values measured using the reference technique) were transformed to have zero mean and unity variance to equalize their contributions in generalization of the model.

Training and testing of the network were carried out using two disjoint datasets, known as the training set and the testing set, respectively. The training set was partitioned into two disjoint subsets, with the datasets corresponding to two-third of the randomly selected cardiac cycles assigned to the estimation set and the remaining ones assigned to the validation set. The weights of the network were initially set to random values. The estimation set was applied repeatedly for training of the network and weight adjustment was carried out in batch mode on an epoch-by-epoch basis for improving the accuracy of the estimated output values with reference to the corresponding target values. The maximum number of epochs during training was set as 10,000. After each epoch, the validation set was used for checking the overfitting of the network. Increase in accuracy over the estimation set with the accuracy over the validation set remaining the same or decreasing was considered to be an indicator of overfitting and validation failure. The training was stopped in the case of 100 successive validation failures. Subsequently, the estimation capability of the trained network was assessed on the testing set.

The commonly used ICG parameters in the different equation-based methods for SV estimation are $L$, $Z_0$, $(-dz/dt)_{\max}$, and $T_{\text{lvet}}$, or some transformations and combinations of these parameters. We have used these ICG parameters along with the R-to-R interval from ECG as the inputs. In addition to them, the subject's age, height, and weight were also used as the inputs. The three-layer feed-forward network was implemented with these eight inputs. Several variations of the network, differing in terms of the number of neurons in the hidden layer, activation function in the hidden layer, and training algorithm for updating the weights, were investigated for selecting the optimal network. A set of informal investigations were used to find a near-optimal network. Subsequently, four investigations were carried out for optimizing the network by examining the effect of varying one aspect of the network at a time while keeping the other aspects fixed: (i) number of neurons in the hidden layer, (ii) activation function, (iii) training algorithm, and (iv) set of input parameters.

The investigations for optimizing the network were carried out using the datasets corresponding to SNH-UR and SNH-PE recordings from subjects with normal health pooled together, referred to as SNH-UR+PE. These datasets were partitioned into two disjoint sets,

with the datasets corresponding to 60% of the randomly selected cardiac cycles assigned to the training set and the remaining 40% assigned to the testing set.

The optimal network as selected on the basis of the results of the earlier four investigations was used for examining the effect of different datasets for training. The training was carried out using training sets obtained from the SNH-UR, SNH-PE, and SNH-UR+PE datasets, resulting in three trained networks. Each of these networks was tested on the testing sets obtained from SNH-UR, SNH-PE, SNH-UR+PE datasets. In each case, the training set comprised randomly selected 60% of the cardiac cycles with the remaining 40% used as the testing set. The three networks were subsequently tested on SCD-UR with 100% of the cardiac cycles used as the testing set. Performances of the three networks were compared with estimations using Kubicek, Sramek, and Bernstein equations as given in (2.8), (2.9), and (2.11), respectively. The blood resistivity $\rho$ was taken as 150 Ω-m for Kubicek equation.

In addition to comparison of the performance indices ($\bar{\varepsilon}$, $\sigma_{\varepsilon}$, and $r$), the mean-versus-difference plots, known as the Bland-Altman plots (Altman and Bland 1983; Bland and Altman 1999), were used to examine the distribution of errors.

## 4.3 Results

Results of the investigations for selection of the optimal network and those for comparison of the ANN and equation based methods for beat-to-beat SV estimation are given in the following two subsections.

### *A. Selection of the Optimal Network*

For selection of the optimal network, the under-rest and post-exercise recordings from subjects with normal health were pooled together, resulting in 1255 cardiac cycles with the mean and standard deviation of the SV values as 86.3 mL and 18.8 mL, respectively. As described earlier, the training set comprised 60% of randomly selected cycles, i.e. there were 753 cycles in the training set and remaining 502 cycles in the testing set. The training set was further partitioned into estimation set with 502 cycles (2/3 of the training set) and validation set with remaining 251 cycles. The network was implemented with 8 input parameters: $L$, $Z_0$, $(-dz/dt)_{\max}$, $T_{\text{lvet}}$, RR (R-to-R interval from ECG), Age, Ht (height), and Wt (weight). Investigations were carried out for examining the effects of (i) number of neurons in the hidden layer, (ii) activation function, (iii) training algorithm for updating the weights, and (iv) set of input parameters.

**Table 4.3** Effect of different number of neurons in the ANN hidden-layer (activation function: hyperbolic tangent, training algorithm: Levenberg-Marquardt). Number of cardiac cycles in the testing set = 502. $N_{epoch}$ = number of epochs for training, $\bar{\varepsilon}$ = mean error, $\sigma_\varepsilon$ = standard deviation of errors, and $r$ = correlation coefficient.

| No. of neurons | $N_{epoch}$ | $\bar{\varepsilon}$ (mL) | $\sigma_e$ (mL) | $r$ |
|---|---|---|---|---|
| 3 | 177 | 0.29 | 9.16 | 0.880 |
| 5 | 18 | −1.14 | 7.64 | 0.924 |
| 8 | 31 | −0.14 | 6.38 | 0.944 |
| 10 | 66 | 0.42 | 6.06 | 0.947 |
| 13 | 29 | −0.45 | 7.06 | 0.934 |
| 15 | 39 | 0.55 | 6.90 | 0.937 |
| 20 | 10 | −0.47 | 7.26 | 0.931 |

($p < 0.000l$ for all $r$ values)

Performance comparison was carried out by tabulating the number of epochs for convergence during training and mean error ($\bar{\varepsilon}$), standard deviation of errors ($\sigma_\varepsilon$), and correlation coefficient ($r$) with reference to the target values for the estimation, validation, and testing sets. In selecting the optimal network, the number of epochs for convergence is given lower precedence than the error related performance indices.

For examining the effect of the number of neurons in the hidden layer, the hyperbolic tangent was selected as the activation function and the Levenberg-Marquardt algorithm was selected for updating the weights. The performance indices for the number of hidden-layer neurons varied from 3 to 20 are given in Table 4.3. The network with three-neuron hidden layer needed the largest number of epochs for training. The $\bar{\varepsilon}$ values were small (< 1 mL) in all cases. On the basis of values of $\sigma_\varepsilon$ and $r$, the networks with 8 or more neurons may be considered to have better performance than those with 3 or 5 neurons and the network with 10 neurons may be considered to be optimal.

The effect of different activation functions was examined for the network with the 10-neuron hidden layer and the Levenberg-Marquardt algorithm for updating the weights. The networks were implemented with three activation functions: radial basis, logistic, and hyperbolic tangent. The results are given in Table 4.4. The number of epochs was smallest for the radial basis function. The $\bar{\varepsilon}$ values were small (< 1 mL) in all cases. The hyperbolic

**Table 4.4** Effect of different activation functions used in the ANN hidden layer (number of hidden-layer neurons: 10, training algorithm: Levenberg-Marquardt). Number of cardiac cycles in the testing set = 502. $N_{epoch}$ = number of epochs for training, $\overline{\varepsilon}$ = mean error, $\sigma_{\varepsilon}$ = standard deviation of errors, and $r$ = correlation coefficient.

| Activation function | $N_{epoch}$ | $\overline{\varepsilon}$ (mL) | $\sigma_e$ (mL) | $r$ |
|---|---|---|---|---|
| Radial basis | 19 | −0.16 | 6.33 | 0.942 |
| Logisitc | 30 | −0.56 | 6.22 | 0.952 |
| Hyperbolic tangent | 66 | 0.42 | 6.06 | 0.947 |

($p < 0.000$l for all $r$ values)

tangent had smallest $\sigma_{\varepsilon}$ values and hence it may be considered to be the optimal choice although it had a somewhat larger number of epochs than the other two functions.

The approximation error and the number of epochs for convergence depend on the training algorithm used for updating the weights (Haykin 2009, Nocedal and Wright 1999). Effect of different training algorithms was examined on the network with 10 neurons in the hidden layer and the hyperbolic tangent activation function. Out of the several training algorithms, nine commonly used ones were used for implementing the networks: Broyden-Fletcher-Goldfarb-Shanno (BFGS) quasi-Newton, Polak-Ribiére conjugate gradient, scaled conjugate gradient, one step secant, resilient back-propagation, conjugate gradient with Powell-Beale restarts, variable learning rate back-propagation, Fletcher-Powell conjugate gradient, and Levenberg-Marquardt. The results are given in Table 4.5. All algorithms resulted in small $\overline{\varepsilon}$ values (< 1.5 mL) and the variation in performance of different algorithms in terms of $\sigma_{\varepsilon}$ and $r$ was small. There was a large variation in the number of epochs for different algorithms. It was smallest for Levenberg-Marquardt algorithm and much lower than that for other algorithms. This algorithm also resulted in nearly the smallest $\sigma_{\varepsilon}$ and highest $r$. Therefore the Levenberg-Marquardt algorithm may be considered as the optimal choice for our application.

The investigations for examining the effect of number of neurons in the hidden layer, activation function, and training algorithm showed the network with 10-neuron hidden layer, hyperbolic tangent activation function, and Levenberg-Marquardt training algorithm was selected as the optimal choice. This was used for investigating the contribution of different non-ICG parameters by excluding them in different combinations. The results of training and

**Table 4.5** Effect of different ANN training algorithms for updating the weights (number of hidden-layer neurons: 10, activation function: hyperbolic tangent. Number of cardiac cycles in the testing set = 502. Algorithms: BFGS (BFGS quasi-Newton), PRCG (Polak-Ribiere conjugate gradient), SCG (scaled conjugate gradient), OSS (one step secant), RBP (resilient back-propagation), CGPB (conjugate gradient with Powell-Beale restarts), VLRB (variable learning rate back-propagation), FPCG (Fletcher-Powell conjugate gradient), LM (Levenberg-Marquardt). $N_{epoch}$ = number of epochs for training, $\overline{\varepsilon}$ = mean error, $\sigma_\varepsilon$ = standard deviation of errors, and $r$ = correlation coefficient.

| Algorithm | $N_{epoch}$ | $\overline{\varepsilon}$ (mL) | $\sigma_e$ (mL) | $r$ |
|---|---|---|---|---|
| BFGS | 9999 | −0.64 | 6.55 | 0.947 |
| PRCG | 2621 | −0.85 | 6.35 | 0.951 |
| SCG | 2030 | 0.34 | 6.90 | 0.929 |
| OSS | 892 | 0.79 | 7.97 | 0.914 |
| RBP | 668 | −0.81 | 7.24 | 0.922 |
| CGPB | 2383 | −0.86 | 7.47 | 0.927 |
| VLRB | 9925 | −1.46 | 7.20 | 0.924 |
| FPCG | 1623 | 0.09 | 6.24 | 0.946 |
| LM | 66 | 0.42 | 6.06 | 0.947 |

($p$ < 0.000l for all $r$ values)

testing of the networks are given in Table 4.6. The exclusion of different input parameters had a large effect on the number of epochs, with range of 14 – 417. For the testing set, the $\overline{\varepsilon}$ values were small (< 1.5 mL) in all cases, the $\sigma_\varepsilon$ values range from 6.1 – 11.8 mL, and the $r$ values range from 0.819 – 0.950. Small number of epochs was generally associated with large $\sigma_\varepsilon$ values in most cases and hence cannot be used by itself as an indicator for comparing the importance of the parameters. Cases with small $\sigma_\varepsilon$ values were generally associated with high $r$ values.

Network with exclusion of none of the input parameter had 66 epochs and smallest $\sigma_\varepsilon$. Among single-parameter exclusions, RR exclusion resulted in largest $\sigma_\varepsilon$ indicating its importance. Among two-parameter exclusions, [RR, age] exclusion had largest $\sigma_\varepsilon$. Among three-parameter exclusions, largest $\sigma_\varepsilon$ was observed for [age, Ht, Wt] exclusion indicating that these parameters were collectively important although not individually. Exclusion of all the non-ICG parameters together had largest number of epochs and largest $\sigma_\varepsilon$, indicating collective importance of these parameters for improving the speed of convergence and

**Table 4.6** Effect of exclusion of different non-ICG parameters (number of hidden-layer neurons: 10, activation function: hyperbolic tangent, training algorithm: Levenberg-Marquardt). Number of cardiac cycles in the testing set = 502. $N_{epoch}$ = number of epochs for training, $\overline{\varepsilon}$ = mean error, $\sigma_\varepsilon$ = standard deviation of errors, and $r$ = correlation coefficient.

| Excluded Parameter(s) | $N_{epoch}$ | $\overline{\varepsilon}$ (mL) | $\sigma_e$ (mL) | $r$ |
|---|---|---|---|---|
| None | 66 | 0.42 | 6.06 | 0.947 |
| Ht | 51 | −0.10 | 6.74 | 0.939 |
| Wt | 62 | −0.43 | 6.78 | 0.950 |
| Age | 205 | 0.45 | 6.79 | 0.938 |
| RR | 27 | 1.08 | 7.10 | 0.919 |
| Ht, Wt | 37 | 0.63 | 6.96 | 0.932 |
| Ht, age | 148 | 0.07 | 6.62 | 0.942 |
| Ht, RR | 147 | 0.24 | 7.49 | 0.906 |
| Wt, age | 213 | −0.07 | 7.31 | 0.941 |
| Wt, RR | 14 | 1.00 | 7.86 | 0.905 |
| Age, RR | 162 | 0.56 | 7.91 | 0.915 |
| Ht, Wt, age | 36 | 1.27 | 9.15 | 0.878 |
| Ht, Wt, RR | 92 | −0.09 | 8.33 | 0.895 |
| Ht, age, RR | 77 | −0.11 | 8.12 | 0.908 |
| Wt, age, RR | 30 | 0.86 | 8.23 | 0.909 |
| Ht, Wt, age, RR | 417 | 0.41 | 11.81 | 0.819 |

($p < 0.0001$ for all $r$ values)

decreasing the error in SV estimation. Therefore, it may be inferred that the four non-ICG parameters are needed for the optimal network and the R-R interval is the most important one out of these parameters.

*B. Comparison of ANN and Equation Based Methods for Beat-to-Beat SV Estimation*

Based on the results of the investigations presented in the previous subsection, ANN with eight inputs ($L$, $Z_0$, $(-dz/dt)_{max}$, $T_{lvet}$, RR, age, Ht, Wt), 10 neurons in the hidden layer, hyperbolic tangent activation function, and Levenberg-Marquardt training algorithm was selected as the optimal network for beat-to-beat SV estimation. Further investigation was carried out to examine the performance of this network for different combinations of the training and testing sets and for comparing its performance with equation-based estimations.

**Table 4.7** Comparison of ANN and equation based beat-to-beat SV estimations: mean error ( $\bar{\varepsilon}$ ), standard deviation of errors ( $\sigma_\varepsilon$ ), and correlation coefficient ( $r$ ) with reference to the SV values obtained using Doppler echocardiography.

| Testing set ($N$ = No. of cardiac cycles) | Perform. index | Estimation method | | | | | |
|---|---|---|---|---|---|---|---|
| | | ANN1 | ANN2 | ANN3 | EQKB | EQSR | EQBR |
| SNH-UR ($N$ = 252) | $\bar{\varepsilon}$ (mL) | 0.37 | −5.62 | −0.39 | −52.70 | −52.31 | −42.03 |
| | $\sigma_\varepsilon$ (mL) | 5.99 | 31.19 | 5.95 | 30.29 | 30.97 | 32.14 |
| | $r$ | 0.950 | 0.716 | 0.951 | 0.154 | 0.198 | 0.265 |
| SNH-PE ($N$ = 250) | $\bar{\varepsilon}$ (mL) | 5.79 | −0.16 | 0.90 | −42.13 | −49.33 | −33.68 |
| | $\sigma_\varepsilon$ (mL) | 15.23 | 7.43 | 7.17 | 56.84 | 34.07 | 40.02 |
| | $r$ | 0.752 | 0.930 | 0.936 | 0.210 | 0.228 | 0.291 |
| SNH-UR+PE ($N$ = 502) | $\bar{\varepsilon}$ (mL) | 3.04 | −2.15 | 0.07 | −47.09 | −50.77 | −37.98 |
| | $\sigma_\varepsilon$ (mL) | 12.65 | 14.30 | 6.59 | 46.23 | 32.61 | 48.73 |
| | $r$ | 0.773 | 0.725 | 0.946 | 0.363 | 0.295 | 0.364 |
| SCD-UR ($N$ = 842) | $\bar{\varepsilon}$ (mL) | 1.36 | −2.21 | −0.10 | −42.08 | −38.21 | −44.84 |
| | $\sigma_\varepsilon$ (mL) | 9.30 | 9.71 | 7.20 | 37.67 | 35.65 | 40.88 |
| | $r$ | 0.829 | 0.812 | 0.933 | 0.292 | 0.163 | 0.329 |

($p < 0.0001$ for all $r$ values)

In the subsequent description, the networks trained on training sets with SNH-UR, SNH-PE, and SNH-UR+PE datasets are referred to as ANN1, ANN2, and ANN3, respectively. The SV estimations using the Kubicek, Sramek, and Bernstein equations are referred to as EQKB, EQSR, EQBR, respectively. The performance comparisons of the ANN-based and the equation-based estimations were carried out for the testing sets corresponding to SNH-UR, SNH-PE, SNH-UR+PE, and SCD-UR.

The results are summarized in Table 4.7. Results for the three trained networks ANN1, ANN2, and ANN3 show that the performance of each trained network was the best when the training and testing sets corresponded to the same datasets, with almost similar pattern for the three performance indices. The network ANN3 resulted in $\bar{\varepsilon}$ = 0.1 mL, $\sigma_\varepsilon$ = 6.6 mL, and $r$ = 0.946 for SNH-UR+PE. The performance of ANN1 on SNH-UR and that of ANN2 on SNH-PE were almost similar. However, the performance of ANN1 on SNH-PE and SNH-UR+PE and that of ANN2 on SNH-UR and SNH-UR+PE were significantly poor. The performance of ANN3 on SNH-UR and SNH-PE was almost similar to that on SNH-UR+PE. These results

indicate that training of the network on the pooled data significantly improved its performance and that ANN3 can be used for SV estimation on all three SNH datasets.

Testing of ANN3 on SCD-UR resulted in $\bar{\varepsilon}$ = −0.1 mL, $\sigma_\varepsilon$ = 7.2 mL, and $r$ = 0.933 and thus only a slight performance degradation compared to the testing on SNH-UR+PE. Testing of ANN1 and ANN2 on SCD-UR gave relatively poor results. These results show that training of the optimal network on the training set obtained by pooling of the under-rest and post-exercise recordings from the subjects with normal health enabled the network for SV estimation on recordings from subjects with cardiovascular disorders.

As seen in Table 4.7, the three equation-based SV estimations resulted in relatively large $\bar{\varepsilon}$, large $\sigma_\varepsilon$, and low $r$ values for all the four testing sets. The performance of Bernstein equation (EQBR) was generally better than that of the other two equations. This equation resulted in $\bar{\varepsilon}$ = −44.8 mL, $\sigma_\varepsilon$ = 40.9 mL, and $r$ = 0.329 for testing on SCD-UR. Thus, the ANN-based method, particularly with the training set obtained by pooling of the under-rest and post-exercise recordings from subjects with normal health, may be considered to be much more effective than the equation-based methods for beat-to-beat SV estimation from subjects with normal health as well as those with cardiovascular disorders.

Figure 4.4 gives plots of the difference of estimations versus the mean of estimations (Bland-Altman plots) for beat-to-beat SV estimation impedance cardiography using ANN3 and Doppler echocardiography for the SNH-UR+PE and SCD-UR datasets, showing the distribution of differences along with 95% confidence interval ($\bar{\varepsilon} \pm 1.96\sigma_\varepsilon$). The plots show that the distribution of differences between the two measurement techniques are similar for both the datasets, indicating that the performance of ANN3 for recordings from the subjects with cardiovascular disorders is similar to that for recordings from the subjects with normal health. There is an increase in the error at the higher SV values, which may be due to sparsity of training data at this end.

Earlier studies (Aust *et al* 1982, Northridge *et al* 1990, Castor *et al* 1994, Mulavara *et al* 1998, van der Meer *et al* 1999, Fellahi *et al* 2009) on evaluation of impedance cardiography with reference to Doppler echocardiography for SV estimation have used estimation over a set of cycles for each subject. In the study by Mulavara *et al* (1998) using ANN-based SV estimation on subjects with normal health, the correlation coefficients for estimations using the Kubicek equation, the Sramek equation, and the ANN-based method were 0.29, 0.32, and 0.88, respectively. For comparison with such studies, the beat-to-beat SV estimations in our study were evaluated for average of SV values across the cardiac cycles for each of the 22 subjects with cardiovascular disorders. All three equation-based estimations

resulted in large $\bar{\varepsilon}$ and $\sigma_\varepsilon$ values, and low $r$ values, with $\bar{\varepsilon}$ = −43.1 mL, $\sigma_\varepsilon$ = 43.5 mL, and $r$ = 0.20 for EQBR. The ANN-based estimations resulted in much lower $\bar{\varepsilon}$ and $\sigma_\varepsilon$ values, and larger $r$ values, with $\bar{\varepsilon}$ = 0.4 mL, $\sigma_\varepsilon$ = 5.7 mL, and $r$ = 0.96 for ANN3. Thus, the ANN-based estimation outperformed the equation-based estimation for beat-to-beat variation as well as for average SV estimation

## 4.4 Discussion

An ANN-based technique for beat-to-beat SV estimation has been proposed and investigated using an ICG-echocardiography database. The ICG parameters are obtained using a technique for automatic detection of the B, C, and X points as presented in the previous chapter. Echocardiography is used as the reference technique, as it is noninvasive, can be used for beat-to-beat SV estimation, and can be used simultaneously along with impedance cardiography. Our approach assumes that the input-output relationships in the datasets from subjects with normal health, with the recordings in the under-rest condition and in the post-exercise condition after the heart rate has been increased by participation of the subject in the Bruce exercise protocol, can also be representative of the input-output relationships in the datasets from subjects with cardiovascular disorders. A three-layer feed-forward network with error back-propagation algorithm was selected for SV estimation. The network was implemented for eight input parameters: inter-electrode distance, basal impedance, ICG peak, left ventricular ejection time, R-R interval, age, height, and weight. Three of these parameters (ICG peak, left ventricular ejection time, and R-R interval) are estimated on beat-to-beat basis and the other five parameters are subject-dependent. The input parameters and the target values were transformed to equalize their contributions in generalization of the model. The investigations were carried out in two stages. The first stage involved optimization of the network by examining the effects of number of neurons in the hidden layer, activation function, and the training algorithm for updating the weights, and set of input parameters. The second stage involved testing of the network by examining the effect of different combinations of training and testing sets and comparison with equation-based estimations.

The investigations for optimizing the network were carried out using the datasets from the subjects with normal health with the under-rest and post-exercise recordings pooled together. These investigations showed the network with 10-neuron hidden layer, hyperbolic tangent activation function, and Levenberg-Marquardt training algorithm as the optimal choice. Exclusion of the four non-ICG parameters (R-R interval, age, height, and weight) in different combinations showed that R-R interval was important in decreasing the error and

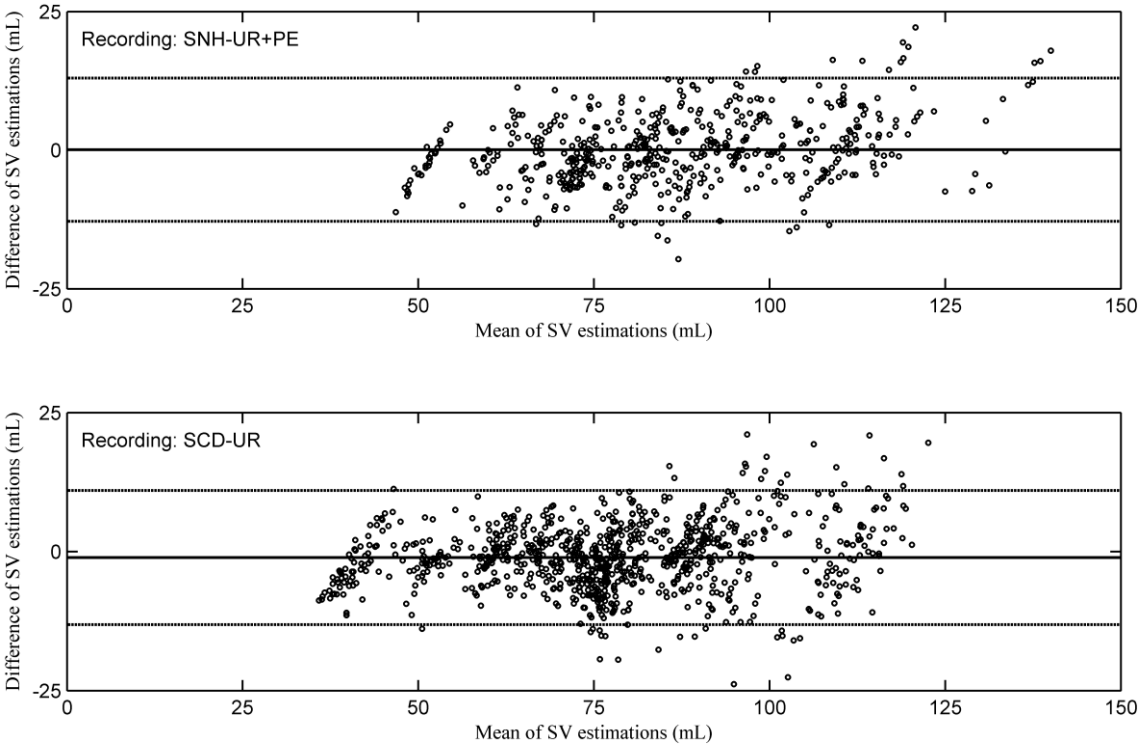


**Figure 4.4** Bland-Altman plots of beat-to-beat SV estimation (mL) using ANN3 on the SNH-UR+PE and SCD-UR recordings with the SV values measured from Doppler echocardiogram as reference (solid line: $\overline{\varepsilon}$ , dotted lines: $\overline{\varepsilon} \pm 1.96\,\sigma_{\varepsilon}$ ).

combination of height, weight, and age together helped in significantly decreasing the number of epochs needed for convergence during training and also the errors. Therefore, it may be inferred that the four non-ICG parameters have an important role in ANN-based estimation. These parameters were retained as part of the inputs for the second stage of the investigation.

The second stage of investigation involved examining the effect of different combinations of training and testing sets on performance of the optimal network and comparing its performance with equation-based estimations. Three network models were developed by using three types of training sets from the recordings from the subjects with normal health: (i) under-rest, (ii) post-exercise, and (iii) under-rest and post-exercise pooled together. All the three trained networks were tested using the three testing sets. Results showed that the performance of each trained network was the best when the training and testing sets corresponded to the same datasets. Performance of the first two networks degraded when tested on different datasets. Performance of the third network did not change much across the testing sets. Performance of the network trained on the pooled datasets did

not degrade during testing on the other two types of datasets. Therefore, this network may be considered as better than the other two.

Performances of the trained networks were compared with the three established equation-based methods (Kubicek, Sramek, and Bernstein), for the recordings from the subjects with normal health and for recordings from the subjects with cardiovascular disorders. In comparison with the ANN-based estimations, the equation-based estimations had poor performance on all indicators. Bernstein equation generally performed better than the other two equations. It provided correlation coefficients of 0.36 and 0.33 for the recordings from the subjects with normal health and for subjects with cardiovascular disorders, respectively. The corresponding values for the best ANN-based estimation were 0.95 and 0.93. The Bland-Altman plots showed the distribution of errors in SV estimation for recordings from the subjects with cardiovascular disorders to be similar to that for recordings from the subjects with normal health.

For a comparison of the results with earlier studies (Aust *et al* 1982, Northridge *et al* 1990, Castor *et al* 1994, Mulavara *et al* 1998, van der Meer *et al* 1999, Fellahi *et al* 2009), the beat-to-beat SV estimations were averaged over the cardiac cycles for each subject. The correlation coefficients for the equation-based estimations were low and similar to those reported in earlier studies. The correlation coefficient for ANN-based estimation was 0.96 and higher than the earlier reported values. Thus, the results show that the ANN-based estimation with training using the pooled datasets from the subjects with normal health can be used for different datasets and pooling is needed for training to extend the use of the trained network for SV estimation for the subjects with cardiovascular disorders. The results further show that the proposed method is useable for measuring SV averaged over a set of cardiac cycles and for beat-to-beat SV monitoring.

Investigations need to be carried out with a large database. Training data from a large number of subjects and particularly with higher levels of exercise can help in reducing sparsity of datasets at the ends of the SV range and in improving the effectiveness of ANN-based estimation. The testing needs to be carried out with a large number of subjects with cardiovascular disorders. Use of other types of networks and techniques for detection of ICG characteristic points with smaller errors should be investigated. Use of the C-C interval in place of the R-R interval in the input parameter set may be helpful in further improving the performance. Effects of inclusion of additional ICG parameters, such as B-C interval, C-X interval, and ICG value at the X point, need to be investigated.

# Chapter 5
# SUMMARY AND CONCLUSION

## 5.1 Introduction

Impedance cardiography is a low-cost noninvasive technique for SV monitoring and it can be used for estimation of several other cardiovascular indices. Due to lack of repeatability in the estimated values and poor agreement between the estimated values and the measurements using the reference techniques, impedance cardiography has not received acceptance for use in clinical diagnosis, continuous monitoring in intensive care units, and for decision making in emergency departments. Our research objective was to develop an ANN-based method for automatic beat-to-beat SV estimation using impedance cardiography to improve the acceptability of this technique for use in clinical practice and as a research tool for the study of SV variability.

Most of the existing methods for SV estimation are based on models of the thoracic impedance and the aortic blood profile along with use of empirically derived scaling factors. Validations of these methods have often used parameters obtained from ensemble-averaged signals and across-the-subjects data. Use of ANN-based SV estimation can help in addressing the inadequacies of the model-based approaches. Further, training and testing of the network for beat-to-beat estimation can help in overcoming the limitations of ensemble averaging and across-the-subjects data. We have used Doppler echocardiography as the reference technique, as it is noninvasive, it can be used for beat-to-beat SV measurements on healthy subjects and patients, and it can be used simultaneously along with impedance cardiography.

The summary of the investigations, the conclusions drawn from the results, and some suggestions for further work are presented in the following sections.

## 5.2 Summary of the Investigations

For developing an ANN-based method for automatic beat-to-beat SV estimation using impedance cardiography, an ICG-echocardiography database was developed. Subsequently, this database was used for two sets of investigations: (i) beat-to-beat detection of the B, C, and X points for obtaining the ICG parameters for use in SV estimation and (ii) optimization and evaluation of the ANN-based SV estimation.

*ICG-echocardiography database:* The ICG, ECG, and Doppler echocardiogram signals were simultaneously recorded in a clinical setting from subjects with normal health and

subjects with cardiovascular disorders, without efforts for gender and age balancing. The gender, age, height, weight, and inter-electrode distance were noted for each of the subjects. The instrumentation and the method used for the recordings have been described in Section 3.3 and Section 4.2 and the format related details of the database are given in Appendix C. There were 18 subjects with normal health and 22 subjects with cardiovascular disorders. All recordings were carried out with the subject in the left-lateral position with no restriction on breathing. For a subject with normal health, two recordings were carried out. The first recording was carried out with the subject having relaxed and rested. The second recording was carried out after the subject underwent an exercise, following the first four stages of the Bruce exercise protocol, to increase the heart rate. The first and second sets of recordings are referred to as 'under-rest' and 'post-exercise' recordings. For a subject with cardiovascular disorder, only the under-rest recording was carried out. The under-rest and post-exercise recordings from the 18 subjects with normal health have 630 and 625 cardiac cycles, respectively. The under-rest recordings from the 22 subjects with cardiovascular disorders have 842 cardiac cycles.

*Automatic detection of ICG characteristic points:* For obtaining the ICG parameters for SV estimation, the B, C, and X points in the ICG waveform need to be detected in an error-free manner. While the C point is generally prominent, the B and X points are much less distinct and their detection gets severely affected by the artifacts and due to morphological variations in the waveform. Based on an empirical examination of the morphological variations of the ICG waveforms, a time-domain technique for automatic detection of B, C, and X points has been proposed, as described in Section 3.2. The proposed technique uses simultaneously acquired ECG and ICG as inputs. It uses R and T peaks of ECG as reference points and multiple time-domain features to reduce errors due to morphological variations. A wavelet-based denoising is employed for suppression of respiratory artifacts in ICG and the technique can be used without any restriction on breathing. It does not require estimation of the baseline and selection of the processing parameters. As high-order derivatives are not used, the detection is not significantly affected by the presence of a moderate level of noise in the input signal. Detection is carried out on beat-to-beat basis after marking of the ICG cycles with reference to the R peaks and hence the techniques avoids inter-cycle smearing. The proposed technique was evaluated on the ICG-echocardiography database comprising simultaneously acquired and time-aligned ICG and Doppler echocardiogram recordings. The performance of the technique was evaluated with reference to the visually marked points in the ICG waveform and with reference to the intervals measured using echocardiography.

*ANN-based SV estimation:* An ANN-based method for SV estimation has been proposed, as described in Section 4.2. It is based on the assumption that the relationship between the SV values and the input parameters can be acquired by the network during its training and the trained network can be used subsequently for SV estimation. The training was carried out on the datasets obtained from the individual cardiac cycles without ensemble averaging. This approach assumes that the input-output relationships in the datasets from subjects with normal health, with the recordings under the resting condition and in the post-exercise condition after the heart rate has been increased by participation of the subject in the Bruce exercise protocol, can also be representative of the input-output relationships in the datasets from subjects with cardiovascular disorders. The ICG parameters to serve as inputs for beat-to-beat SV estimation were obtained using the proposed technique for automatic detection of the B, C, and X points. Beat-to-beat SV measurements from Doppler echocardiograms were used as the target values. A three-layer feed-forward network with error back-propagation algorithm was selected for SV estimation and implemented for 8 input parameters: $L$, $Z_0$, $(-dz/dt)_{\max}$, $T_{\text{lvet}}$, R-R interval from ECG, age, height, and weight. The investigations on ANN-based SV estimation were carried out in two stages: (i) optimization of the network by examining the effects of number of neurons in the hidden layer, activation function, training algorithm for updating the weights, and set of input parameters and (ii) testing of the network with different combinations of training and testing sets and comparison with equation-based estimations.

## 5.3 Conclusions

The conclusions from the results of the investigations for evaluating the performance of the proposed technique for automatic detection of the B, C, and X points may be summarized as the following:

i) There were no significant differences in the performance of the proposed technique across the three sets of recordings in the database, despite large heart rate and morphological variations in the data.

ii) The proposed technique performed better than the established techniques reported earlier. The performance of the proposed technique may be attributed to the use of artifact suppression, use of R and T peaks as reference points for marking ICG segments for locating the features, and use of multiple time-domain features for resolving ambiguities caused by morphological variations.

iii) The bias related error (mean of differences) and the precision related error (standard deviations of differences), as referred to the mean R-R interval, for estimation of the B-X interval were 3.2% and 7.1%, respectively. Thus the proposed technique may be considered to be suitable for obtaining ICG parameters for automatic beat-to-beat SV estimation.

The investigations for optimizing the network for ANN-based SV estimation, its testing with different combinations of training and testing sets, and comparison with equation-based estimations resulted in the following conclusions:

i) The investigations involving training and testing with the pooling of the under-rest and post-exercise datasets from the subjects with normal health showed that the best performance was provided by the network with 10-neuron hidden layer, hyperbolic tangent activation function, Levenberg-Marquardt training algorithm, and the set of 8 input parameters.

ii) Testing of the network models developed by using three types of training sets from the recordings from the subjects with normal health showed that the training using the pooled datasets can be used for all types of datasets and that training on the pooled datasets is needed for extending the use of trained network for SV estimation for the subjects with cardiovascular disorders.

iii) The ANN-based SV estimation using the optimal network resulted in mean error $\bar{\varepsilon}$ = 0.1 mL, standard deviation of errors $\sigma_\varepsilon$ = 6.6 mL, and correlation coefficient $r$ = 0.946 for testing sets from subjects with normal health. The results for testing sets from subjects with cardiovascular disorders were $\bar{\varepsilon}$ = −0.1 mL, $\sigma_\varepsilon$ = 7.2 mL, and $r$ = 0.933, showing only a slight performance degradation. Among the equation-based estimations, Bernstein equation provided better performance than the other two equations, but its performance with $\bar{\varepsilon}$ = −44.8 mL, $\sigma_\varepsilon$ = 40.9 mL, and $r$ = 0.329 was significantly inferior to the ANN-based estimation.

In summary, it may be concluded that the proposed ANN-based method using the optimized network and the ICG parameters obtained by automatic beat-to-beat detection of the B, C, and X points can be used for SV estimation with low bias and high precision from different types of datasets. The proposed technique may be helpful in improving the acceptability of impedance cardiography for use in clinical practice and as a research tool for the study of SV variability.

## 5.4 Suggestions

For extending the applications of impedance cardiography as a low-cost diagnostic tool, the proposed technique for beat-to-beat detection of the B, C, and X points needs to be evaluated for estimation of other cardiovascular indices and study of their variabilities. Further

investigations for improving the detection technique, particularly for improving the agreement of the detected X point with the point of aortic valve closure, may help in improving the performance of ANN-based SV estimation. The proposed method needs to be investigated using other types of networks and a larger database.

# Appendix A
# SV MEASUREMENT
# USING DOPPLER ECHOCARDIOGRAPHY

## A.1 Introduction

Echocardiography is an ultrasound-based noninvasive technique for detection of cardiovascular disorders. Several modes of this technique are used clinically: A-mode, B-mode, M-mode, 2D, and Doppler (Quinones *et al* 2002, Oh *et al* 2006, Solomon and Bulwer 2007). In the A-mode (amplitude mode), a short ultrasound pulse is transmitted and the received echoes are plotted as a function of time, with the position and intensity of the echoes being related to the distance of the reflecting tissues and their acoustic characteristics, respectively. In the B-mode (brightness mode), echoes are represented as dots along a line representing transmission path of the ultrasonic pulse, with the echo intensity represented by the brightness of the corresponding dot. In the M-mode (motion mode), B-mode display along with repeated transmission of pulses is used to provide a one-dimensional view of movements of the reflecting tissues. In 2D-mode (two-dimensional mode), a phased-array transducer is used to steer the pulse along different directions and M-mode display of the received echoes along the corresponding transmission paths is used to provide a two-dimensional scan of the reflecting tissues. Doppler echocardiography uses detection of Doppler shift in the echo for measuring blood flow velocity. It is useful in detection of cardio-valvular insufficiency, stenosis, and other abnormal blood flow conditions. In pulsed wave Doppler (PWD), short bursts of ultrasound are transmitted and the resulting echoes are received, using a single transducer, to measure the blood velocities from a selected discrete region of the heart. In continuous wave Doppler (CWD), two transducers are used for simultaneous transmission and reception for measuring the velocities of the blood cells in the transmission path.

The study of different structures of the heart and their movements involves imaging the heart using multiple transducer positions (parasternal, suprasternal, subcostal, and apical) and from multiple cross-sectional views (long axis, short-axis, four-chamber, five-chamber) (Henry *et al* 1980). Parasternal long-axis view is used for visualizing right ventricle, ventricular septum, ascending aorta, anterior and posterior cups of the aortic valve, mitral valve, left atrium, and right ventricular outflow tract. Parasternal short-axis view helps in visualizing, mitral valve, right ventricle, and left ventricular cavity dimension and wall thickness. In apical four-chamber view, the four heart chambers can be visualized simultaneously. Apical

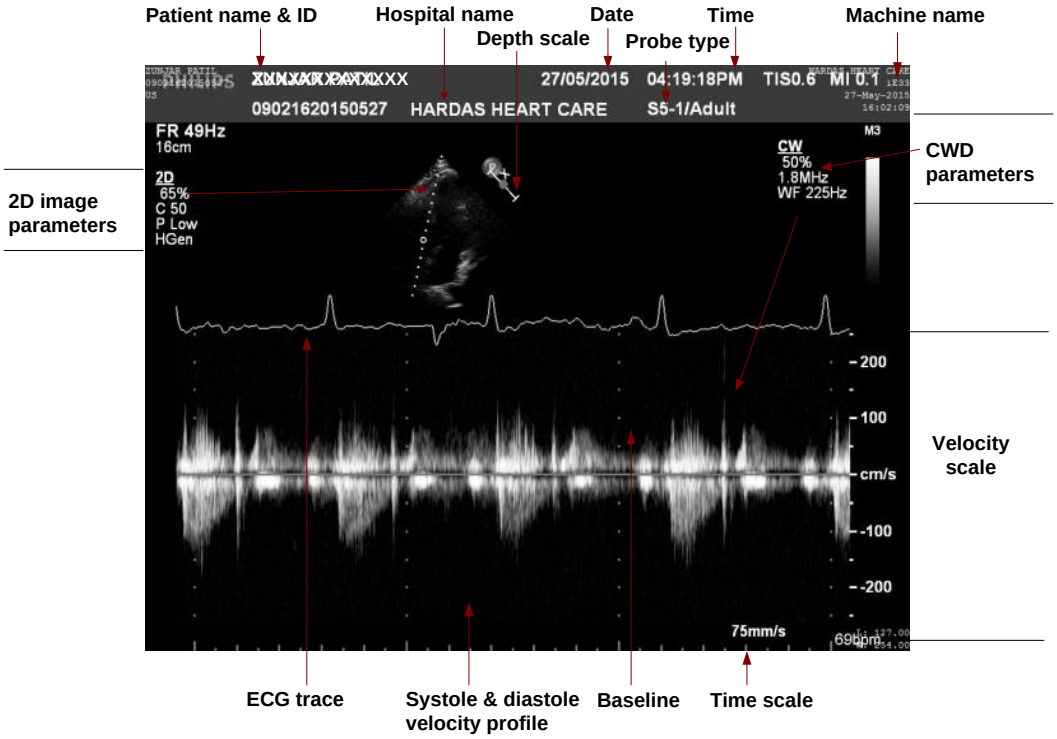


**Figure A.1** Echocardiogram (2D and CWD) in apical five-chamber view (machine: Philips 'iE33') recorded from the subject SNH-ZP, along with description of different fields in the display.

five-chamber view can be used for visualizing the left ventricular outflow tract, right and left leaflets of the aortic valve, and ascending aorta.

An example of echocardiogram for a subject with normal health is shown in Figure A.1 and that for a subject with cardiovascular disorders is shown in Figure A.2. The textual information has the subject name and ID, the transducer type and frequency, power, gain, and pulse repetition frequency. In the graphical part of the display, the 2D gray sector image provides the structural and functional information of the heart. In the superimposed color flow Doppler mapping (CFM) image, blood flow is shown using the BART scale for velocity with blue representing the flow away from the transducer and red representing the flow towards it. Lower half of the display shows the blood flow velocity profile obtained using CWD in apical five-chamber view along with tracing of simultaneously acquired ECG.

A graphical representation of an aortic segment from LVOT to ascending aorta with markings of the diameter at different levels is shown in Figure A.3. The aortic blood velocity profile was recorded in apical five-chamber view of the ascending aorta using CWD as shown in Figure A.2. The aortic diameter was measured from 2D sector image in parasternal long-axis view at the level of the aortic annulus during mid-systole, as shown in Figure A.4.

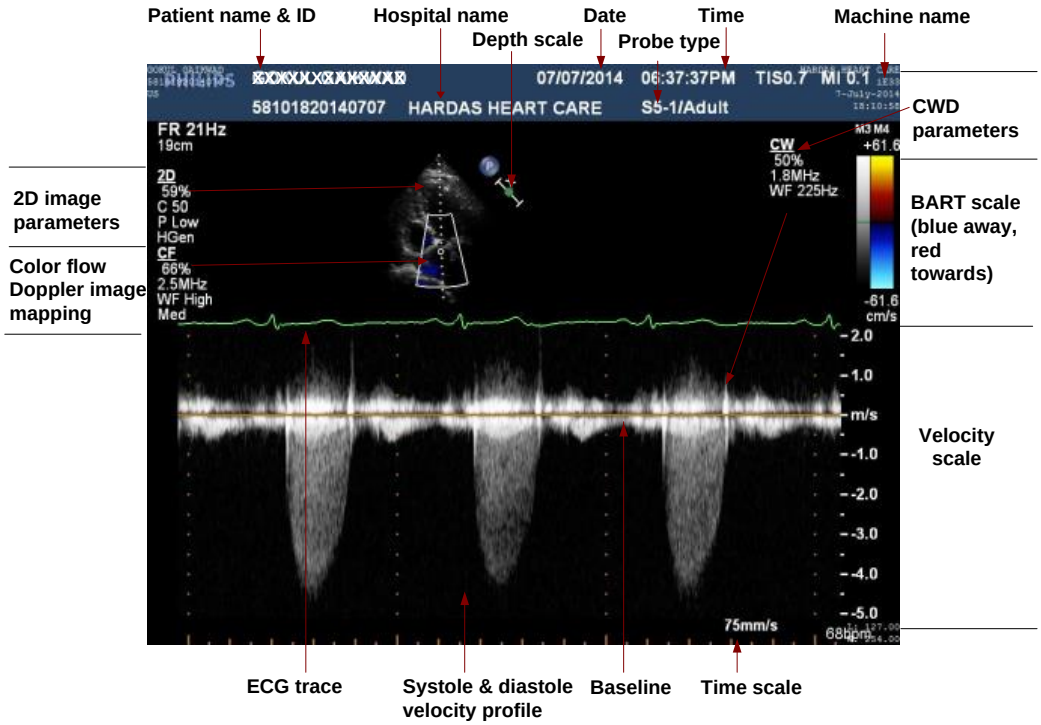


**Figure A.2** Echocardiogram (2D and CWD) in apical five-chamber view (machine: Philips 'iE33') recorded from the subject SCD-GG, along with description of different fields in the display.

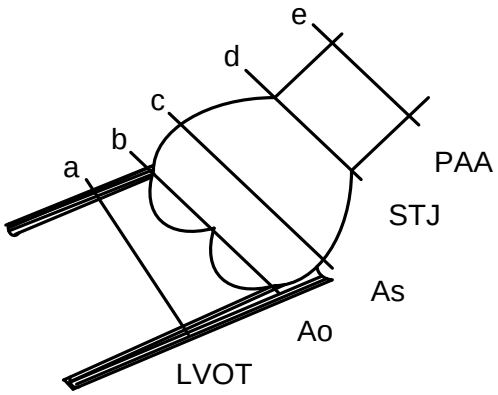


**Figure A.3** Locations for measurement of VTI and CSA in the segment from LVOT to ascending aorta: (a) LVOT, around 5 – 10 cm proximal from the aortic valve, (b) aortic annulus/root AO, (c) aortic sinus AS, (d) sino-tubular junction STJ, and (e) proximal ascending aorta PAA.

## A.2 SV Measurement

The blood flow rate is the product of blood velocity in the aorta and cross-sectional area (CSA) of the aorta at the velocity measuring site. The sites for blood flow measurement using Doppler echocardiography, in descending preference order, are (i) left ventricular outflow tract (LVOT) or aortic annulus, (ii) mitral annulus, and (iii) pulmonic annulus (Quinones *et al*

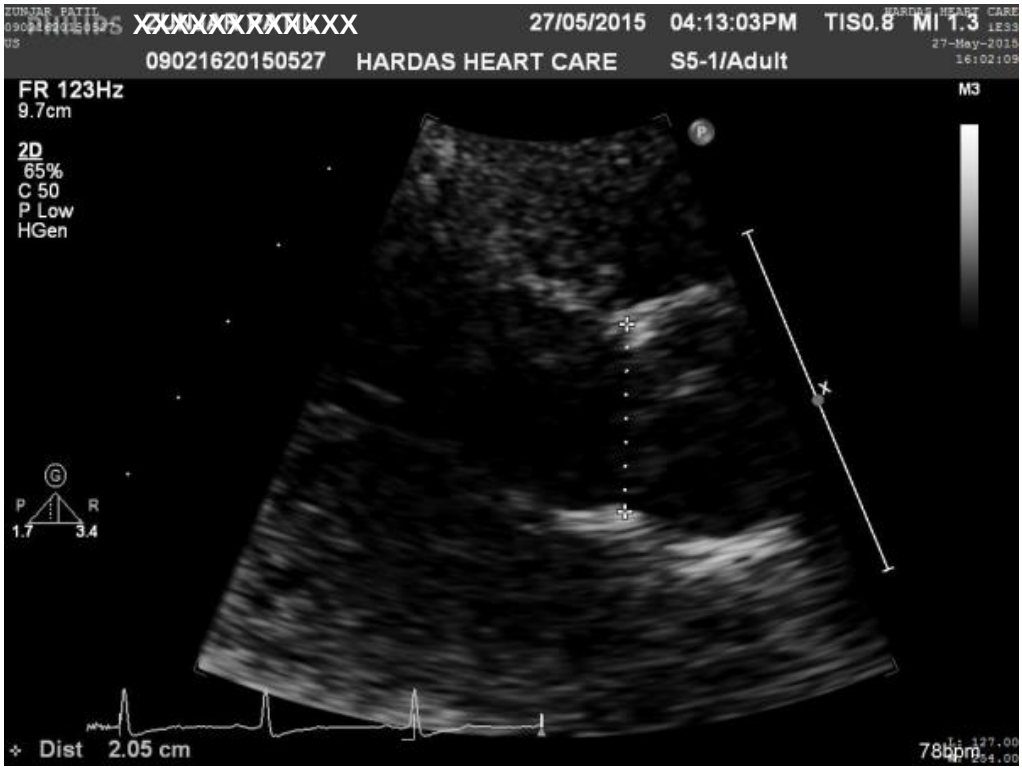


**Figure A.4** 2D echocardiogram in parasternal long-axis view (machine: Philips 'iE33') for measurement of aortic annulus diameter, recorded from the subject SNH-ZP.

2002, Baumgartner *et al* 2009). As the flow is pulsatile and the velocity varies during the cardiac cycle, velocity-time integral (VTI) is calculated over the ejection phase by finding the area between the envelope of the Doppler spectrum and its baseline. It is equal to the stroke distance i.e. the average distance travelled by the ejected blood in each cardiac cycle. SV is calculated as the product of VTI and CSA. The aortic CSA of aorta is calculated from the measurement of aortic diameter at the annulus assuming circular cross-section.

The agreement of results of left ventricular SV measurement using Doppler echocardiography with other SV estimation methods has been reported by several researchers (Rasmussen *et al* 1982, Lewis *et al* 1984, Bouchard *et al* 1987, Northridge *et al* 1990). Some of these studies have used PWD and rest have used CWD for VTI calculation from the Doppler spectrum. In calculation of CSA, some have measured the aortic valve diameter, some have used the LVOT diameter, and some have measured the diameter at a level of aortic annulus/root or ascending aorta. When PWD is used, the ultrasound should be directed to the location being used for CSA calculation. In this method, there is a possibility of location mismatch and aliasing in the measurement of high velocities. These difficulties get avoided by using CWD.

## A.3 Consistency of VTI Estimation for SV Measurement

As described in the previous section, SV measurement involves manual tracing of the blood velocity for VTI estimation. To assess the consistency of VTI estimation, the velocity tracings were carried out on the recordings from two subjects by three trained operators (A, B, and C). The first subject was suffering from hypertension and the second subject had severe aortic stenosis. The VTI values for the second subject were about three times those for the first subject. The statistical measures (minimum, maximum, mean, and S.D.) of the beat-to-beat values as estimated from the manual tracings of the blood velocity profile by three operators for the two subjects are given in Table A.1 and these values show good match across the operators. For a quantitative assessment of the consistency of the measurements, agreement between the VTI values estimated on beat-to-beat basis was examined by calculating the mean difference ($\bar{\varepsilon}$), standard deviation of differences ($\sigma_\varepsilon$), and correlation coefficient ($r$) for the three operator pairs (AB, BC, CA) and the results are given in Table A.2. The inter-operator biases, indicated by the $\bar{\varepsilon}$ values, are very small. The inter-operator random differences, indicated by the $\sigma_\varepsilon$ values are 1.67 – 2.24 cm or less than 7% (considering mean VTI of about 25 – 30 cm for most subjects). The $r$ values are higher than 0.99, showing high inter-operator consistency in VTI estimation.

**Table A.1** Measurements of VTI (cm) by three operators (A, B, C) on recordings from two subjects (SCD-AB with hypertension, SCD-GG with severe aortic stenosis): minimum (min), maximum (max), mean, and standard deviation (S.D.).

| Measure | Subject SCD-AB (No. of cycles = 41) | | | Subject SCD-GG (No. of cycles = 36) | | |
|---|---|---|---|---|---|---|
| | Op. A | Op. B | Op. C | Op. A | Op. B | Op. C |
| min | 27.7 | 28.1 | 27.9 | 89.7 | 88.9 | 88.3 |
| max | 32.4 | 31.9 | 31.7 | 114 | 113 | 113 |
| mean | 29.9 | 29.9 | 29.7 | 104 | 104 | 105 |
| S.D. | 1.08 | 0.79 | 0.92 | 5.71 | 5.11 | 5.29 |

**Table A.2** Consistency measures of manual estimation of VTI by three operator pairs: mean difference ($\bar{\varepsilon}$), standard deviation of differences ($\sigma_\varepsilon$), and correlation coefficient ($r$). Number of cardiac cycles = 77 (cycles from two subjects pooled together).

| Measure | Operator pair AB | Operator pair BC | Operator pair CA |
|---|---|---|---|
| $\bar{\varepsilon}$ (cm) | 0.19 | −0.34 | 0.15 |
| $\sigma_\varepsilon$ (cm) | 2.22 | 1.67 | 2.24 |
| $r$ | 0.998 | 0.999 | 0.998 |

# Appendix B
# ARTIFICIAL NEURAL NETWORK BASICS

## B.1 Introduction

Artificial neural networks (ANN) are distributed processing systems having certain features of biological neural systems and may be trained with input-output data or may operate in a self-organizing mode. These systems have been used in many applications involving estimation or classification (Leahy *et al* 1991, Gajdar *et al* 1997, Tan and Saif 1997, Silipo and Marchesi 1998, Jain and Fanelli 2000, Bose 2001, Papaloukas *et al* 2002, Ceylan and Ozbay 2007, Haykin 2009, Ghorbanian *et al* 2010, Ramana and Raghu 2010). This appendix provides an overview of ANN basics (commonly used structures, activation functions, type of networks, and learning algorithms) and some of the estimation related applications.

## B.2 ANN Structure and Types of Networks

An ANN comprises a network of basic processing units with each unit representing a neuron, which receives inputs $x_n$, sums them with synaptic weights $w_n$ along with bias $b$, and produces output $y$ using activation function $f$ (usually a sigmoid function). The relation between the neuron inputs and its output is given as

$$y = f\left(\sum_{n=1}^{m} w_n x_n + b\right) \tag{B.1}$$

Knowledge is acquired by the network through a learning process and is stored in the form of synaptic weights. The network structure consists of layers, each layer having one or more neurons. The first layer is the input layer with the number of neurons in it usually equal to the number of inputs. The last layer is the output layer. Between these two layers, there can be one or more hidden layers. The neurons in the input layer generally have linear activation function and those in the hidden layers have sigmoid activation function. The output layer neurons may have linear, sigmoid, or signum activation function (as described in the next section) depending on the application.

The network has to be configured by setting the weights such that the application of a set of inputs produces the desired set of outputs. The weights may be set using a prior knowledge. In most applications, they are set through a training process by feeding a specific set of inputs and in accordance with a learning rule. In supervised learning, the network is

trained by applying inputs and corresponding targets (desired output values). In unsupervised learning or self-organizing operation, no targets are provided and the network is trained to respond to clusters of the pattern by discovering statistically salient features in the inputs.

The networks can be classified as (i) feed-forward with signal flow only in the forward direction and (ii) feedback or recurrent with some of the neuron outputs applied as inputs to the neurons in an earlier layer. Applications involving estimation problems invariably use feed-forward networks with supervised learning. A three-layer feed-forward ANN, with training using error back-propagation algorithm and nonlinear activation function in the hidden-layer is shown earlier in Figure 4.1.

## B.3 Activation Functions

The activation function transforms the weighted sum of the neuron inputs and bias to the output (Samarasinghe 2006, Haykin 2009, Beale *et al* 2011). The output has two saturation values, usually 0 and 1 for uniploar function and −1 and 1 for bipolar function. Some of the activation functions are shown in Figure B.1. The linear activation function is used in linear approximators and the signum function is used in binary classifiers. Sigmoid functions are S-shaped differentiable functions, with logistic and hyperbolic tangent being the most commonly used ones. The logistic function is unipolar and is given as

$$f(t) = \frac{1}{1+e^{-\alpha t}} \tag{B.2}$$

where $\alpha$ is the slope parameter and $t$ is the weighted sum of inputs and bias. The hyperbolic tangent function is bipolar and is given as

$$f(t) = \tanh(t) \tag{B.3}$$

Both functions have highest slope at zero input and progressively decreasing slope for input increasing in either direction. These functions are extensively used in nonlinear approximation applications.

## B.4 Methods for Supervised Learning of Feed-Forward Networks

In training with supervised learning, the network is fed with a sequence of input vectors and corresponding targets. Learning involves simultaneous and incremental adjustments of the weights in order to progressively decrease the error (difference between the network output value and the target) to a minimum value (Bianchini *et al* 1995, Singh and Kumar 2004, Samarasinghe 2006, Haykin 2009, Zakaria *et al* 2010). The network processes each input vector and the output is compared with the target and a measure of the error over the input vectors is calculated, with the mean-square error (MSE) being the most commonly used

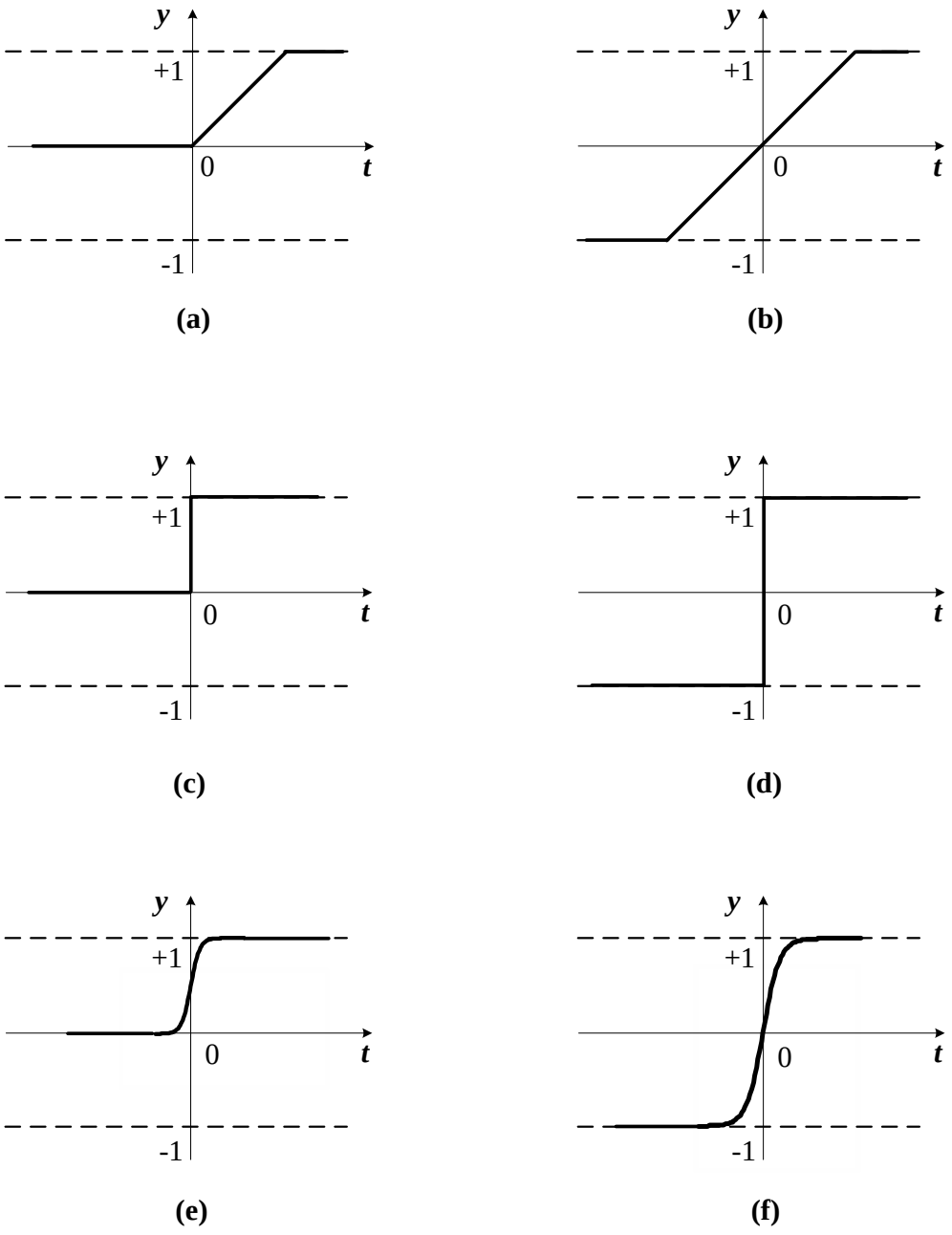


**Figure B.1** Activation functions: (a) linear unipolar, (b) linear bipolar, (c) unipolar signum, (d) bipolar signum, (e) unipolar logistic, and (f) bipolar hyperbolic tangent.

measure. In the error back-propagation method, the partial derivatives of the error with respect to each of the weights are calculated using mathematical model of the neurons in the network and chain rule. A number of learning algorithms for adjusting the weights in accordance with these derivatives are used. The weights are initially set to random values and adjustments can be done in two ways. In online or sequential learning, the weights are

adjusted after application of each input vector and corresponding target. In offline or batch learning, the weights are adjusted after all the input vectors have been presented once, known as an epoch. For improving the accuracy of the estimated output values with reference to the corresponding targets, the weight adjustments are carried out on an epoch-by-epoch basis by repeatedly applying the input vectors.

In gradient descent algorithm (Haykin 2009), the error gradient is used to reach the lowest point on the error surface, by applying corrections to the synaptic weights in proportion to corresponding partial derivatives. This algorithm applies the same learning rate to all weights. For higher convergence, other algorithms use correction factors with the factor for each weight calculated as a function of its distance from its optimal value. In the steepest descent algorithm (Samarasinghe 2006, Haykin 2009, Sahu *et al* 2011), the error is reduced along the negative gradient of the error surface. However, the learning rate, which is the same for all of the weights, is adapted internally during training.

Levenberg-Marquardt (LM) algorithm (Levenberg 1944, Marquardt 1963, Samarasinghe 2006, Haykin 2009) is a second-order error minimizing algorithm in which the gradient descent concept is extended to include the curvature of the error surface for speeding up the leaning process. The learning rate is set to unity and a new logarithmic term is added to the second derivative error term, which is used along with the first derivative term in computing the new weights. The second-order algorithms converge faster to reach the threshold MSE value and take less training time.

Broyden-Fletcher-Goldfarb-Shanno quasi-Newton algorithm (Fletcher 1987, Haykin 2009) constructs an approximation for the second derivative of error information represented as a square matrix called Hessian, from an arbitrary function using the cost function evaluated at the current and previous points. It is updated using the error gradient evaluated at each epoch and is used as a correction factor to the synaptic weights to reach the lowest point on the error surface. Conjugate gradient algorithm (Fletcher 1987, Shewchuk 1994, Haykin 2009) is a second-order learning algorithm with faster learning rate and less computational requirements. In this algorithm, the error is reduced along the conjugate gradient direction. Minimization of the error gradient is achieved by assigning a value proportional to the conjugate vector scaled with a learning rate to the synaptic weights. This algorithm has several forms on the basis of the procedure adapted for calculating the conjugate direction vectors or a scaling factor which is a function of these vectors. In the case of scaled conjugate descent algorithm, successive vectors of the quadratic cost function (error surface) are generated at each epoch as successive conjugate gradient vectors. Fletcher-Powell, Powell-

Beale, and Polak-Ribiére proposed different formulas to calculate the scaling factor without explicit knowledge of conjugate direction vectors.

One-step secant algorithm (Battiti 1992) uses the Hessian to reach the lowest point on the error surface by applying it as the correction to the synaptic weights. The storage and computation requirements are reduced by storing the partial Hessian and assuming the previous Hessian at each epoch as an identity matrix. It permits calculation of the new search direction without having to compute the Hessian inverse.

In the resilient back-propagation algorithm (Riedmiller and Braun 1993), the lowest point on the error surface is reached by using the sign of the error gradient to determine the direction of the search for weight update and correction to the synaptic weights applied by a separate weight correction value. The weight correction is increased by a predefined value for no sign change in two successive epochs, it is decreased by a predefined value for a sign change in the gradient, and it is not changed for zero gradient. Use of sigmoid activation functions in the hidden layers eliminates the effect of small-magnitude gradients. Magnitude of weight correction is reduced in case the weights oscillate and it is increased if the weights continue to change in the same direction for several epochs.

In the variable learning rate back-propagation algorithm (Hagan *et al* 1996), the learning rate is changed during the training process adaptively based on the error surface. Initial network weights and bias are calculated using the current learning rate and then the new errors are calculated. If the new errors are larger than the old by a predefined ratio, the new weights and bias are discarded and the learning rate is decreased by a predefined percentage. Otherwise, the new weights are kept unchanged and the learning rate is increased by a predefined percentage.

## B.5 ANN Applications for Estimation

Leahy *et al* (1991) used multilayer perceptron structure with two hidden layers for estimation in robot control to enhance the high-speed tracking accuracy of the robot manipulator. In this network, error back-propagation algorithm was used for training the network, with maximization of the estimation accuracy and minimization of the mean-square error as the training criteria. Wang and Feng (1992) proposed a linear recurrent neural network for real-time parameter estimation, as it converges faster and is easier to realize than Hopfield network or quasi-linear ANNs. Several ANN applications in power electronics have been reported by Bose (2001) using both feed-forward and feedback networks.

Gajdar *et al* (1997) designed feed-forward ANN to estimate the friction coefficient in wheel train system. The network had two hidden layers, with the first hidden layer having 14

hyperbolic tangent neurons and the second layer having 7 linear neurons, and it was trained using error back-propagation and 201-sample dataset. The friction coefficient calculated using formula was also considered as one of the inputs. They reported that their approach reduced the training time compared to pure ANN-based approaches.

Blackwell *et al* (2008) used multilayer feed-forward network to estimate atmospheric profiles, with the networks having one or two hidden layers with hyperbolic tangent activation function and the output layer with linear activation functions. The network weights were initialized using Nguyen-Widrow method (Nguyen and Widrow 1990), which selects the weights for evenly distributing the active region of the activation function across the layer's input space. They used Levenberg-Marquardt learning method and separate datasets for training, validation, and testing. DeLuccia and Werner (2007) used ANN combined with global optimizer such as genetic algorithm for estimating the suitable element spacing in broadband non-uniformly spaced phased-array antennas.

The review of ANN applications for estimation show that different applications need a careful selection of ANN structure, learning method, the number of layers in the structure, and the number of linear and nonlinear neurons in each layer. Pre-processing or the methods used for data preparation and the network parameters also need to be carefully selected.

As described in the fourth chapter, our investigations for ANN-based SV estimation using impedance cardiography with Doppler echocardiography as the reference technique were carried out using the three-layer feed-forward network. The input parameter set consisted of up to eight parameters. The optimal network was selected by examining the effects of the following:

(i) The number of neurons in the hidden-layer: 3, 5, 8, 10, 13, 15, and 20;

(ii) Activation functions: radial basis, logistic, and hyperbolic tangent; and

(iii) Training algorithm for updating the weights: BFGS quasi-Newton, Polak-Ribiére conjugate gradient, scaled conjugate gradient, one-step secant, resilient back-propagation, conjugate gradient with Powell-Beale restarts, variable learning rate back-propagation, Fletcher-Powell conjugate gradient, and Levenberg-Marquardt.

# Appendix C
# CLINICAL RECORDING DATABASE

The ICG and Doppler echocardiogram signals were simultaneously recorded in a clinical setting at Hardas Heart Care (Pune, Maharashtra, India), after approval of the protocol by the Ethics Committee of the hospital. The subjects for participating in the study were recruited from among the persons visiting the hospital for health check-up, diagnosis, or post-operative treatment. They were informed about the study and they read and signed the consent if willing to participate in it. There was no monetary cost or benefit for participation.

The subjects with normal health had no known history of cardiovascular disorders and were screened by a cardiologist on the basis of physical examination and ECG report. The subjects with cardiovascular disorders were the patients undergoing post-operative treatment or with past history of cardiovascular disorders. They were screened for suitability to participate in the study by the concerned cardiologist. The gender, age, height, and weight of the subjects were noted. The group of subjects with normal health comprised seventeen males and one female with age of 26 – 65 years (mean = 46.3 years, S.D. = 10.7 years), height of 1.54 – 1.80 m (mean = 1.69 m, S.D. = 0.06 m), and weight of 61 – 100 kg (mean = 76.2 kg, S.D. = 10.0 kg). The group of subjects with cardiovascular disorders had nineteen males and three females with age of 24 – 78 years (mean = 51.5 years, S.D. = 15.8 years), height of 1.43 – 1.76 m (mean = 1.66 m, S.D. = 0.08 m), and weight of 52 – 97 kg (mean = 71.6 kg, S.D. = 11.7 kg). The recordings were carried out during the period extending from June 2014 to June 2015.

The ICG related signals were recorded using 'HIC-2000 Impedance Cardiograph' from Bio-Impedance Technology (Chapel Hill, NC, USA). The impedance sensing was carried out using four-electrode configuration with Ag-AgCl disposable ECG spot electrodes. The outer two electrodes were used for injecting the excitation current and the resulting voltage was picked-up across the inner two electrodes. The upper current electrode was placed above the suprasternal notch on the front of the neck, with the lower one placed below the xiphoid process on the left lateral side of the thorax. The upper voltage electrode was placed at the base of the neck below the upper current electrode and the lower voltage electrode was placed at the level of xiphoid process on the left lateral side of the thorax above the lower current electrode. The placement of ICG electrodes is shown earlier in Figure 3.3. The instrument used 1 mA excitation current of 100 kHz and provided analog output signals corresponding to basal impedance ($Z_0$), deviation from basal impedance ($-z(t)$), and ICG ($-dz/dt$) with the

sensitivities of 40 mV/Ω, 0.5 V/Ω, and 400 mV/(Ω·s$^{-1}$), respectively. It also provided analog ECG signal as sensed using the voltage electrodes. The output signals from the ICG instrument were acquired using the 8-channel, 12-bit signal acquisition module 'KUSB-3102' from Keithley Instruments (Cleveland, Ohio, USA) and connected through USB to a battery-powered Notebook PC. The sampling frequency was set at 500 Hz. The distance between the voltage sensing electrodes was noted.

The echocardiography recordings were carried out using 'iE33 echocardiography system' from Philips Ultrasound (Bothell, Wash., USA) with a 5 MHz phased-array probe placed on the chest after applying an ultrasound gel for good contact with the skin. The aortic blood flow velocity profile was recorded using apical five-chamber view of the ascending aorta. The aortic diameter was measured using parasternal long-axis view at the level of aortic annulus during mid-systole. The VTI was estimated as the area between the envelope of the Doppler spectrum and its baseline with the help of the built-in software of the echocardiography machine by tracing the spectral envelope with its track ball. The machine has a facility for three-electrode ECG recording and this facility was used, with electrode placement as shown earlier in Figure 3.3, for time-aligned display of ECG and Doppler echocardiogram waveforms. As the recordings of ICG and Doppler echocardiogram waveforms employed independent time bases, the cardiac cycles of the two recordings were synchronized by alignment of the corresponding ECG-R peaks.

For a subject with normal health, two recordings were carried out. The first recording was carried out with the subject having relaxed and rested. The ICG electrodes and echocardiography probe were placed as described earlier and simultaneous recording of the ICG and Doppler echocardiogram signals was carried out, with the subject lying in the left-lateral position with slight folding of the right leg. The second recording was carried out after the subject had undergone an exercise to significantly increase the heart rate. The exercise was carried out, following the first four stages of the Bruce exercise protocol (Bruce *et al* 1949), for about ten minutes on the 'GE T-2100' treadmill from GE Healthcare (Wauwatosa, Wis., USA) attached with 'Smart Biphasic' defibrillator from Philips Healthcare (Andover, Mass., USA). The recording was carried out soon after cessation of the exercise and in the same way as the first recording. The subject was advised to avoid any movements during both the recordings in order to minimize the motion artifacts, but no restrictions were placed on breathing. The first and second sets of recordings are referred to as 'under-rest' and 'post-exercise' recordings. For a subject with cardiovascular disorder, only the under-rest recording was carried out. A summary of information on subjects with normal health and subjects with

cardiovascular disorders along with the corresponding values of aortic annulus diameter, R-R interval of ECG, and stroke volume estimated using Doppler echocardiography are given earlier in Table 3.1 and Table 3.2, respectively. The under-rest (UR) and post-exercise (PE) recordings from the 18 subjects with normal health (SNH) have 630 and 625 cardiac cycles, respectively and these are referred to as SNH-UR and SNH-PE. The under-rest recordings from the 22 subjects with cardiovascular disorders (SCD) have 842 cardiac cycles and these are referred to as SCD-UR.

The recordings were organized as a database to be used for ICG-related research. The database has information on individual subjects and the simultaneously recorded ICG and Doppler echocardiograms. The database folder is named as 'icg_database' and its organization is given in Table C.1. Information on the subjects with normal health and those with cardiovascular disorders are tabulated in the files named as 'icg_database_ healthy_hhc2nov16' and 'icg_database_patients_hhc2nov16', using the format as given in Table C.2. Each row in the table has subject code, name, gender, address, age, height, weight, medical history, voltage sensing electrodes distance, and hyperlink to the respective data folder of subject. The Doppler echocardiogram, ICG signal recording, and medical report of each subject are saved in a folder named with the respective subject code. Consent forms and reports (with masked subject identity) of all the subjects are saved in the folders named as 'consent' and 'reports', respectively. The columns with personal information are masked in the sharable database.

Organization of the folders 'icg_consent_n_report_healhty' and 'icg_consent_n_report_ patients' with consent forms and medical reports of 'SNH' subjects and 'SCD' subjects is tabulated in Table C.3. Organization of the folders 'icg_data_healthy' and 'icg_data_patients' with data from 'SNH' subjects and 'SCD' subjects is given in Table C.4. Organization of the folders 'SS_data' from 'SNH' subjects and 'SCD' subjects is given in Table C.5.

The ICG data files may be input for processing using the following code:

```
%Matlab code for loading the icg data file
   clc; close all; clear all;
   load SS_icg_pre_ex.mat % loading data file
   ch1 = data(:,1);  % Zo
   ch2 = data(:,2);  % -z(t)
   ch3 = data(:,3);  % -dz/dt
   ch4 = data(:,4);  % ECG
   ch5 = data(:,5);  % synchronous pulse
   figure;
   subplot(511); plot(ch1);
   subplot(512); plot(ch2);
   subplot(513); plot(ch3);
```

```
subplot(514); plot(ch4);
subplot(515); plot(ch5);
title('Acquired 5ch: Zo, z(t), dz/dt, ECG, and synch
pulse')
```

**Table C.1** Organization of the main folder 'icg_database' of the clinical recording database, SNH: Subjects with normal health, SCD: Subjects with cardiovascular disorders).

| Folders and files | Description |
|---|---|
| icg_database_healthy_hhc2nov16 | File with information on 'SNH' subjects (format as in Table C.1) |
| icg_database_patients_hhc2nov16 | File with information on 'SCD' subjects (format as in Table C.1) |
| icg_consent_n_report_healhty | Folder with consent forms and medical reports of 'SNH' subjects (pdf files) |
| icg_consent_n_report_patients | Folder with consent forms and medical reports of 'SCD' subjects (pdf files) |
| icg_data_healthy | Folder with data from SNH |
| icg_data_patients | Folder with data from SCD |

**Table C.2** Format of the tables used for recording information from subjects with normal health (SNH) and subjects with cardiovascular disorders (SCD). 'SS': Subject code.

| Sr. no. | Sub. code | Name, Gender, Age, Address, Consent, Clinical report | Gender, Age, Ht. (cm), Wt. (kg) | Medical history | L (condition, cm) | Data (ICG & Doppler Echo.) |
|---|---|---|---|---|---|---|
| 1 | SS | -- | -- | -- | -- | -- |
| -- | -- | -- | -- | -- | -- | -- |
| -- | -- | -- | -- | -- | -- | -- |

**Table C.3** Organization of the folders 'icg_consent_n_report_healhty' and 'icg_consent_n_report_patients' with consent forms and medical reports of 'SNH' subjects and 'SCD' subjects. 'SS': subjects code.

| Files | Description |
|---|---|
| SS_consent | Scanned copy of signed consent forms of 'SNH' subjects and 'SCD' subjects (format as given in Appendix D) |
| -- | -- |
| -- | -- |
| SS_report | Scanned copy of medical reports of 'SNH' subjects and 'SCD' subjects |
| -- | -- |
| -- | -- |

**Table C.4** Organization of the sub-folders 'icg_data_healthy' and 'icg_data_patients' with data from 'SNH' subjects and 'SCD' subjects. 'SS': subjects code.

| Sub-folders | Description |
|---|---|
| icg_data_healthy\SS_data | Sub-folders each with Doppler echocardiograms, ICG data files, and medical report of 'SNH' subjects |
| -- | -- |
| -- | -- |
| icg_data_patients\SS_data | Sub-folders each with Doppler echocardiograms, ICG data files, and medical report of 'SNH' subjects |
| -- | -- |
| -- | -- |

**Table C.5** Organization of the sub-folders 'SS_data' from 'SNH' subjects and 'SCD' subjects.

| Files | Description |
|---|---|
| SS_de_pre_ex_IM_NNNN.jpg | Doppler echocardiogram frame recorded from subject 'SS' under pre-exercise condition, as 'jpg' image file. |
| -- | -- |
| -- | -- |
| SS_de_post_ex_IM_NNNN .jpg | Doppler echocardiogram frame recorded from subject 'SS' under post-exercise condition, as '.jpg' image file. |
| -- | -- |
| -- | -- |
| SS_icg_pre_ex.mat | ICG recorded from subject 'SS' under rest condition (corresponding to several Doppler echocardiogram files), waveform samples as '.mat' file. |
| SS_icg_post_ex.mat | ICG recorded from subject 'SS' under post-exercise condition (corresponding to several Doppler echocardiogram files), waveform samples as '.mat' file. |
| SS_icg_pre_ex.fig | Plots of ICG waveform samples 'SS_icg_pre_ex.mat' as '.fig' file. |
| SS_icg_post_ex.fig | Plots of ICG waveform samples 'SS_icg_post_ex.mat' as '.fig' file. |

# Appendix D

# SUBJECT CONSENT FORM

### Informed Consent for Participation in a Research Study

## I Project Title

Monitoring of cardiovascular indices using impedance cardiography (Investigators: Dr. Suhas P. Hardas, Hardas Heart Care, Shivajinagar, Pune, India; Prof. P. C. Pandey, S. M. M. Naidu, and Uttam R. Bagal, IIT Bombay).

## II Introduction

You are invited to participate in a research study. It is important that you read this description of the study and understand the nature and risk of participation. Please give your consent to participate in this clinical study only if you have completely understood the nature and course of this study and if you are aware of your rights as a participant.

## III Purpose of the Study

Echocardiography is one of the established non-invasive techniques for the diagnosis of cardiovascular disorders. Some of the cardiovascular indices can also be obtained using Impedance Cardiography, which is a relatively inexpensive technique and can be used for monitoring these indices during critical care or during stress test as needed by the physician. The purpose of the study is to carry out recordings using echocardiography and impedance cardiography simultaneously for a comparison of the test results with the objective of evaluating the effectiveness of impedance cardiography and further improving it.

## IV Expected Duration of the Study and Number of Subjects

You will be one of approximately fifty persons who will participate in this study. You will be in the study for about an hour during your visit to the hospital.

## V Study Procedures to be Followed

If you agree to participate in this study, (a) you will be asked about previous medical problems, your current health, and your medications; (b) you will have a brief physical examination, and (c) you need to undergo ECG and Echocardiography tests. The test results will be reviewed by a doctor and you will be informed if you are eligible to participate in the study.

This study involves non-invasive recordings related to cardiovascular functioning with an impedance cardiograph and Doppler Echocardiograph. Recordings will be taken by using surface electrodes connected to an impedance cardiograph. Four ECG disposable pre-gelled electrodes will be placed for approximately 30 min duration. During these recordings, Doppler Echocardiogram will also be acquired, in left lateral position. At the end of the recordings, the electrodes will be removed. The study may involve several recordings before and

after mild levels of exercise. In case you are undergoing a treatment, you may be invited to participate in the study again during your follow-up visit to the hospital.

## VI Risks and Discomforts of Participating

No risks related to use of Echocardiography and Impedance Cardiography have been reported. The tests will be conducted under the supervision of a doctor. It may involve a mild level of exercise, resulting in an increase in the heart rate and the breathing rate. The level of exercise will be similar to that in a stress test. You can stop the exercise in case you feel any discomfort.

## VII Possible Benefits of the Study

The study is being carried out to gain knowledge to develop better and low-cost instruments and techniques for diagnosis of cardiovascular disorders in the future. There are no direct benefits to you of participating in this study. No diagnostic information or clinical inference based on the recordings taken from you will be made available to you.

## VIII Compensation for Participation

Participation in this study will be at no cost to you. The tests and the clinical recordings to be used in the study will be free of charge. No compensation will be provided for your participation.

## IX Compensation for Study Related Injury

In the rare event of a physical injury or illness that may occur as a direct result of your participation in this study, you will be provided medical care at no cost to you. You will not give up any of your legal rights by signing this form.

## X Right to Withdraw from the Study

Your participation in this study is entirely voluntary. You may choose not to take part or you may leave the study at any time. Your decision will not affect your further treatment at this institute.

## XI Confidentiality

All study records will be kept confidential at all times. Your identity will not be revealed except as required by law. Records related to your tests and treatment may be published for scientific reasons. Your identity will not be revealed in these publications.

## XII Contact for Further Information

Thank you for taking the time to read the information about this study, or have had it read to you. Before signing this document, you should ask questions about anything that you do not understand. The study staff will be happy to answer your questions before, during, and after the study. If you have any questions about your rights as a research participant or complaints regarding the research study, you may contact Dr. Suhas P. Hardas, on telephone number 020 4102 8999.

## XIII Consent

1) I have read (or have had it read to me) the information given in the informed Consent Document for this study entitled "Monitoring of cardiovascular indices using impedance cardiography".
2) I have received an explanation of the nature, purpose, duration and foreseeable effects and risks of participation and what I will be expected to do. My questions have been answered satisfactorily.
3) I understand that my participation is voluntary and that I may refuse to participate or may withdraw from the study at any time, without penalty or loss of benefits to which I may otherwise be entitled.
4) I further understand that any information that becomes available during the course of the study that may affect my willingness to take part will be informed to me.
5) Institutional review board authorities may wish to examine my medical records to verify the information collected. By signing this document, I give permission for this review of my records.
6) I understand that my identity will not be revealed in any report or publication.
7) I agree to take part in the above study.

Signature/thumb impression of Subject: ----------

Name of Subject: ----------

Date: ----------

Place: ----------

# REFERENCES


Altman D G and Bland J M 1983 Measurement in medicine: the analysis of method comparison studies *The Statistician* **32** 307–17

Arbol J R, Perakakis P, Garrido A, Mata J L, Fernandez-Santaella M C and Vila J 2016 Mathematical detection of aortic valve opening (B point) in impedance cardiography: a comparison of three popular algorithms *Psychophysiology* **54** 350–7

Arora D, Chand R, Mehta Y and Trehan N 2007 Cardiac output estimation after off-pump coronary artery bypass: a comparison of two different techniques *Ann. Card. Anaesth.* **10** 132–6

Aust P E, Belz G G, Belz G and Koch W 1982 Comparison of impedance cardiography and echocardiography for measurement of stroke volume *Eur. J. Clin. Pharmacol*. **23** 475–7

Barrows A K, Yoshizawa M and Yasuda Y 1995 Filtering noncorrelated noise in impedance cardiography *IEEE Trans. Biomed. Eng.* **42** 324–7

Battiti R 1992 First and second order methods for learning: between steepest descent and Newton's method *Neural Comput.* **4** 141–66

Baumgartner H, Hung J, Bermejo J, Chambers J B, Evangelista A, Griffin B P, Iung B, Otto C M, Pellikka P A and Quinones M 2009 Echocardiographic assessment of valve stenosis: EAE/ASE recommendations for clinical practice *Eur. J. Echocardiogr.* **10** 1–25 doi:10.1093/ejechocard/jen303

Baura G D 2001 Noninvasive continuous cardiac output monitor *US Patent* 6186955 B1

Beale M H, Hagan M T and Demuth H B 2011 *Neural Network Toolbox User's Guide* (Natick, MA: The MathWorks, Inc.)

Bernstein D P 1986 A new stroke volume equation for thoracic electrical bioimpedance: theory and rationale *Crit. Care Med.* **14** 904–9

Bernstein D P 2010 Impedance cardiography: pulsatile blood flow and the biophysical and electrodynamic basis for the stroke volume equations *J. Electr. Bioimp*. **1** 2–17

Bernstein D P and Lemmens H J 2005 Stroke volume equation for impedance cardiography *Med. Biol. Eng. Comput.* **43** 443–50

Bianchini M, Frasconi P and Gori M 1995 Learning in multilayered networks used as autoassociators *IEEE Trans. Neural Netw.* **6** 512−15

Blackwell W J, Chen F W, Jairam L G and Pieper M 2008 Neural network estimation of atmospheric profiles using AIRS/IASI/AMSU data in the presence of clouds *Proc. Int. Geosci. Remote Sensing Symp.* (Boston, MA: IEEE) pp 122–5 doi: 10.1109/IGARSS.2008.4778808

Bland J M and Altman D G 1999 Measuring agreement in method comparison studies *Stat. Methods Med. Res.* **8** 135–60

Bonjer F H, Van Den Berg J and Dirken M N 1952 The origin of the variations of body impedance occurring during the cardiac cycle *Circulation* **6** 415–20

Boomsma D I, de Vries J and Orlebeke J F 1989 Comparison of spot and band impedance cardiogram electrodes across different tasks *Psychophysiology* **26** 695–9

Bose B K 2001 Artificial neural network applications in power electronics *Proc. 27th Annu. Conf. IEEE Ind. Electron. Soc.* (Denver, CO: IEEE) pp 1631–8 doi: 10.1109/IECON.2001.975533

Bouchard A, Blumlein S, Schiller N B, Schlitt S, Byrd B F 3rd, Ports T and Chatterjee K 1987 Measurement of left ventricular stroke volume using continuous wave Doppler echocardiography of the ascending aorta and M-mode echocardiography of the aortic valve *J. Am. Coll. Cardiol.* **9** 75–83

Bour J and Kellett J 2008 Impedance cardiography: a rapid and cost-effective screening tool for cardiac disease *Eur. J. Intern. Med.* **19** 399–405

Braun M U, Schnabel A, Rauwolf T, Schulze M and Strasser R H 2005 Impedance cardiography as a noninvasive technique for atrioventricular interval optimization in cardiac resynchronization therapy *J. Interv. Card. Electrophysiol.* **13** 223–9

Bruce R A, Lovejoy F W Jr, Pearson R, Yu P N G, Brothers G B and Velasquez T 1949 Normal respiratory and circulatory pathways of adaptation in exercise *J. Clin. Invest.* **28** 1423–30

Carvalho P, Paiva R P, Henriques J, Antunes M, Quintal I and Muehlsteff J 2011 Robust characteristic points for icg: definition and comparative analysis *Proc. Int. Conf. Bio-inspired Systems and Signal Processing* (Rome, Italy: Scitepress Digital Library) pp 161–8

Castor G, Klocke R K, Stoll M, Helms J and Niedermark I 1994 Simultaneous measurement of cardiac output by thermodilution, thoracic electrical bioimpedance and Doppler ultrasound *Br. J. Anaesth.* **72** 133–8

Ceylan R and Ozbay Y 2007 Comparison of FCM, PCA and WT techniques for classification ECG arrhythmias using artificial neural network *Expert Sys. Appl.* **33** 286–95

DeLuccia C S and Werner D H 2007 Nature-based design of aperiodic linear arrays with broadband elements using a combination of rapid neural-network estimation techniques and genetic algorithms *IEEE Antennas Prop. Mag.* **49** 13–23

De Maria A N and Raisinghani A 2000 Comparative overview of cardiac output measurement methods: has impedance cardiography come of age? *Congest Heart Fail.* **6** 60–73

DeMarzo A P and Lang R M 1996 A new algorithm for improved detection of aortic valve opening by impedance cardiography *Proc. Comput. Cardiol.* (Indianapolis: IEEE) pp 373–6 doi: 10.1109/CIC.1996.542551

Elstad M and Walloe L 2015 Heart rate variability and stroke volumevariability to detect central hypovolemia during spontaneousbreathing and supported ventilation in young, healthy volunteers *Physiol. Meas.* **36** 671–81

Ermishkin V V, Kolesnikov V A and Lukoshkova EV 2014 Age-dependent and 'pathologic' changes in ICG waveforms resulting from superposition of pre-ejection and ejection waves *Physiol. Meas.* **35** 943–63

Ernst J M, Litvack D A, Lozano D L, Cacioppo J T and Berntson G G 1999 Impedance pneumography: noise as signal in impedance cardiography *Psychophysiology* **36** 333–8

Fellahi J L, Caille V, Charron C, Deschamps-Berger P H and Vieillard-Baron A 2009 Noninvasive assessment of cardiac index in healthy volunteers: a comparison between thoracic impedance cardiography and Doppler echocardiography *Anesth. Analg.* **108** 1553–9

Fletcher R 1987 *Practical Methods of Optimization* 2nd edn (New York: Wiley)

Fortin J *et al* 2006 Non-invasive beat-to-beat cardiac output monitoring by an improved method of thransthoracic bioimpedance measurement *Comp. Biol. Med.* **36** 1185–203

Gajdar T, Rudas I and Suda Y 1997 Neural network based estimation of friction coefficient of wheel and rail *Proc. Int. Conf. IEEE Intell. Eng. Syst.* (Budapest, Hungary: IEEE) pp 315–18 doi: 10.1109/INES.1997.632437

Ghorbanian P, Ghaffari A, Jalali A and Nataraj C 2010 Heart arrhythmia detection using continuous wavelet transform and principal component analysis with neural network classifier *Proc. Comput. Cardiol.* (Belfast, UK: IEEE) pp 669−72

Guyton A C and Hall J E 2006 *Textbook of Medical Physiology* 11th edn, ed Schmitt W and Gruliow R (Saunders: Elsevier)

Hagan M T, Demuth H B and Beale M H 1996 *Neural Network Design* 2nd edn (Boston, MA: PWS Publishing)

Haykin S 2009 *Neural Networks and Learning Machines* 3rd edn, ed Horton M J and Dworkin A (New York: Prentice Hall/Pearson)

Heinroth K M, Elster M, Nuding S, Schlegel F, Christoph A, Carter J, Buerke M and Werdan K 2007 Impedance cardiography: a useful and reliable tool in optimization of cardiac resynchronization devices *Europace* **9** 744–50

Henry W L *et al* 1980 Report of the American Society of Echocardiography Committee on nomenclature and standards in two-dimensional echocardiography *Circulation* **62** 212–7

Hill D W and Lowe H J 1973 The use of the electrical-impedance technique for the monitoring of cardiac output and limb blood flow during anaesthesia *Med. Biol. Eng.* **11** 534–45

Hoff I E, Hoiseth L O, Hisdal J, Roislien J, Landsverk S A and Kirkeboen K A 2014 Respiratory variations in pulse pressure reflect central hypovolemia during noninvasive positive pressure ventilation *Crit. Care Res. Pract.* 2014 doi: 10.1155/2014/712728

Holme N L, Rein E B and Elstad M 2016 Cardiac stroke volume variability measured non-invasively by three methods for detection of central hypovolemia in healthy humans *Eur. J. Appl. Physiol.* **116** 2187–96

Hu X, Chen X, Ren R, Zhou B, Qian Y, Li H and Xia S 2014 Adaptive filtering and characteristics extraction for impedance cardiography *J. Fiber Bioeng. Informat.* **7** 81–90

Hurwitz B E, Shyu L Y, Reddy S P, Schneiderman N and Nagel J H 1990 Coherent ensemble averaging techniques for impedance cardiography *Proc. 3rd IEEE Symposium Computer-Based. Med. Sys.* (Chapel Hill, NC: IEEE) pp 228–35 doi: 10.1109/CBMSYS.1990.109403

Ikarashi A, Nogawa M, Yamakoshi T, Tanaka S and Yamakoshi K 2006 An optimal spot-electrodes array for electrical impedance cardiography through determination of impedance mapping of a regional area along the medial line on the thorax *Proc. IEEE Eng. Med. Biol. Soc.* (New York, NY: IEEE) pp 3202–5 doi: 10.1109/IEMBS.2006.260748

Jain L and Fanelli A M 2000 *Recent Advances in Artificial Neural Networks Design and Applications* ed Jain L C (New York: CRC Press)

Jensen L, Yakimets J and Teo K K 1995 A review of impedance cardiography *Heart & Lung: J. Acute Critical Care* **24** 183–93

Jindal G D, Ananthakrishnan T S, Kataria S K, Jain R K, Mandlik S A, Sinha V, Deepak K K and Deshpande A K 2003 25 Years of impedance plethysmography *BARC Newsletter* (Mumbai, India: BARC) **236**

Kamath S A, Drazner M H, Tasissa G, Rogers J G, Stevenson L W and Yancy C W 2009 Correlation of impedance cardiography with invasive hemodynamic measurements in patients with advanced heart failure: the bioimpedance cardiography (BIG) substudy of the evaluation study of congestive heart failure and pulmonary artery catheterization effectiveness (ESCAPE) Trial *Am. Heart J.* **158** 217–23

Karnegis J N and Kubicek W G 1970 Physiological correlates of the cardiac thoracic impedance waveform *Am. Heart J.* **79** 519–23

Kerr A J, Simmonds M B and Stewart R A 1998 Influence of heart rate on stroke volume variability in atrial fibrillation in patients with normal and impaired left ventricular function *Am. J. Cardiol.* **82** 1496–500

Kieback A G, Borges A C, Schink T, Baumann G and Laule M 2010 Impedance cardiography versus invasive measurements of stroke volume index in patients with chronic heart failure *Int. J. Cardiol.* **143** 211–3

Kim D W 1989 Detection of physiological events by impedance *Yonsei Med. J.* **30** 1–11

Kim D W, Baker L E, Pearce J A and Kim W K 1988 Origins of the impedance change in impedance cardiography by a three-dimensional finite element model *IEEE Trans. Biomed. Eng.* **35** 993–1000

Kim D W, Song C G and Lee M H 1992 A new ensemble averaging technique in impedance cardiography for estimation of stroke volume during treadmill exercise *Front Med. Biol. Eng.* **4** 179–88

Kizakevich P N, Hazucha M, Van Hoose L, Bolick K, Jochem W J, McCartney M and McMaster L 1994 Reproducibility of impedance cardiogram waveform analysis in lower-body and upper-body exercise *Proc. IEEE 7th Sym. Comp. Based Med. System* (Winston-Salem, NC: IEEE) pp 181–6 doi: 10.1109/CBMS.1994.316008

Kizakevich P N, Teague S M, Jochem W J, Nissman D B, Niclou R and Sharma M K 1989 Detection of ischemic responses during treadmill exercise by computer-aided impedance cardiography *Proc. 2nd Annu. IEEE Symp. Comput. Based Med. Syst.* (Minneapolis, MN: IEEE) pp 10–5 doi: 10.1109/CBMSYS.1989.47351

Kizakevich P N, Teague S M, Nissman D B, Jochem W J, Niclou R and Sharma M K 1993 Comparative measures of systolic ejection during treadmill exercise by impedance cardiography and Doppler echocardiography *Biol. Psychol.* **36** 51–61

Korhonen I, Koobi T and Turjanmaa V 1999 Beat-to-beat variability of stroke volume measured by whole-body impedance cardiography *Med. Biol. Eng. Comput*. **37** 61–2

Krivoshei A, Kukk V and Min M 2008 Decomposition method of an electrical bioimpedance signal into cardiac and respiratory components *Physiol. Meas.* **29** S15–S25

Kubicek W G 1989 On the source of peak first time derivative (dZ/dt) during impedance cardiography *Annals Biomed. Eng.* **17** 459–62

Kubicek W G, Karnegis J N, Patterson R P, Witsoe D A and Mattson R H 1966 Development and evaluation of an impedance cardiac output system *Aerosp. Med.* **37** 1208–12

Kubicek W G, Kottke J, Ramos M U, Patterson R P, Witsoe D A, Labree J W, Remole W, Layman T E, Schoening H and Garamela J T 1974 The Minnesota impedance cardiograph-theory and applications *Biomed. Eng.* **9** 410–6

Kubicek W G, Patterson R P and Witsoe D A 1970 Impedance cardiography as a noninvasive method of monitoring cardiac function and other parameters of cardiovascular system *Ann. New York Acad. Sci.* **170** 724–32

Lababidi Z, Ehmke D A, Durnin R E, Leaverton P E and Lauer R M 1970 The first derivative thoracic impedance cardiogram *Circulation* **41** 651–8

Lababidi Z, Ehmke D A, Durnin R E, Leaverton P E and Lauer R M 1971 Evaluation of impedance cardiac output in children *Pediatrics* **47** 870–9

Leahy M R, Johnson M A and Rogers S K 1991 Neural network payload estimation for adaptive robot control *IEEE Trans. Neural Netw.* **2** 93–100

Levenberg K 1944 A method for the solution of certain non-linear problems in least squares *Quart. Appl. Math.* **12** 164–68

Lewis J F, Kuo L C, Nelson J G, Limacher M C and Quinones M A 1984 Pulsed Doppler echocardiographic determination of stroke volume and cardiac output: clinical validation of two new methods using the apical window *Circulation* **70** 425–31

Liu H, Yambe T, Sasada H, Nanka S, Tanaka S, Nagatomi R and Nitta S 2004 Comparison of heart rate variability and stroke volume variability *Auton. Neurosci.* **116** 69–75

Lo H Y, Liao S C, Ng C J, Kuan J T, Chen J C and Chiu T F 2007 Utility of impedance cardiography for dyspneic patients in the ED *Am. J. Emerg. Med.* **25** 437–41

Lopez-Saucedo A, Hirt M, Appel P L, Curtis D L, Harrier H D and Shoemaker W C 1989 Feasibility of noninvasive physiologic monitoring in resuscitation of trauma patients in the emergency department *Crit. Care Med*. **17** 567–8

Marik P E, Cavallazzi R, Vasu T and Hirani A 2009 Dynamic changes in arterial waveform derived variables and fluid responsiveness in mechanically ventilated patients: a systematic review of the literature *Crit. Care Med.* **37** 2642–7

Marquardt D W 1963 An algorithm for least-squares estimation of nonlinear parameters *J. Soc. Indust. Appli. Math.* **11** 431–41

Meijer J H, Boesveldt S, Elbertse E and Berendse H W 2007 Using time interval parameters from impedance cardiography to evaluate autonomic nervous function in Parkinson's disease *Proc. 13th Int. Conf. Electr. Bioimpedance & 8th Conf. Electr. Impedance Tomography* (Graz: IFMBE) pp 596–9 doi: 10.1007/978-3-540-73841-1_154

Miyamoto Y, Tamura T and Mikami T 1981 Automatic determination of cardiac output using an impedance plethysmography *Biotelem. Patient Monit.* **8** 189–203

Moody J O and Antsaklis P J 1996 The dependence identification neural network construction algorithm *IEEE Trans. Neural Netw.* **7** 3–15

Mulavara A P, Timmons W D, Nair M S, Gupta V, Kumar A A and Taylor B C 1998 Electrical impedance cardiography using artificial neural networks *Ann. Biomed. Eng.* **26** 577–83

Nagel J H, Shyu L Y, Reddy S P, Hurwitz B E, McCabe P M and Schneiderman N 1989 New signal processing techniques for improved precision of noninvasive impedance cardiography *Ann. Biomed. Eng.* **17** 517–34

Naidu S M M, Pandey P C and Pandey V K 2011 Automatic detection of characteristic points in impedance cardiogram *Proc. Comput. Cardiol.* (Hangzhou, China: IEEE) pp 497–500

Nelson N and Janerot-Sjoberg B 2001 Beat-to-beat changes in stroke volume precede the general circulatory effects of mechanical ventilation: a case report *Crit. Care* **5** 41–5

Nguyen D and Widrow B 1990 Improving the learning speed of 2-layer neural networks by choosing initial values of the adaptive weights *Proc. Int. Joint Conf. Neural Netw.* (San Diego, California: IEEE) doi: 10.1109/IJCNN.1990.137819

Nocedal J and Wright S J 1999 *Numerical Optimization* (New York: Springers)

Northridge D B, Findlay I N, Wilson J, Henderson E and Dargie H J 1990 Non-invasive determination of cardiac output by Doppler echocardiography and electrical bioimpedance *Br. Heart J.* **63** 93–7

Nyboer J 1970 *Electrical Impedance Plethysmography* 2nd edn, ed Thomas C C (Massachusetts: Springfield)

Nyboer J, Kreider M M and Hannapel L 1950 Electrical impedance plethysmography a physical and physiologic approach to peripheral vascular study *Circulation* **2** 811–21

Oh J K, Seward J B and Tajik A J 2006 *The Echo Manual* 3rd edn (New Delhi: Wolters Kulwer)

Ono T, Miyamura M, Yasuda Y, Ito T, Saito T, Ishiguro T, Yoshizawa M and Yambe T 2004 Beat-to-beat evaluation of systolic time intervals during bicycle exercise using impedance cardiography *Tohoku J. Exp. Med.* **203** 17–29

Packer M *et al* 2006 Utility of impedance cardiography for the identification of short-term risk of clinical decompensation in stable patients with chronic heart failure *J. Am. Coll. Cardiol.* **47** 2245–52

Papaloukas C, Fotiadis D I, Likas A and Michalis L K 2002 An ischemia detection method based on artificial neural networks *Artif. Intell. Med*. **24** 167–78

Pan J and Tompkins W J 1985 A real-time QRS detection algorithm *IEEE Trans. Biomed. Eng.* **32** 230–6

Pandey V K and Pandey P C 2005 Cancellation of respiratory artifact in impedance cardiography *Proc. of the 27th Annu. Int. Conf. IEEE Eng. Med. Biol. Soc*. (Shanghai, China: IEEE) pp 5503–6

Pandey V K and Pandey P C 2007 Wavelet based cancellation of respiratory artifacts in impedance cardiography *Proc. 15th Int. Conf. Digital Signal Processing* (Cardiff, UK: IEEE) pp 191–4 doi: 10.1109/ICDSP.2007.4288551

Pandey V K and Pandey P C 2009 Wavelet based denoising for suppression of motion artifacts in impedance cardiography *Proc. Int. Symp. Emerging Areas Biotechnol. Bioeng.* (Mumbai, India) pp 21–2

Pandey V K, Pandey P C and Sarvaiya J N 2008 Impedance simulator for testing of instruments for bioimpedance sensing *IETE J. Research* **54** 203–7

Pandey V K, Pandey P C, Burkule N J and Subramanyan L R 2011 Adaptive filtering for suppression of respiratory artifact in impedance cardiography *Proc. 33rd Annu. Int. Conf. IEEE Eng. Med. Biol. Soc.* (Boston, Massachusetts: IEEE) pp 7932–6 doi: 10.1109/IEMBS.2011.6091956

Patterson R P 1989 Fundamentals of impedance cardiography *IEEE Eng. Med. Biol. Mag.* **8** 35–8

Patterson R P 2010 Impedance cardiography: what is the source of the signal? *Proc. J. Physics: Conf. Ser.* **224** 012118

Patterson R P, Wang L and Raza S B 1991 Impedance cardiography using band and regional electrodes in supine, sitting, and during exercise *IEEE Trans. Biomed. Eng.* **38** 393–400

Penney B C, Patwardhan N A and Wheeler H B 1985 Simplified electrode array for impedance cardiography *Med. Biol. Eng. Comput.* **23** 1–7

Peterson G E, Brickner M E and Reimold S C 2003 Transesophageal echocardiography: clinical indications and applications *Circulation* **107** 2398–402

Pianosi P and Garros D 1996 Comparison of impedance cardiography with indirect Fick (CO2) method of measuring cardiac output in healthy children during exercise *Am. J. Cardiol.* **77** 745–9

Qu M H, Zhang Y J, Webster J G and Tompkins W J 1986 Motion artifact from spot and band electrodes during impedance cardiography *IEEE Trans. Biomed. Eng.* **33** 1029–36

Quiñones M A, Otto C M, Stoddard M, Waggoner A and Zoghbi W A 2002 Recommendations for quantification of Doppler echocardiography: a report from the Doppler Quantification Task Force of the Nomenclature and Standards Committee of the American Society of Echocardiography *J. Am. Soc. Echocardiogr.* **15** 167–84

Raaijmakers E, Faes T J, Goovaerts H G, de Vries P M and Heethaar R M 1997 The inaccuracy of Kubicek's one-cylinder model in thoracic impedance cardiography *IEEE Trans. Biomed. Eng.* **44** 70–6

Ragheb A O, Geddes L A, Bourland J D and Tacker W A 1992 Tetrapolar electrode system for measuring physiological events by impedance *Med. Biol. Eng. Comput.* **30** 115–7

Ramana K V and Raghu B K 2010 Neural network based classification and diagnosis of brain haemorrhages *Int. J. Artificial Intell. Expert Sys.* **1** 7–25

Rasmussen S, Corya B C, Phillips J F and Black M J 1982 Unreliability of M-mode left ventricular dimensions for calculating stroke volume and cardiac output in patients without heart disease *Chest* **81** 614–9

Raza S B, Patterson R P and Wang L 1992 Filtering respiration and low-frequency movement artefacts from the cardiogenic electrical impedance signal *Med. Biol. Eng. Comput.* **30** 556–61

Riedmiller M and Braun H A 1993 A direct adaptive method for faster backpropagation learning: the RPROP algorithm *Proc. IEEE Int. Conf. Neural Netw.* (San Francisco, CA: IEEE) pp 586–91 doi: 10.1109/ICNN.1993.298623

Riese H, Groot P F C, Berg M V D, Kupper N H M, Magnee E H B and Rohaan E J 2003 Large-scale ensamble averaging of ambulatory impedance cardiograms *Behav. Res. Methods Instrum. Comput.* **35** 467–77

Rizzi M, Aloia M D and Castagnolo B 2009 High sensitivity and noise immune method to detect impedance cardiography characteristic points using wavelet transform *J. App. Sci.* **9** 1412–21

Rosell J and Webster J G 1995 Signal-to-motion artifact ratio versus frequency for impedance pneumography *IEEE Trans. Biomed. Eng.* **42** 321–3

Sahu D R, Wong N C and Yao J C 2011 A generalized hybrid steepest-descent method for variational inequalities in Banach spaces *Fixed Point Theory Appl.* **754702** pp 1–28 doi: 10.1155/2011/754702

Sakamoto K and Kanai H 1979 Electrical characteristics of flowing blood *IEEE Trans. Biomed. Eng.* **26** 686–95

Samarasinghe S 2006 *Neural Networks for Applied Sciences and Engineering* (New York: Auerbach Publications/Taylor and Francis)

Saunders C E 1988 The use of transthoracic electrical bioimpedance in assessing thoracic fluid status in emergency department patients *Am. J. Emerg. Med.* **6** 337–40

Scherhag A, Kaden J J, Kentschke E, Sueselbeck T and Borggrefe M 2005 Comparison of impedance cardiography and thermodilution-derived measurements of stroke volume and cardiac output at rest and during exercise testing *Cardiovasc. Drugs Ther.* **19** 141–7

Sherwood A, Allen M T, Fahrenberg J, Kelsey R M, Lovallo W R and van Doornen L J 1990 Methodological guidelines for impedance cardiography *Psychophysiology* **27** 1–23

Sherwood A, McFetridge J and Hutcheson J S 1998 Ambulatory impedance cardiography: a feasibility study *J. Appl. Physiol*. **85** 2365–9

Shewchuk J R 1994 *An introduction to the conjugate gradient method without the agonizing pain* (Pittsburgh: Carnegie Mellon University)

Shyu L Y, Lin Y S, Liu C P and Hu W C 2004 The detection of impedance cardiogram characteristic points using wavelet transform *Comput. Biol. Med.* **34** 165–75

Shyu L Y, Reddy S P, Nagel J H and Schneiderman N 1988 New signal processing techniques for improved reliability of impedance cardiography *Proc. Annu. Int. Conf. IEEE Eng. Med. Biol. Soc.* (New Orleans, LA: IEEE) pp 41–2 doi: 10.1109/IEMBS.1988.94395

Siebert J, Drabik P, Lango R and Szyndler K 2004 Stroke volume variability and heart rate power spectrum in relation to posture changes in healthy subjects *Med. Sci. Monitor* **10** 31–7

Siebert J, Wtorek J and Rogowski J 1999 Stroke volume variability-cardiovascular response to orthostatic maneuver in patients with coronary artery diseases *Ann. N.Y. Acad. Sci.* **873** 182–90

Silipo R and Marchesi C 1998 Artificial neural networks for automatic ECG analysis *IEEE Trans. Signal Process.* **46** 1417–25

Singh S K and Kumar D R 2004 A comparison of different neural network training algorithms for hydromechanical deep drawing *Int. J. Mater. Product Tech.* **21** 186−99

Sodolski T and Kutarski A 2007 Impedance cardiography: a valuable method of evaluating haemodynamic parameters *Cardiol. J.* **14** 115–26

Solomon S D and Bulwer B E 2007 *Essential echocardiography* (Totowa, NJ: Humana Press)

Sramek B 1984 Noninvasive continuous cardiac output monitor *US Patent* 4450527

Sramek B, Rose D M and Miyamoto A 1983 Stroke volume equation with a linear base impedance model and its accuracy as compared to thermodilution and magnetic

flowmeter techniques in humans and animals *Proc. 6th Int. Conf. Electr. Bioimp.* (Zadar, Yugoslavia: ISEBI) 38

Strickberger S A, Conti J, Daoud E G, Havranek E, Mehra M R, Piña I L and Young J 2005 Patient selection for cardiac resynchronization therapy *Circulation* **111** 2146–50

Summers R L, Parrott C W, Quale C and Lewis D L 2004 Use of noninvasive hemodynamics to aid decision making in the initiation and titration of neurohormonal agents *Congest Heart Fail.* **10** 28–31

Summers R L, Shoemaker W C, Peacock W F, Ander D S and Coleman T G 2003 Bench to bedside: electrophysiologic and clinical principles of noninvasive hemodynamic monitoring using impedance cardiography *Acad. Emerg. Med.* **10** 669–80

Summers R L, Woodward L H and Kolb J C 1999 Correlation of radiographic cardiothoracic ratio with cardiac function in patients with acute congestive heart failure *Emerg. Radiol.* **6** 153–6

Takada K, Fujinami T, Senda K, Nakayama K and Nakano S 1977 Clinical study of "A waves" (atrial waves) in impedance cardiograms *Am. Heart. J.* **94** 710–7

Tan Y and Saif M 1997 Nonlinear dynamic modelling of automotive engines using neural networks *Proc. Int. Conf. IEEE Control App.* (Hartford, CT: IEEE) doi: 10.1109/CCA.1997.627607

Tang W H and Tong W 2009 Measuring impedance in congestive heart failure: current options and clinical applications *Am. Heart J.* **157** 402–11

Tassan-Mangina S, Codorean D, Metivier M, Costa B, Himberlin C, Jouannaud C, Blaise AM, Elaerts J and Nazeyrollas P 2006 Tissue Doppler imaging and conventional echocardiography after anthracycline treatment in adults: early and late alterations of left ventricular function during a prospective study *Eur. J. Echocardiogr.* **7** 141–6

Ulbrich M, Mühlsteff J, Teichmann D, Leonhardt S and Walter M 2015 A thorax simulator for complex dynamic bioimpedance measurements with textile electrodes *IEEE Trans. Biomed. Circuits Syst.* **9** 412–420

Van De Water J M, Miller T W, Vogel R L, Mount B E and Dalton M L 2003 Impedance cardiography: the next vital sign technology? *Chest* **123** 2028–33

van der Meer N J, Vonk Noordegraaf A, Kamp O and de Vries P M 1999 Noninvasive measurement of cardiac output: two methods compared in patients with mitral regurgitation *Angiology* **50** 95–101

Ventura H O, Pranulis M F, Young C and Smart F W 2000 Impedance cardiography: a bridge between research and clinical practice in the treatment of heart failure *Congest Heart Fail.* **6** 94–102

Visser K R, Lamberts R, Poelmann A M and Zijlstra W G 1977 Origin of the impedance cardiogram investigated in the dog by exchange transfusion with a stroma-free haemoglobin solution *Pflugers Arch.* **368** 169–71

Visser K R, Mook G A, van der Wall E and Zijlstra W G 1993 Theory of the determination of systolic time intervals by impedance cardiography *Biol. Psychol.* **36** 43–50

Wang J and Feng X 1992 Analysis and design of a recurrent neural network for real-time parameter estimation *Proc. Int. Joint Conf. Neural Netw.* (Baltimore, MD: IEEE) pp 925–30 doi: 10.1109/IJCNN.1992.226869

Wang L and Patterson R 1995 Multiple sources of the impedance cardiogram based on 3-D finite difference human thorax models *IEEE Trans. Biomed. Eng.* **42** 141–8

Wang L, Paterson R P and Raza S B 1991 Respiratory effects on cardiac related impedance indices measured under voluntary cardio-respiratory synchronization (VCRS) *Med. Biol. Eng. Comput.* **29** 505–10

Wang X A, Sun H H, Adamson D and Van de Water J M 1989 An impedance cardiography system: a new design *Ann. Biomed. Eng.* **17** 535–56

Webster J G 1998 *Medical Instrumentation-Application and Design* 3rd edn (John Wiley: New Delhi)

Welham K C, Mohapatra S N, Hill D W and Stevenson L 1978 The first derivative of the transthoracic electrical impedance as an index of changes in myocardial contractility in the intact anaesthetised dog *Intens. Care Med.* **4** 43–50

Woltjer H H, Bogaard H J and de Vries P M 1997 The technique of impedance cardiography *Eur. Heart J.* **18** 1396–403

Woltjer H H, Bogaard H J, Scheffer G J, van der Spoel H I, Huybregts M A and de Vries P M 1996 Standardization of non-invasive impedance cardiography for assessment of stroke volume: comparison with thermodilution *Br. J. Anaesth.* **77** 748–52

Wong M M, Pickwell-Macpherson E and Zhang Y T 2009 Impedance cardiography for cuffless and non-invasive measurement of systolic blood pressure *Proc. 31st Ann. Int.*

*Conf. IEEE Eng. Med. Biol. Soc.* (Minneapolis, MN: IEEE) pp 800–2 doi: 10.1109/IEMBS.2009.5333521

Yamakoshi Ken-ichi, M. Nogawa, Tanaka S and Takada S 2003 A new proposal of optimal spot-electrode array for electrical impedance cardiography through the measurement of thoracic impedance mapping *Proc. 25th Annu. Int. Conf. IEEE Eng. Med. Biol. Soc.* (Cancun, Mexico: IEEE) doi: 10.1109/IEMBS/2003/1280799

Yamamoto Y, Tamura M S, Mouth Y, Miyasita M and Hamamoto H 1998 Design and implementation for beat-by-beat impedance cardiography *IEEE Trans. Biomed. Eng.* **35** 1086–90

You-Ten K E, Terblanche N, Borges B and Carvalho J 2008 Hypotension during cesarean delivery: role of impedance cardiography *Canadian J. Anesth.* **55** 4755741–2

Yu B H, Nelesen R, Ziegler M G and Dimsdale J E 2001 Mood states and impedance cardiography-derived hemodynamics *Ann. Behav. Med.* **23** 21–5

Zakaria Z, Mat Isa N A and Suandi S A 2010 A study on neural network training algorithm for multiface detection in static images *World Acad. Sc. Engg. Tech.* **62** 505–10

Zhang H and Li J K 2008 Noninvasive monitoring of transient cardiac changes with impedance cardiography *Cardiovasc. Eng.* **8** 225–31

Zhang Y, Qu M, Webster J G, Tompkins W J, Ward B A and Bassett D R 1986 Cardiac output monitoring by impedance cardiography during treadmill exercise *IEEE Trans. Biomed. Eng.* **33** 1037–41

Zhao S, Fang Y, Zhao H and Tang M 2005 Detection of impedance cardiography's characteristic points based on wavelet transform *Proc. of the 27th Annu. Int. Conf. IEEE Eng. Med. Biol. Soc*. (Shanghai, China: IEEE) pp 2730–2

# Author's Resume and Thesis Related Publications

## Author's Resume

Mr. S. Mohan Mahalakshmi Naidu received the degrees of BTech in electronics & instrumentation engineering from Andhra University (India) in 2001 and MTech in electrical engineering with specialization in control & instrumentation from Motilal Nehru National Institute of Technology, Allahabad (India) in 2005. He is an Associate Professor in the Department of Electronics and Communication Engineering, Koneru Lakshmaiah University, Guntur (India) and concurrently pursuing PhD at IIT Bombay (India). His research interests include biomedical instrumentation and signal processing.

## PhD Thesis Related Publications


B B Patil, P C Pandey, V K Pandey, and S M M Naidu, "A high sensitivity bioimpedance detector," *Proc. National Conference on Virtual and Intelligent Instrumentation (NCVII-09)*, Pilani, India, 2009.

S M M Naidu, P C Pandey, and V K Pandey, "Automatic detection of characteristic points in impedance cardiogram," *Proc. Comput. Cardiol. 2011*, Hangzhou, China, pp. 497–500, 2011.

T Sebastian, P C Pandey, and S M M Naidu, "Wavelet based denoising for suppression of respiratory and motion artifacts in impedance cardiography," *Proc. Computing Cardiol. 2011*, Hangzhou, China, pp. 501–504, 2011.

S M M Naidu, U R Bagal, P C Pandey, S Hardas, and N D Khambete, "Detection of characterisitc points of impedance cardiogram and validation using Doppler echocardiography," *Proc. 11th Annu. Conference of the IEEE India Council (INDICON 2014)*, Pune, India, 2014, doi: 10.1109/INDICON.2014.7030596

S M M Naidu, U R Bagal, P C Pandey, S Hardas, and N D Khambete, "Monitoring of stroke volume through impedance cardiography using an artificial neural network," *Proc. 21st National Conference on Communications (NCC 2015)*, Mumbai, India, 2015, doi: 10.1109/NCC.2015.7084896

U R Bagal, P C Pandey, S M M Naidu, and S Hardas, "Detection of opening and closing of the aortic valve using impedance cardiography and its validation by Doppler echocardiography," *Biomed. Physics Eng. Express*, 2017, Online 12 Sept. 2017, doi: 10.1088/2057-1976/aa8bf5

S M M Naidu, P C Pandey, U R Bagal, and S Hardas, "Beat-to-beat estimation of stroke volume using impedance cardiography and artificial neural networks," *Med. Biol. Eng. Comput.*, 2017, Epub 18 Nov. 2017, doi: 10.1007/s11517-017-1752-5

# Acknowledgements

With heartfelt regards and respect, I would like to express my sincere gratitude to my supervisor Prof. P. C. Pandey for his continuous support and invaluable guidance during the course of entire PhD study, investigation, and thesis preparation. His immense knowledge and patience has helped me throughout my research journey. I am grateful to Prof. S. Mukherjee and Prof. V. Rajbabu, members of the research progress committee for their valuable suggestions and encouragement at various stages of the work.

I wish to sincerely thank Dr. Suhas P. Hardas, Hardas Heart Care, Pune, who provided me an opportunity to join his team and for giving me an access to the laboratory and research facilities. Special thanks are to Dr. I. Zanwar, Dr. V. Shah, Dr. N. Sawant, Dr. V. Dixit, Mrs. A. Thakkar, and Mr. D. Gaje for their invaluable and extended support for my research.

I am grateful to Dr. N. D. Khambete and Dr. V. N. Desurkar of Deenanath Mangeshkar Hospital and Research Center, Pune, Dr. V. D. Chavan and Dr. S. R. Kalkekar of Mahatma Gandhi Mission Hospital, Navi Mumbai, and Dr. D. Patil of Madhavbaug Ayurvedic Cardiac Hospital, Raigad for support for clinical recordings and many insightful discussions.

I am thankful to everyone in the Signal Processing and Instrumentation Laboratory for their encouragement and extending support. Special thanks are to my friends Uttam, Vinod, Vidhyadhar, Bhupesh, Mithun, Praveen, Pandurang, Jayan, Natraj, Rajath, Jagbandhu, Toney, Nitya, Santosh, Saketh, Hirak, and other friends for their suggestions and joyful interactions.

I wholeheartedly thank Mrs. A. M. Katara, President, International Institute of Information Technology, Pune for sponsoring my doctoral studies under College Teacher scheme. I am thankful to Dr. V. P. Bhatkar, Dr. A. Rakshit, Prof. S. S. Pujari, Prof. R. Henry, and all other former colleagues at the institute for their good wishes and encouragement. Special thanks are due to Mrs. Vaidehi Banerjee and Mr. Adesh Patwardhan for the initiatives which helped in establishing the collaboration for clinical recordings.

Special thanks are due to Dr. S. Krishnamoorthy, Advisor and Mr. Albert W. D'souza, Chairman, St. John College of Engineering and Management, Palghar and Dr. L. S. S. Reddy, Vice Chancellor and Dr. A. S. C. S. Sastry, Head of the Electronics and Communication Engineering Department of K. L. University, Guntur for their timely support.

My deepest gratitude goes to my parents, brothers, sister, and parents-in-law for being so supportive all the time during the course of research. Special thanks to my wife Swathi for her throughout unfailing support and encouragement.

S. Mohan Mahalakshmi Naidu